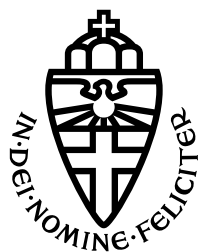


RADBOUD UNIVERSITY NIJMEGEN



FACULTY OF SCIENCE

Power Grid Failures

Theory of Fluctuating Renewables

THESIS BSC MATHEMATICS

Author:
Fons VAN DER PLAS

Supervisor:
dr. Henk DON

Second reader:
prof. dr. Eric CATOR

July 2019

Summary

Limiting global warming requires a rapid transition towards renewable generation of electric energy. For this purpose, global energy demand becomes increasingly dependent on solar and wind energy. Unlike conventional energy sources, these stochastic sources inject a fluctuating amount of power into the electric grid. Large-scale fluctuations change the electric current through high-voltage lines of the transmission network, possibly evoking a line overload. Moreover, the failure of one line can result in a cascade of other failures, eventually causing a blackout.

In this thesis, we will study the effect of fluctuating renewables on the robustness of electric power transmission. To this end, we develop a mathematical framework that models the transmission of stochastic generation and predicts the line failure probability. The model accounts for correlated fluctuations among different network buses, which arise from correlated weather. The model extends the classical DC approximation to the stochastic case and uses algebraic graph theory to study the flow redistribution after multiple line outages.

Inspired by a recent study (Nesti et al., 2018a), we demonstrate the applicability of this theory by identifying the most vulnerable lines in the German transmission network, and simulating the resulting cascades. This case study illustrates the usefulness and limitations of our model to predict line failures caused by fluctuating renewables. Using such methods in practice helps us to evaluate the risks of stochastic generation more precisely, allowing for higher shares of renewable generation to be installed.

Notation

\mathbf{Y} is a matrix or vector

$Y_{i,j}$ is an element of a matrix or vector

Y is a (real or complex) number

\mathbb{Y} is a physical quantity (like ‘admittance’)

$\bar{\mathbf{Y}}$ is the *element-wise complex conjugate* of \mathbf{Y}

\mathbf{Y}^* is the *adjoint* of \mathbf{Y} (which is equivalent to
the *transpose* for real-valued \mathbf{Y})

$[n] = \{1, \dots, n\}$

\ddagger *end of example*

\spadesuit *end of proof*

Contents

I Theory of Electric Power Networks	1
1 Graph theory	2
1.1 Directed graph	2
1.2 Flow	3
1.3 Image of K	6
1.4 Kernel of K	8
2 Probability Theory	11
2.1 Multivariate Gaussian distribution	11
2.2 One linear condition	13
3 The Electric Grid	17
3.1 Overview	17
3.2 Generators	17
3.3 Loads	18
3.4 Transmission	19
3.5 Grid security	21
3.6 The energy market	22
4 Modelling Transmission Networks	27
4.1 The model	27
4.2 Grid structure	28
4.3 Power grid state	29
4.4 State validity	30
4.5 Power Flow	35
4.6 DC approximation	36
4.7 Nodal susceptance matrix	41
4.8 Linear Power Flow	42

4.9	Stochastic power injections	43
4.10	Redistribution of flow	46
II	Predicting failures in Germany's grid	51
5	Methods	52
5.1	Constructing a complete dataset	53
5.2	LPF	55
5.3	Exploratory data analysis	55
5.4	Stochastic power injection	57
5.5	Most likely power injection	59
5.6	Cascading line failures	60
6	Results	61
6.1	SciGRID data	61
6.2	Bus covariance	63
6.3	Line covariance	64
6.4	Most vulnerable lines	67
6.5	Most likely injection	68
6.6	Discussion	71

Part I

Theory of Electric Power Networks

Chapter one

Graph theory

The power grid forms an interconnected *network* of transmission lines, which makes graph theory a logical choice for modelling it. In fact, most electrical systems are modelled using graphs. In circuit theory, *lines* represent individual electrical components (resistors, voltage sources) and *nodes* represent the conductive material between them.¹ We will study the electrical properties of the transmission network in Chapter 4, but for now, we will simply accept that the transmission network consists of *nodes* and *lines*, and that the lines can transfer power between nodes in a straightforward (linear) way. Physically, the power flows are determined by the amount of power injected at each node, which in turn is determined by the devices that we connect to the transmission network. In this chapter, we will study the *converse*:

What does the flow of power tell us about the power injection at the nodes?

To do so, we will build upon the tools of linear algebra and graph theory, as covered in most elementary textbooks on these subjects.

In this section, we will use, without proof:

- *Every connected graph contains a minimum spanning tree.*
- *A connected (di)graph is a tree if and only if the number of lines is one fewer than the number of nodes.*
- *By removing a leaf from a tree, we obtain a new tree.*
- *Given two nodes in a tree, there is a unique path between these nodes that crosses any line at most once.*

1.1 Directed graph

When studying the flow of current in a network, it is necessary to fix a direction for each line, relative to which the flow along that line can be expressed. We do so using a *digraph*, where lines are not defined as two-element sets (like they are in a classical *graph*), but as *ordered pairs*.

Definition 1.1.1. A *directed graph* is a pair $(\mathcal{N}, \mathcal{L})$ such that the set of *nodes* \mathcal{N} is finite, and the set of *lines* $\mathcal{L} \subseteq \mathcal{N} \times \mathcal{N}$ satisfies:

¹This simplification is only true for components with 2 terminals. A transistor has 3 terminals, for example.

- If $(i, j) \in \mathcal{L}$, then $(j, i) \notin \mathcal{L}$. (i.e. there are no 'loops' between two nodes.)
- For each $i \in \mathcal{N}$: $(i, i) \notin \mathcal{L}$. (i.e. no node is directly connected to itself.)

A classical graph can be converted to a *digraph* by (arbitrarily) choosing a direction for each line. Some authors prefer to use a classical graph, combined with an *incidence function*: a function that maps an unordered pair of nodes $\{i, j\}$ to an ordered pair, (i, j) or (j, i) .²

1.2 Flow

For the remainder of this section, assume that $G = (\mathcal{N}, \mathcal{L})$ is a directed graph, where the nodes are labelled $\mathcal{N} = \{1, 2, \dots, n\} = [n]$ for some $n \in \mathbb{N}$. The $m = \#\mathcal{L}$ lines of the network are labelled $\mathcal{L} = \{\mathcal{L}_1, \mathcal{L}_2, \dots, \mathcal{L}_m\}$.

We also fix a field \mathbb{K} , which we will use to define *injections* and *flows* on G . When studying *real power flows*, we will take $\mathbb{K} = \mathbb{R}$.

Definition 1.2.1. An *injection* on G is an element of \mathbb{K}^n ; a *flow* on G is an element of \mathbb{K}^m .

One should view an injection $\mathbf{p} \in \mathbb{K}^n$ as the vector that encodes how much power is being put into the network at each node. When p_i is negative, this means that power is being *consumed* at node i . Similarly, a flow $\mathbf{f} \in \mathbb{K}^m$ represents the amount of power transmitted along each line. For a line $\mathcal{L}_k = (i, j) \in \mathcal{L}$, f_k expresses the amount of power being transmitted along the line, from node i to node j .

Of course, the notions *positive* and *negative* only exist when \mathbb{K} is a totally ordered set. Otherwise, we simply have to be satisfied with the meaning provided by Definition 1.2.2.

When $\mathbb{K} = \mathbb{F}_2$, a flow can be seen as a subset of the collection of lines \mathcal{L} , since any flow entry is either 1 or 0.

Definition 1.2.2. An injection $\mathbf{p} \in \mathbb{K}^n$ is *induced* by a flow $\mathbf{f} \in \mathbb{K}^m$ if:

$$p_i = \sum_{\mathcal{L}_k=(i,j) \in \mathcal{L}} f_k - \sum_{\mathcal{L}_k=(j,i) \in \mathcal{L}} f_k \quad (1.1)$$

for each node $i \in \mathcal{N}$. ($p_i = 0$ for isolated nodes.)

Note that \mathbf{p} is uniquely defined for every choice of \mathbf{f} . This allows us to define a function:

Definition 1.2.3. Suppose G has no isolated nodes. We define the *Flow Response Transformation* (K) as the function

$$K : \mathbb{K}^m \rightarrow \mathbb{K}^n$$

that maps a flow $\mathbf{f} \in \mathbb{K}^m$ to the unique injection $\mathbf{p} \in \mathbb{K}^n$ that it induces.

²Slepian (1968) takes this one step further by *only* considering the incidence function: the set of lines can be retrieved as the *domain* of the incidence function, and the set of nodes is the *union* of the set of lines.

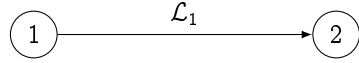


Figure 1.1: The simple *two-node* network of two nodes and one line.

From (1.1), it follows that K is a linear map, which means that we can write K as a matrix: \mathbf{K} . We can find an explicit expression for the entries $K_{i,k}$, noting that its *rows* are determined by (1.1), and that there are no ‘double’ lines in the digraph.

$$K_{i,k} = \begin{cases} 1 & \text{if } \mathcal{L}_k = (i, j) \text{ for some } j \in [n], \\ -1 & \text{if } \mathcal{L}_k = (j, i) \text{ for some } j \in [n], \\ 0 & \text{otherwise.} \end{cases}$$

This matrix can be seen as the familiar *incidence matrix* of a classical graph, adapted to digraphs. For this reason, \mathbf{K} is often called the *vertex-edge incidence matrix* of G . The ordered set of lines is uniquely defined by the vertex-edge incidence matrix.

Example 1.2.4 (Two-node network). A very simple digraph is one with just two nodes, and a single line connecting them. This *two-node network* is drawn in Figure 1.1. Although real networks are much bigger, this example is useful to illustrate some of the concepts introduced in Chapter 4.

We have:

$$\begin{aligned} \mathcal{N} &= \{1, 2\} \text{ and} \\ \mathcal{L} &= \{\mathcal{L}_1\} \text{ with } \mathcal{L}_1 = (1, 2). \end{aligned}$$

Since $n = 2$ and $m = 1$, \mathbf{K} is a 2×1 matrix:

$$\mathbf{K} = \begin{pmatrix} 1 \\ -1 \end{pmatrix}.$$

■

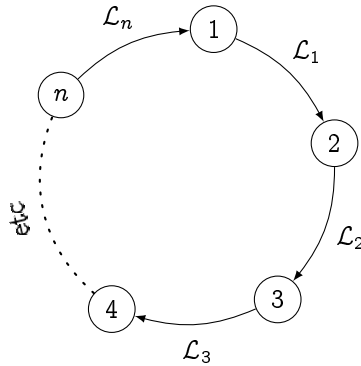


Figure 1.2: The *n-loop* network with n nodes and n lines.

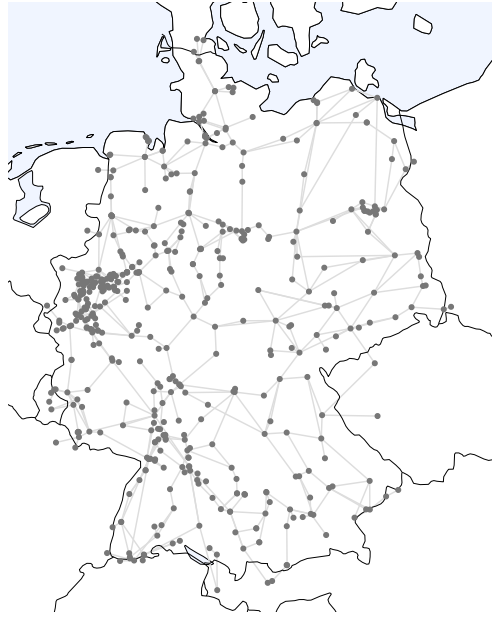


Figure 1.3: The $n = 489$ buses and $m = 695$ lines of the SciGRID network. A description of this dataset is given in Part II.

Example 1.2.5 (Loop network). A less trivial digraph is the *n-loop network*, shown in Figure 1.2. It consists of n nodes, connected in a circular fashion (using n lines).

Note that this network is 2-edge connected, meaning that the network remains connected when any edge is removed. (Although removing *any* two lines will disconnect the network.)

We have:

$$\begin{aligned}\mathcal{N} &= \{1, \dots, n\} = [n] \text{ and} \\ \mathcal{L} &= \{\mathcal{L}_1, \dots, \mathcal{L}_n\} \text{ with } \mathcal{L}_i = (i, i+1) \text{ for } 1 \leq i < n \text{ and } \mathcal{L}_n = (n, 1).\end{aligned}$$

Since $m = n$, \mathbf{K} is an $n \times n$ matrix:

$$\mathbf{K} = \begin{pmatrix} 1 & & & & -1 \\ -1 & 1 & & & \\ & -1 & 1 & & \\ & & \ddots & \ddots & \\ & & & 1 & \\ & & & -1 & 1 \end{pmatrix}.$$

(All unspecified elements are 0).

Note that the *columns* of \mathbf{K} correspond to the lines of the network. □

Example 1.2.6 (SciGRID Germany). In Part II, we will apply our theory to the SciGRID dataset, which contains the network shown in Figure 1.3. This network is much more

realistic than the previous examples, as it is based on the real-world structure of the transmission network in Germany.

It is common for transmission networks to have a well-connected ‘core’, with some branches out of the core towards the outer regions of the network. This means that in general, $m > n$.

Indeed, in this network we have $n = 489$ and $m = 695$. The vertex-edge incidence matrix \mathbf{K} has dimensions 489×695 , and it is *sparse*: most entries are zero.

It is important to note that this is only a *section* of the actual transmission network of continental Europe, which is highly connected among different countries. As we will discuss in Section 5.1, accurate datasets of continental Europe do exist, but they are hard to obtain and analyse. \square

The fact that \mathbf{K} is a linear map raises an interesting question: how can the image and kernel of \mathbf{K} be interpreted in the context of digraph flows? The reader is invited to revisit Example 1.2.5 to visualise these sets.

One can interpret the image of \mathbf{K} as the set of injections that can be redistributed along the network. Because a flow only serves to redistribute injections from one node to another, nothing is lost or gained in the network. This imposes the condition that an injection vector must have *zero sum*. Moreover, when G is connected, *all* zero sum injections can be induced by a flow.

The kernel can be interpreted as the set of all flows that result in zero injections. Besides the trivial case of zero flow, any constant flow along a loop induces zero injection. We will find that these *loop flows* generate *all* flows in the kernel of \mathbf{K} .

When G is a planar graph, loops around the faces of G actually form a *basis* for the kernel. In the more general case that G is connected, but not necessarily planar, such a basis can also be constructed by fixing a *minimum spanning tree* of G .

As an added bonus, applying the Rank-Nullity theorem to \mathbf{K} when G is planar provides us with an alternative demonstration of Euler’s Formula.

These statements will be made more precise in the next sections, when we study the image and kernel of \mathbf{K} in more detail.

1.3 Image of \mathbf{K}

We start with the following definition:

Definition 1.3.1. The function $\sigma : \mathbb{K}^n \rightarrow \mathbb{K}$ defined by

$$\sigma : \mathbf{p} \mapsto \sum_{i=1}^n p_i$$

is the linear map from an injection vector \mathbf{p} to the *net injection* of \mathbf{p} .

The kernel of σ is the set of zero-sum injections:

$$\ker \sigma = \left\{ \mathbf{p} \in \mathbb{K}^n \mid \sum_{i=1}^n p_i = 0 \right\}.$$

When G is connected, this is exactly the set of injections that can be induced by a flow on G :

Theorem 1.3.2. *Suppose that G is connected. Then*

$$\text{Im } K = \left\{ \mathbf{p} \in \mathbb{K}^n \mid \sum_{i=1}^n p_i = 0 \right\} \cong \mathbb{K}^{n-1} \quad (1.2)$$

We will prove this equality by considering the two inclusions \subseteq and \supseteq separately. The first inclusion follows from the observation that K is the vertex-edge incidence matrix of G .

Lemma 1.3.3. *Suppose that G is connected.*

$$\text{Im } K \subseteq \ker \sigma \quad (1.3)$$

Proof. We write $\mathbf{e}^1, \dots, \mathbf{e}^m$ for the standard basis of \mathbb{K}^m .

Since K is linear, one only needs to verify that $K(\mathbf{f}) \in \ker \sigma$ for each $\mathbf{f} = \mathbf{e}^k$ in the basis. The vectors $K(\mathbf{e}^1), \dots, K(\mathbf{e}^m)$ are exactly the columns of the matrix K , which all have zero sum: a column corresponds to a line in G , and has exactly two non-zero entries: 1 for the entering node, and -1 for the leaving node. \checkmark

To prove the inclusion \supseteq implied by Theorem 1.3.2, we first consider the special case that G is a *tree*.

Lemma 1.3.4. *Suppose that G is a (connected) tree.*

$$\text{Im } K \supseteq \ker \sigma \quad (1.4)$$

Proof. G is a tree, so $m = n - 1$. Because \mathbb{K}^m and $\ker \sigma$ both have dimension $n - 1$, we only need to prove that K is injective: when K has nullity 0, it must have rank $n - 1$.

If $n = 1$, then the digraph consists of a single node, and no lines. It then follows from (1.1) that the only injection that can be induced is $\mathbf{p} = (0) \in \mathbb{K}^1$, so K can only be injective.

If $n > 1$, we will use the fact that the statement holds for any tree with fewer than n nodes. (*Proof by induction.*)

Suppose that $\mathbf{f} \in \mathbb{K}^m$, such that $\mathbf{p} = K(\mathbf{f}) = \mathbf{0}$. Because G is a tree, we can³ pick a leaf $i \in \mathcal{N}$, which has a unique line \mathcal{L}_k connecting i to some $j \in \mathcal{N}$. (We have either $\mathcal{L}_k = (i, j)$ or $\mathcal{L}_k = (j, i)$.)

Only one line is connected to i , so (1.1) gives: $p_i = \pm f_k$. (The sign depends on the orientation of \mathcal{L}_k .) We assumed $p_i = 0$, so we must have $f_k = 0$.

By removing node i and line \mathcal{L}_k , we obtain a smaller tree, for which the statement already holds. The Flow Response Transformation of this subtree is essentially the

³Write $\text{gr}(i)$ for the number of lines connected to i . G is connected, so $\text{gr}(i) \geq 1$ for each $i \in \mathcal{N}$. If no i exists with $\text{gr}(i) = 1$, then $\text{gr}(i) \geq 2$ for each $i \in \mathcal{N}$, giving $\sum_{i=1}^n \text{gr}(i) \geq 2n$. On the other hand, each of the $n - 1$ lines connects exactly two nodes, so $\sum_{i=1}^n \text{gr}(i) = 2(n - 1) < 2n$, a contradiction.

restriction of K to the set $\{\mathbf{f} \in \mathbb{K}^m \mid f_k = 0\}$. Because the restriction is injective, all other coefficients of \mathbf{p} are also zero. This shows that K is injective, and the result follows. 

Proof of Theorem 1.3.2. To prove $\text{Im } K = \ker \sigma$, it remains to show that

$$\text{Im } K \supseteq \ker \sigma \quad (1.5)$$

holds for *any* connected G , not just for trees.

Since G is connected, we can choose a minimum spanning tree: choose $T \subseteq [m]$ with $\#T = n - 1$ such that $G_T = (\mathcal{N}, \{\mathcal{L}_k\}_{k \in T})$ is such a connected subdigraph.

Define $F_T = \text{Span}\{\mathbf{e}^k\}_{k \in T} \subseteq \mathbb{K}^m$ as the subset of flows on G that are zero outside of G_T . Because F_T is a linear subspace of \mathbb{K}^m , we have

$$\text{Im } K = K(\mathbb{K}^m) \supseteq K(F_T),$$

which reduces the problem to $K(F_T) \supseteq \ker \sigma$, which follows from Lemma 1.3.4. 

This shows that

$$\text{Im } K = \ker \sigma.$$

Because $\sigma : \mathbb{K}^n \rightarrow \mathbb{K}$ is surjective, it has rank 1. It therefore has nullity $n - 1$, or equivalently, $\ker \sigma \cong \mathbb{K}^{n-1}$. 

1.4 Kernel of K

Again, let us assume that G is connected. In Theorem 1.3.2, we derived an explicit formulation for the image of K , showing that $\text{rank } K = n - 1$.

Concerning the kernel of K , we already know that $\mathbf{0} \in \ker K$, reflecting the fact that zero flow induces zero injection. In the special case that G is a tree, this is the only such flow. In general, however, the kernel of K is much bigger.

Proposition 1.4.1. *Suppose that G is connected. The dimension of $\ker K$ equals*

$$\text{null } K = m - (n - 1).$$

Proof. This follows directly from the Rank-Nullity theorem, applied to Theorem 1.3.2. 

Corollary 1.4.1.1. *If G is a tree, then $\ker K = \{\mathbf{0}\}$, and K is an isomorphism between \mathbb{K}^m and $\ker \sigma$.*

Proof. Applying Proposition 1.4.1 with $m = n - 1$, we find that $\text{null } K = 0$, so that $\ker K = \{\mathbf{0}\}$. Together with Theorem 1.3.2, we find the result. 

1.4.1 Loop flows

What do the elements of $\ker K$ look like? As we will see, any flow along a *loop*⁴ results in zero power injection. When interpreting a loop as an element \mathbf{f} of \mathbb{K}^m , we must be careful to *flip the sign of f_k if the line L_k is traversed in reverse*.

Theorem 1.4.2. *Suppose that G is connected and that (i_1, i_2, \dots, i_p) is a loop that visits each line at most once. Then the loop flow $\mathbf{f} \in \mathbb{K}^m$ defined by:*

$$f_k = \begin{cases} 1 & \text{if } (i_s, i_{s+1}) = L_k \text{ for any } 1 \leq s < p, \\ -1 & \text{if } (i_{s+1}, i_s) = L_k \text{ for any } 1 \leq s < p, \\ 0 & \text{otherwise,} \end{cases} \quad (1.6)$$

for each line L_k , is an element of the kernel of K .

Proof. We will verify that $\mathbf{p} = K(\mathbf{f})$ is zero. Choose any $i \in N$.

Because the loop is closed, there is an *even* number (possibly zero) of lines with non-zero flow that connect to i . This means that the sums in (1.1) cancel each other (note the negative sign for reversed lines in (1.6)), resulting in $p_i = 0$. \checkmark

Remark. Because K is linear, multiplying a loop flow with a scalar $\gamma \in \mathbb{K}$, or adding two loop flows, creates a new flow that induces zero injection. (The result of addition is a flow, but in general not a *loop* flow.)

Now that we know the dimension of $\ker K$, a natural next step is to look for a *basis* that generates the kernel. Motivated by the previous theorem, we will look for a basis consisting of *loop flows*.

A logical choice for this basis would be the set of all flows in *loops surrounding the faces contained in the graph*. This approach, which only works for *planar graphs*, will be discussed in the next section.

For now, we would like to find a basis of loop flows for the more general case that G is connected, but not necessarily planar. We proceed as follows:

Definition 1.4.3. Suppose that G is connected, and that $T \subseteq [m]$ is a minimum spanning tree. For each remaining line $L_k = (i, j) \in \{L_k \in \mathcal{L} \mid k \notin T\}$, there exists a *unique path along the tree* from j to i that crossed any line at most once, say

$$(i_1, i_2, \dots, i_p), \quad \text{where } i_1 = j \text{ and } i_p = i.$$

By adding the chosen line L_k to this path, we find a loop in G : $(i_1, i_2, \dots, i_p, j)$, which defines a loop flow \mathbf{f}^k .

We define the *spider web basis on T* as the set of loop flows defined this way: $\{\mathbf{f}^k\}_{k \in [m] \setminus T}$. (If T were to represent a physical tree, a spider could spin a web from i to j by attaching a strand to j and then walking the path to i .⁵)

⁴We define a *path* by the ordered sequence of nodes that it visits, including the initial and final node. Although we are studying directed graphs, lines can be traversed in either direction by a path. A *loop* is a path where the initial and final node coincide.

⁵It turns out that this is not how most spiders cover large distances: instead, they produce a long thread, and let it drift in the wind until it sticks to another surface. Clever!

Theorem 1.4.4. *The spider web basis on T constructed in Definition 1.4.3 is a basis for $\ker K$.*

Proof. Because T is a minimum spanning tree, it has $n - 1$ elements, and so the spider web basis consists of $m - (n - 1)$ loop flows. Because the number of elements in the basis equals the dimension of $\ker K$, one only needs to prove that they are linearly independent. Indeed, for each $k \in [m] \setminus T$, the loop flow \mathbf{f}^k is the only element for which the k^{th} entry is non-zero. Therefore, \mathbf{f}^k cannot be written as linear combination of the other fundamental loops. 

1.4.2 Planar Graphs

The spider web basis can be constructed for any connected graph. When the graph is also *planar*, a more intuitive basis exists. Without providing a rigorous definition, we simply say that a graph is *planar* if it can be ‘drawn on a piece of paper without any crossing lines’. Such a drawing creates *faces*: areas enclosed by lines.⁶ Different drawings can produce different collections of faces.

If we fix a collection of faces for a planar graph, then each face is enclosed by some of the lines, which form a loop in the graph. We define the *planar basis on this drawing* as the set of loop flows defined by those loops: each face becomes an element in the basis. Rewriting Theorem 1.4.1, we find:

Corollary 1.4.4.1 (Euler’s Formula). *In a planar, connected graph, we have:*

$$v + f - e = 1$$

where v is the number of vertices, e is the number of edges, and f is the number of faces enclosed by edges, excluding the ‘exterior face’.

⁶We do not consider the infinite enclosing area as one of the faces.

Chapter two

Probability Theory

2.1 Multivariate Gaussian distribution

This presentation of the multivariate Gaussian distribution is heavily based on Chapter VIII of Mathematical Statistics by Pestman (1998), which provides proofs to all theorems listed below.

One distribution that will be particularly useful in our analysis is the *multivariate Gaussian distribution*, which generalises the (one-dimensional) normal distribution. In the simplest case, we have a stochastic vector $\mathbf{E} = (E_1, \dots, E_p)$, which is the combination of p Gaussian distributed, *independent* scalar variables. In general, however, we wish to study stochastic vectors produced by applying a *linear transformation* $\mathbf{L} \in \mathcal{L}(\mathbb{R}^p, \mathbb{R}^q)$ to \mathbf{E} . In this case, the coordinate variables $(\mathbf{L}\mathbf{E})_1, \dots, (\mathbf{L}\mathbf{E})_q$ are not always independent! For example, the map $(E_1, E_2) \mapsto (E_1, E_1 + E_2)$ transforms two independent normals into two dependent ones.

2.1.1 Normal and Gaussian

Although they are often used interchangeably, we make a clear distinction between a *normal* distribution and a *Gaussian* distribution. The former should be familiar:

Definition 2.1.1. A scalar variable E is said to be *normally distributed* with parameters μ and σ if

$$x \mapsto \frac{1}{\sigma\sqrt{2\pi}} \exp\left[\frac{-(x-\mu)^2}{2\sigma^2}\right] \quad (2.1)$$

is the probability density of E .

Definition 2.1.2. A scalar variable E is said to be *Gaussian distributed* if it is either normally distributed or constant.

One could interpret a constant E with value μ as a normally distributed variable with mean μ and ‘standard deviation 0’. A linear combination of normally distributed *scalar* variables is also normally distributed, and the same is true for Gaussian distributed scalars.

Definition 2.1.3. A stochastic vector $\mathbf{E} = (E_1, \dots, E_p)$ is *elementary normally distributed* if the scalar variables E_i are independent and normally distributed ($i \in [p]$).

\mathbf{E} is *elementary Gaussian distributed* if the scalar variables E_i are independent and Gaussian distributed.

Definition 2.1.4. A stochastic vector $\mathbf{X} = (X_1, \dots, X_p)$ is *normally distributed* if there exists an orthogonal operator \mathbf{Q} such that $\mathbf{Q}\mathbf{X}$ is elementary normally distributed. \mathbf{X} is *Gaussian distributed* if there exists an orthogonal operator \mathbf{Q} such that $\mathbf{Q}\mathbf{X}$ is elementary Gaussian distributed.

We state, without proof, the following properties of Gaussian distributed vectors:

Proposition 2.1.5. *The distribution of a Gaussian distributed vector \mathbf{X} is uniquely determined by its expectation $\boldsymbol{\mu} = \mathbb{E}[\mathbf{X}]$ and covariance matrix $\Sigma = \mathcal{C}(\mathbf{X})$, and we write $\mathbf{X} \sim \mathcal{N}(\boldsymbol{\mu}, \Sigma)$. \mathbf{X} is normally distributed if and only if Σ is invertible.*

Translating or applying a linear map to a Gaussian distribution results in a new Gaussian distribution. Note that this can be *any* linear map, not necessarily a bijective, orthogonal one.

Theorem 2.1.6. *Suppose \mathbf{X} is a $\mathcal{N}(\boldsymbol{\mu}, \Sigma)$ -distributed p -vector.*

For any $\mathbf{a} \in \mathbb{R}^p$:

$$\mathbf{X} + \mathbf{a} \sim \mathcal{N}(\boldsymbol{\mu} + \mathbf{a}, \Sigma), \quad (2.2)$$

and for any linear map $\mathbf{L} \in \mathcal{L}(\mathbb{R}^p, \mathbb{R}^q)$:

$$\mathbf{L}\mathbf{X} \sim \mathcal{N}(\mathbf{L}\boldsymbol{\mu}, \mathbf{L}\Sigma\mathbf{L}^*). \quad (2.3)$$

Remark. If \mathbf{X} is normally distributed, and $\mathbf{L} \in \mathcal{L}(\mathbb{R}^p, \mathbb{R}^q)$, then $\mathbf{L}\mathbf{X}$ is Gaussian distributed, but not necessarily normally distributed! A trivial example is the zero map: any normally distributed scalar is mapped to a constant (0), which does not exhibit a probability density function.

Corollary 2.1.6.1. *For any $\mathbf{b} \in \mathbb{R}^p$, the mapping*

$$\langle \mathbf{b}, \cdot \rangle : \mathbb{R}^p \rightarrow \mathbb{R} : \mathbf{x} \mapsto \langle \mathbf{b}, \mathbf{x} \rangle$$

is linear, and therefore the scalar variable $\langle \mathbf{b}, \mathbf{X} \rangle$ is Gaussian distributed.

In particular, when applying Corollary 2.1.6.1 to each element of the standard basis $(\mathbf{e}_1, \dots, \mathbf{e}_p)$ of \mathbb{R}^p , we find that each of the *coordinates* of \mathbf{X} is Gaussian distributed:

Proposition 2.1.7. *Suppose $\mathbf{X} = (X_1, \dots, X_p)$ is a $\mathcal{N}(\boldsymbol{\mu}, \Sigma)$ -distributed p -vector. Then each for each $i \in [p]$, the marginal distribution is given by:*

$$X_i \sim \mathcal{N}(\mu_i, \Sigma_{ii}).$$

For normally distributed vectors, a probability density function exists:

Theorem 2.1.8. *Suppose \mathbf{X} is a normally distributed p -vector with expectation $\boldsymbol{\mu} = \mathbb{E}[\mathbf{X}]$ and covariance matrix $\Sigma = \mathcal{C}(\mathbf{X})$. Then \mathbf{X} has a probability density function given by*

$$\mathbf{x} \mapsto \frac{1}{\sqrt{\det(\Sigma)} (2\pi)^{p/2}} \exp \left[-\frac{1}{2} (\mathbf{x} - \boldsymbol{\mu})^* \Sigma^{-1} (\mathbf{x} - \boldsymbol{\mu}) \right] \quad (2.4)$$

Remark. The condition that \mathbf{X} is normally distributed is necessary: if \mathbf{X} is Gaussian, but not normal, it will take values in an *affine subspace* of \mathbb{R}^p (such as a plane, as subspace of \mathbb{R}^3). If a density function were to exist, it would have support of zero measure, and integrating over \mathbb{R}^p would yield 0, instead of 1.

2.2 One linear condition

Definition 2.2.1. Given a $\mathbf{r} \in \mathbb{R}^p$ and $b \in \mathbb{R}$, the set $A \subseteq \mathbb{R}^p$ of solutions to the equation

$$\langle \mathbf{r}, \mathbf{x} \rangle = b$$

is called a *plane in \mathbb{R}^p* . The set $B \subseteq \mathbb{R}^p$ of solutions to

$$\langle \mathbf{r}, \mathbf{x} \rangle \leq b$$

is a *half-space in \mathbb{R}^p* . When $b = 1$, we write \mathbf{r}_A (or \mathbf{r}_B), and we say that \mathbf{r}_A (\mathbf{r}_B) is a *pillar* for A (or B). Two planes are called *parallel* if they do not intersect.

Remark. When $b \neq 1$, we can scale \mathbf{r} to create a pillar for A or B , unless $b = 0$ (which is the case if and only if $\mathbf{0} \in A$).

Remark. A is the *boundary* of B , i.e. $A = \partial B$.

Geometrically, a pillar can be interpreted as a vector from the origin that crosses the plane orthogonally. Its length is *not* the distance between the origin and the plane, but rather the *inverse* of this distance.

Definition 2.2.2. A *convex polyhedron in \mathbb{R}^p* is the intersection of finitely many half-spaces in \mathbb{R}^p , and can be written as the set of solutions to

$$\mathbf{R}\mathbf{x} \leq \mathbf{b},$$

where each i th row of \mathbf{R} , together with b_i , defines one of the intersecting half-spaces.

The boundary of a convex polyhedron is contained in the union of planes corresponding to the half-spaces. This relation is strict, in general.

The convex polyhedra in \mathbb{R} are exactly all (possibly infinite) closed intervals. Convex polyhedra in \mathbb{R}^3 are familiar shapes, like a cube or a pyramid, but they might also be unbounded, like a pyramid with infinitely deep foundations. Objects that are *not* convex polyhedra are spheres (no finite intersection of half-spaces) and donuts (not convex, which as the name suggest, is a property of any convex polyhedron¹).

2.2.1 Feasibility region

In this thesis, we model the *power injection* of a grid as a normally distributed stochastic vector, where each coordinate corresponds to the amount of power injected at a node of the network. Positive values denote net generation (injection) and negative values are assigned to net consumption. The stochastic behaviour originates from *renewable sources*: wind and solar, and their correlations arise from correlated weather.

The transmission network was built to transfer power from one node to another, i.e. have a non-zero power injection. In Chapter 3, we will learn that not all power injections are *feasible*, as some might cause one of the transmission lines to overload. The *feasibility*

¹Using the linearity of the inner product, one easily finds that half-spaces are convex, and so are their intersections.

region (the set of power injections that can be used) is, to some approximation,² a *convex polyhedron*.

Using historical generation series, we can estimate the covariance of this power injection. Because the amount of current flowing through a line is a linear function of the power injection (by the same approximation), we can use Corollary 2.1.6.1 to determine the marginal distribution of line current, which gives the probability of an overload failure. A failure of this kind (i.e. caused by a fluctuation of renewable injection) is called an *emergent failure*.

Current studies (notably Nesti et al. (2018a) and Chertkov et al. (2011)) take this one step further, by determining *the most probable power injection that caused the emergent failure to occur*. We follow the approach of Nesti et al. (2018a), which is generalised in the following Theorem. Here, the plane A can be taken to be one of the *boundary planes of the feasibility region, corresponding to one of the lines*, and the event $\mathbf{X} \in A$ is the *event that this line overloads*.

Theorem 2.2.3. *Let $\mathbf{X} \sim \mathcal{N}(\boldsymbol{\mu}, \boldsymbol{\Sigma})$ be a normally distributed p -vector with density function $f_{\mathbf{X}}$, and let $A \subseteq \mathbb{R}^p$ be a plane, given by a pillar $\mathbf{r}_A \in \mathbb{R}^p$. Then $\mathbf{X} | \mathbf{X} \in A$ is Gaussian distributed, and has mode*

$$\tilde{\mathbf{x}}_A = \operatorname{argmax}_{\mathbf{x} \in A} f_{\mathbf{X}}(\mathbf{x}) = \boldsymbol{\mu} + \frac{1 - \langle \boldsymbol{\mu}, \mathbf{r}_A \rangle}{\langle \boldsymbol{\Sigma} \mathbf{r}_A, \mathbf{r}_A \rangle} \boldsymbol{\Sigma} \mathbf{r}_A. \quad (2.5)$$

Proof. We will start with the special case of $\boldsymbol{\Sigma} = \mathbf{I}$, and work our way towards the general case.³

Step 1. The case of unit covariance.

Suppose \mathbf{X} is *elementary* normally distributed, with all marginal variances equal to one, i.e. $\boldsymbol{\Sigma} = \boldsymbol{\Sigma}^{-1} = \mathbf{I}$. The probability density function of X (see Equation (2.4)) then reduces to:

$$\mathbf{x} \mapsto \frac{1}{(2\pi)^{p/2}} \exp \left[\frac{-\|\mathbf{x} - \boldsymbol{\mu}\|^2}{2} \right].$$

This is a *decreasing* function of the *distance between \mathbf{x} and $\boldsymbol{\mu}$* , and so its mode is obtained when this distance is minimal.

Because A is an affine subspace of \mathbb{R}^p , the distance between $\mathbf{x} \in A$ and $\boldsymbol{\mu}$ is minimal when \mathbf{x} is the *orthogonal projection* of $\boldsymbol{\mu}$ onto A , which is given by:

$$\tilde{\mathbf{x}}_A = \boldsymbol{\mu} + \frac{1 - \langle \boldsymbol{\mu}, \mathbf{r}_A \rangle}{\langle \mathbf{r}_A, \mathbf{r}_A \rangle} \mathbf{r}_A.$$

Step 2. The case of an arbitrary elementary normal distribution.

Let us drop the assumption that all marginal variances are equal to one. There exist $\lambda_1, \dots, \lambda_p \in \mathbb{R}_{>0}$ such that $\boldsymbol{\Sigma} = \boldsymbol{\Lambda} = \operatorname{diag}(\lambda_1, \dots, \lambda_p)$, and $\boldsymbol{\Lambda}^t = \operatorname{diag}(\lambda_1^t, \dots, \lambda_p^t)$ for any $t \in \mathbb{R}$. With $t = -\frac{1}{2}$, we find that $\boldsymbol{\Lambda}^{-\frac{1}{2}} \mathbf{X}$ is elementary normally distributed, with mean $\boldsymbol{\Lambda}^{-\frac{1}{2}}$ and unit covariance matrix (Theorem 2.1.6). Applying the same transformation $\boldsymbol{\Lambda}^{-\frac{1}{2}}$ to A yields a new plane, which has pillar $\boldsymbol{\Lambda}^{\frac{1}{2}} \mathbf{r}_A$ (not $\boldsymbol{\Lambda}^{-\frac{1}{2}} \mathbf{r}_A$!):

For each $\mathbf{x} \in \mathbb{R}^p$, we have

²We make this *DC approximation* more precise in Chapter 4.

³This process uses the so-called the *standardised form* of \mathbf{X} .

$$\mathbf{x} \in A \iff$$

$$\begin{aligned} \langle \mathbf{x}, \mathbf{r}_A \rangle = 1 &\iff \sum_{i=1}^p x_i r_{A,i} = 1 \iff \sum_{i=1}^p \lambda_i^{-\frac{1}{2}} x_i \lambda_i^{\frac{1}{2}} r_{A,i} = 1 \iff \\ \left\langle \Lambda^{-\frac{1}{2}} \mathbf{x}, \Lambda^{\frac{1}{2}} \mathbf{r}_A \right\rangle = 1 &\iff \left\langle \Lambda^{-\frac{1}{2}} \mathbf{x}, \mathbf{r}_{\Lambda^{-\frac{1}{2}}(A)} \right\rangle = 1 \\ &\iff \Lambda^{-\frac{1}{2}} \mathbf{x} \in \Lambda^{-\frac{1}{2}}(A). \end{aligned}$$

This means that the plane $\Lambda^{-\frac{1}{2}}(A)$ is defined by the pillar $\Lambda^{\frac{1}{2}} \mathbf{r}_A$.

We can now apply our earlier result, and we find:

$$\begin{aligned} \tilde{\mathbf{x}}_A &= \Lambda^{\frac{1}{2}} \overline{\left(\Lambda^{-\frac{1}{2}} \mathbf{x} \right)_{\Lambda^{-\frac{1}{2}}(A)}} = \Lambda^{\frac{1}{2}} \left(\Lambda^{-\frac{1}{2}} \boldsymbol{\mu} + \frac{1 - \langle \Lambda^{-\frac{1}{2}} \boldsymbol{\mu}, \Lambda^{\frac{1}{2}} \mathbf{r}_A \rangle}{\langle \Lambda^{\frac{1}{2}} \mathbf{r}_A, \Lambda^{\frac{1}{2}} \mathbf{r}_A \rangle} \Lambda^{\frac{1}{2}} \mathbf{r}_A \right) \\ &= \boldsymbol{\mu} + \frac{1 - \langle \Lambda^{-\frac{1}{2}} \boldsymbol{\mu}, \Lambda^{\frac{1}{2}} \mathbf{r}_A \rangle}{\langle \Lambda^{\frac{1}{2}} \mathbf{r}_A, \Lambda^{\frac{1}{2}} \mathbf{r}_A \rangle} \Lambda \mathbf{r}_A = \boldsymbol{\mu} + \frac{1 - \langle \boldsymbol{\mu}, \mathbf{r}_A \rangle}{\langle \Lambda \mathbf{r}_A, \mathbf{r}_A \rangle} \Lambda \mathbf{r}_A. \end{aligned}$$

Step 3. The general case.

Finally, we consider the general case where \mathbf{X} is normally distributed. If so, there exists orthogonal \mathbf{Q} such that $\boldsymbol{\Sigma} = \mathbf{Q} \boldsymbol{\Lambda} \mathbf{Q}^{-1}$, with $\boldsymbol{\Lambda}$ a diagonal matrix. In other words, the orthogonal map \mathbf{Q}^{-1} maps \mathbf{X} into an *elementary* normally distributed vector.⁴ Applying the same transformation \mathbf{Q}^{-1} to A yields a new plane, which is defined by the pillar $\mathbf{Q}^{-1} \mathbf{r}_A$. This derivation is more straightforward, since \mathbf{Q}^{-1} is orthogonal:

For each $\mathbf{x} \in \mathbb{R}^p$, we have

$$\mathbf{x} \in A \iff$$

$$\begin{aligned} \langle \mathbf{x}, \mathbf{r}_A \rangle = 1 &\iff \langle \mathbf{Q}^{-1} \mathbf{x}, \mathbf{Q}^{-1} \mathbf{r}_A \rangle = 1 \iff \langle \mathbf{Q}^{-1} \mathbf{x}, \mathbf{r}_{\mathbf{Q}^{-1}(A)} \rangle = 1 \\ &\iff \mathbf{Q}^{-1} \mathbf{x} \in \mathbf{Q}^{-1}(A). \end{aligned}$$

Using our previous result, we find:

$$\begin{aligned} \tilde{\mathbf{x}}_A &= \mathbf{Q} \overline{(\mathbf{Q}^{-1} \mathbf{x})_{\mathbf{Q}^{-1}(A)}} = \mathbf{Q} \left(\mathbf{Q}^{-1} \boldsymbol{\mu} + \frac{1 - \langle \mathbf{Q}^{-1} \boldsymbol{\mu}, \mathbf{Q}^{-1} \mathbf{r}_A \rangle}{\langle \boldsymbol{\Lambda} \mathbf{Q}^{-1} \mathbf{r}_A, \mathbf{Q}^{-1} \mathbf{r}_A \rangle} \boldsymbol{\Lambda} \mathbf{Q}^{-1} \mathbf{r}_A \right) \\ &= \boldsymbol{\mu} + \frac{1 - \langle \mathbf{Q}^{-1} \boldsymbol{\mu}, \mathbf{Q}^{-1} \mathbf{r}_A \rangle}{\langle \boldsymbol{\Lambda} \mathbf{Q}^{-1} \mathbf{r}_A, \mathbf{Q}^{-1} \mathbf{r}_A \rangle} \boldsymbol{\Lambda} \mathbf{Q}^{-1} \mathbf{r}_A = \boldsymbol{\mu} + \frac{1 - \langle \boldsymbol{\mu}, \mathbf{r}_A \rangle}{\langle \boldsymbol{\Lambda} \mathbf{Q}^{-1} \mathbf{r}_A, \mathbf{r}_A \rangle} \boldsymbol{\Lambda} \mathbf{Q}^{-1} \mathbf{r}_A \\ &= \boldsymbol{\mu} + \frac{1 - \langle \boldsymbol{\mu}, \mathbf{r}_A \rangle}{\langle \boldsymbol{\Sigma} \mathbf{r}_A, \mathbf{r}_A \rangle} \boldsymbol{\Sigma} \mathbf{r}_A. \end{aligned}$$



When we replace the *plane* A by a *half-space* B in Theorem 2.2.3, there are two cases to consider. If $\boldsymbol{\mu} \in B$, then $\tilde{\mathbf{x}}_B = \boldsymbol{\mu}$, because the mode of \mathbf{X} is $\boldsymbol{\mu}$, which is contained in B .

⁴ $\mathbf{Q}^{-1} \mathbf{X}$ is elementary normally distributed, but it does not necessarily have a unit covariance matrix.

In the non-trivial case of $\mu \notin B$, we find that $\tilde{\mathbf{x}}_B = \tilde{\mathbf{x}}_A$, where $A := \partial B$ is the *boundary* of B , which is a plane, given by the same pillar: $\mathbf{r}_A = \mathbf{r}_B$. A geometrical argument is as follows: by reducing to the case of an elementary normally distributed \mathbf{X} with a unit covariance matrix, the mode is the point of B that minimises the distance to μ . Since $\mu \notin B$, this point must lie on the boundary of B , i.e. $\tilde{\mathbf{x}}_B \in A$. Because A is a subset of B , we can proceed to compute $\tilde{\mathbf{x}}_A$, which is then necessarily the mode of $\mathbf{X} | B$.

For a half-plane B , we now have an explicit expression for $\tilde{\mathbf{x}}_B$, i.e. the *most likely value* of \mathbf{X} , given that $\mathbf{X} \in B$. What can we say about the *expected value* of $\mathbf{X} | B$? Geometrically, one can imagine that $\mathbb{E}[\mathbf{X} | \mathbf{X} \in B]$ lies close to $\tilde{\mathbf{x}}_B$, but ‘shifted inwards’, away from ∂B (in the direction of its pillar). We have not found a direct method to compute this expected value. Nesti et al. (2018a) introduce a scaling factor $\epsilon > 0$ to the covariance of \mathbf{X} (i.e. $\mathbf{X}_\epsilon \sim \mathcal{N}(\mu, \epsilon \Sigma)$), and show that the expected value *converges* to $\tilde{\mathbf{x}}_B$, the mode,⁵ as $\epsilon \rightarrow 0$, using the tools of Large Deviations Theory.

One can interpret this result as saying that the probability density of $\mathbf{X}_\epsilon | B$ gets *concentrated close to the boundary of B* . In the one-dimensional case, this statement⁶ is easy to demonstrate, see e.g. Touchette (2009).

⁵The factor ϵ disappears in (2.5).

⁶i.e. the *tail distribution* of $X \sim \mathcal{N}(0, \epsilon^2)$, given $X \geq 1$, becomes *steeper* as $\epsilon \rightarrow 0$.

Chapter three

The Electric Grid



This chapter is based on two books: Electric Power Systems by von Meier (2006), which provides a clear summary of the working and operation of electric grids, and Electric Power Principles: Sources, Conversion, Distribution and Use by Kirtley (2010), a more quantitative approach to the subject.

3.1 Overview

The electric grids of this world are some of the largest machines built by humans. As this system was built by clever engineers, its behaviour is, on a small scale (individual lines, transformers, and so on) *well-understood*. In fact, one of the reasons that all transmission lines, substations and switchboxes look so similar, is to increase the *homogeneity* of the network.

On a larger scale, however, the behaviour of this machine is not always well understood, as complex behaviour arises from the interconnection of generators, transmission lines and loads. When the transmission network fails, the consequences can be dramatic. For example, filtering and supply of drinking water, telecommunication and heating all rely on a functioning power grid. The large scale of a transmission network makes it more stable, but it also increases the potential effect of its failure. The two largest blackouts (at the time of writing) occurred in north-eastern India on 30 and 31 July, 2012, affecting 400 million and 620 million people, respectively. These blackouts were due to a peak in consumption caused by extreme heat and drought.¹

3.2 Generators

Almost all sources of electric power in the electric grid use an *AC generator* to convert (rotational) kinetic energy to electric energy.² At a hydroelectric plant, the weight of water applies direct torque to the water pumps, mechanically connected to the generator

¹Air-conditioning and irrigation pumps increased consumption; hydroelectric generation was limited.

²A notable exception is the photovoltaic cell (PV cell) used in solar panels. PV cells produce a direct current, which is converted to AC power at nominal voltage using an *inverter*. Solar inverters are often complicated systems, capable of using battery storage, synchronising with the AC grid and varying PV operating voltage to maximise PV efficiency.

shaft.³ At most other types of plants (including coal-fired and nuclear plants), generators are powered by steam pressure.

The term *AC generator* denotes a specific device that uses *electromagnetic induction* to convert rotational kinetic energy into AC power. Somewhat confusingly, we use the term *generator* to denote *any* energy source connected to the grid, where we consider a power plant (which might house multiple AC generators) as a single generator. Solar parks and lithium batteries are generators, but they do not use an AC generator. They use an AC inverter, which *mimics*, to some extent, the behaviour of a classical AC generator.

3.3 Loads

Unlike other utilities like gas and water, the transfer of electrical energy is *instantaneous*.⁴ Of course, energy storage does exist,⁵ but this energy is not stored as ‘high-voltage AC energy’, but as *potential* (mechanical or chemical) energy. Potential energy needs to be converted before it can be transmitted, which is not instantaneous. When switching on your lights, there will be an *instant* increase in demand, which must be generated somewhere (otherwise it would violate the Law of Conservation of Energy). Of course, via the electric grid, your light bulb is connected to generators, which then start converting an additional 10 W to power the light bulb. But how do the generators know when to increase their output, if you never called them to say that you are turning on your lights?

The answer is called *electric inertia*. A classic AC generator (in a hydroelectric plant, for example) contains a heavy rotor, which is spinning at (a rational fraction of) the grid frequency. Because of its weight, a lot of energy is stored in the spinning of the rotor. When the total load on an AC network is increased, there is no instantaneous increase in burning of fuel, flowing of water, or otherwise. Instead, this increase in power demand will ‘take’ its energy from the *inertial energy* of all rotational AC generators in the grid, *slowing down* their rotation. As a result, the AC frequency of the entire grid starts slowing down. When grid operators notice a drop in AC frequency (we are talking about differences on the order of 0.001 Hz here), they can increase the amount of fuel being burned, open water valves or lift control rods from between radioactive cores to increase the amount of energy converted by the AC generator. This will start to increase the AC frequency again, until it settles at the predetermined utility frequency (60 Hz in North America and Northern South America; 50 Hz in the rest of the world, with some exceptions). Most modern AC generators have an automatic feedback loop to control the steam valve, to allow for frequency adjustments on the smallest scale.

³Some hydroelectric plants are *reversible*: their generators can be used as electric motors, pumping water back up into a reservoir. This is a form of large-scale *energy storage*, which can increase the usability of intermittent renewable energy sources.

⁴Within the limits of special relativity, of course. That is, while the drift speed electrons is nowhere near the speed of light, the actual *signal* propagates at about two thirds the speed of light, depending on the type of cable.

⁵Most commonly as *reversible* hydro-electric generators; other examples include hydrogen storage (electrolysis of water produces hydrogen and oxygen, which can be stored and combusted at a later time) and lithium storage (very large phone batteries) (some electric vehicles can also return energy back to grid!)

3.4 Transmission

The voltage of AC power can be shifted up and down using transformers. We typically use higher voltages for long-range transmission, since high-voltage AC is much more efficient (less power is lost in heating the transmission lines). This is why high-voltage lines can afford to have relatively thin wires, given the amount of power that they transmit. The network of high-voltage lines (which operate at voltages on the order of 100 kV) is called the *transmission network*. Transmission lines usually run interrupted for long distances (on the order of kilometres) between two *substations*. At these endpoints, transformers connect the high-voltage transmission lines to medium-voltage (on the order of 10 kV) *distribution lines*, which eventually make it to all generators and consumers in the area that the substation serves.

3.4.1 Three-phase transmission

Depending on where you live, your wall socket will likely have *two* connectors. Most modern sockets also have a third connector, the *ground wire*, but this third connector does not have the purpose of carrying a current, like the other two (under normal circumstances).

This makes sense, since most electrical devices only need a *potential difference* (between *two* wires) to function. In the early days of transmission systems, however, this caused a problem for factories using AC motors to power their production line. When a (single-phase) AC current is used to power a motor, the amount of *torque*⁶ is not constant: when the potential difference is zero, which happens twice every 1/50th of a second, no electric field is present in the armature windings, and no torque is applied to the rotor.

To solve this problem, both the AC generator and AC motor are equipped with *three* identical sets of armature windings, each oriented 120° relative to the others. One end of each winding is connected to the common ground, and the remaining three connection points form the *three-phase connection* between generator and motor.⁷

As the generator rotor is moving, there will always be one armature winding which is close⁸ to being perpendicular to the rotor windings, and will therefore have a relatively high induced current.

In fact, when writing down the three currents in exact form (three sinusoids with the same frequency and magnitude, with phases 0°, 120° and 240°), we find that *the sum of their squares*, i.e. the total amount of transmitted power, is *constant*! Although the amount of power transmitted on just one of the phases (square of the sinusoid current) is not constant, the combination of the three is. This means that the torque of a motor, which is the sum of torques applied by each armature winding, is constant.

Figure 3.1a shows one cycle of single-phase, two-phase and three-phase current, and the

⁶i.e. rotational force. In most systems, torque is proportional to *change in rotational velocity* (change in rpm).

⁷This method of connecting three coils (or more generally, impedances) to three-phase AC is called the *Wye configuration*. Another method is to connect the impedances between each pair of two phases, with no common ground connection. This method, called the *Delta configuration*, is described in more detail in von Meier (2006).

⁸within 30°

total amount of power transmitted by the phases. Here we see that the total amount of power is constant when more than one phase is used. So why not use two phases, instead of three?

Because electricity needs to flow in a *closed circuit*, each phase needs *two wires* to transmit its power; this second wire is called the *return wire*. When we have more than one phase, their circuits are distinct, and we can combine their return wires into a single return wire for all phases.⁹ This means that one-phase, two-phase and three-phase transmission requires two, three and four wires, respectively: one additional wire is the common return wire.

This return current is generally greater than each of the individual phase currents (see Figure 3.1a). However, when three-phase transmission is used with relative phase angles 0° , 120° and 240° , the return current is zero. This means that the return wire can be thinner (i.e. cheaper), or it can be omitted completely.¹⁰ It is for these two reasons (constant power and no return current) that three-phase AC is used almost everywhere.

When looking at AC transmission systems, you will often find three identical copies of the same component. For example, high-voltage AC transmission lines always have three, six or nine wires, which are identical in material, thickness and length.

Single-line approximation

There are a number of reasons to build transmission systems this way. One benefit of having three copies of the exact same network is that they will behave the same way, saving grid operators up to two thirds of potential headaches!

As a result, it is very common to model the grid as a single-line network (with a global, zero-impedance ground). Because of the homogeneity of the transmission system, there are only some special cases where considering the three phases separately is necessary. See Kirtley (2010) for a more detailed account.

3.4.2 Line failures

When a transmission line stops transmitting power, we speak of a *line failure*. In most cases, a line failure is not caused by a broken or molten wire, but by a disconnection at one of its ends, as a safety measure. Some line failures are caused by a *fault*, or *power surge* a sudden abnormal peak in current, caused by anomalies like fallen trees or lightning strikes. A high current is detected by *circuit breakers*, which then automatically breaks its connection. A household fuse is an example of a circuit breaker, although modern circuit breakers use a mechanical switch. (These can be reset, instead of requiring a replacement fuse.) In high-voltage systems, circuit breakers can be quite advanced, sometimes using pressurised gas or oil to prevent arcing inside the switch.

Another type of line failure, the one most relevant to this thesis, is an *overload*. All transmission lines have a *thermal limit*: a maximum current that the line can sustain

⁹using the Wye configuration described previously

¹⁰In high-voltage transmission lines, one can often see a fourth (or seventh, or tenth), thinner wire: this is the return wire. This wire accounts for small imbalances in the load connected to each phase, which cause a non-zero return current. In some (older) medium-voltage lines, there is no return wire. In this case, the Delta configuration is often used: loads are connected to two of the three phases.

without risking overheating, causing sagging or even melting of transmission cables. To prevent these dangerous scenarios, transmission lines automatically disconnect when the current exceeds the predetermined *line threshold*.

It is important to note that grid operators cannot control the amount of current - and therefore - power that flows through a transmission line: grid operators can only connect or disconnect the line from the grid. The impedance of a wire does not act as a *bottleneck* (like a small-diameter pipe would do in an irrigation network). From Ohm's law ($ZI = V$), one could mistakenly conclude that the amount of current passing through a transmission line is inversely proportional to its resistance. However, the electric potential (V) in this equation is *not* the potential between the wire and the ground (e.g. 220 kV), but rather the potential difference between the two ends of the wire (which is not zero!). This difference (known as *line drop*) is quite low, compared to the potential between one of the ends and the ground (220 kV transmission lines usually have a 1% line drop). The amount of current carried by a wire is dominated by the current being 'generated' and 'used' at its ends.

3.5 Grid security

Historically, failures of transmission network have had dramatic effects. The effects of such outages are even visible from space, since almost every light source depends on a functioning transmission network.

Power outages can also be dangerous to human health. During the two-day blackout of Ontario and eight North-Eastern US states in 2003, almost 100 deaths were attributed to unavailable emergency services, stress, increased air pollution and the use of candles and backup generators.

When the first power grids were built, grid security was ensured by *redundancy*. Transmission lines were designed to carry currents much greater than predicted. One of the criteria for building a network was *N-1 redundancy*: the network should remain operational after the failure of *any* line. In graph theory, this is equivalent to building a 2-edge-connected graph.

Nowadays, the capacity of power grids is being pushed to its limits. The main reason is that it is *economically beneficial* to do so: most electricity networks have become *privatised* since they were built, and are being used and upgraded in a way that minimises costs. A second reason is an increase in renewable generation, which requires the grid to be used in a way different from its design. This has led to "more situations in which transmission lines are loaded close to their thermal limits." (Ronellenfitsch et al., 2017)

There are many mechanisms in place that ensure grid security. For example, a grid operator has a *load shedding scheme*: a predefined order of loads that will be cut off from the network when needed. The most important tool to maintain grid security is *load profiling* (i.e. predicting future load), combined with control over generation: the grid operator gets the final say in deciding which generators will be used at what time. We will discuss this decision-making process in Section 3.6.

Given the net amount of power injected at each node of the transmission network, the current that will flow through each line is determined by physics. We use a *Power Flow* (PF) algorithm to calculate these currents, which we can use to check whether no line

current exceeds its threshold. We will study the Power Flow equations in Chapter 4.

3.5.1 Power islanding

Because nodes often house both loads and generators, the disconnection of a single node, or of a subset of nodes, does not always lead to a power outage, since local power generation might be sufficient to serve the load. This situation, where a subsection of the transmission network still operates after being disconnected, is called a *power island*.

Since the power island and the remaining network have been operating independently of each other, it is likely that their AC phase angles no longer line up.¹¹ Unless this phase drift is corrected for (by temporarily increasing or decreasing the AC frequency on either side), the power island cannot be reconnected, since this phase drift likely exceeds the power angle limit of a new transmission line.

3.6 The energy market

Modern power grids play the role of a competitive economic market. There are many possible ways to supply everyone with power, because there is more *installed capacity* than there is demand. As a result, generation shares are largely determined by *bidding*. Different generation technologies (gas, wind, etc.) form a *stacking order*: in general, wind energy will always be cheaper than coal. Yet, it is not uncommon for renewable, cheap energy sources to be *curtailed*, in favour of more expensive, possibly non-renewable energy sources. One of the reasons for grid operators to do so, is to protect vulnerable lines from overloading.

In this section, we will describe a very simplified version of the energy market, to illustrate how grid operators ensure grid security while minimising costs.

Every hour, all parties involved in the generation and transmission of power come together, to decide *what the configuration during the following hour will be*. For the sake of simplicity, we will assume that each power plant (renewable or non-renewable) is owned by its own company, and that the entire transmission network is owned by a single grid operator.

Phase one: offering prices

First, all generators offer to supply energy during the coming hour *for a certain price per kWh*. Generally, company A, which owns a wind farm, will offer their energy for a lower price than company B, which owns a coal plant. The price offered by company A is lower because a wind farm has zero *marginal cost* - the cost of generating an additional unit of electricity, once the turbine has been built. No fuel or labour is needed to generate power using a wind turbine, it simply needs to not be turned off.

Besides marginal cost, there are two more factors that influence the offered price:

¹¹This misalignment likely occurs right after the disconnection, when the total generation in the power island is substantially higher or lower than the total load. Until this mismatch has settled, the AC frequency will be higher or lower, respectively, than the target frequency (say, 50 Hz).

- Company A needs to pay back their initial investment, which increases the offered price.
- Government subsidies, which promote the use of low-carbon energy, reduce the offered price.

In general, one can assume that the price offered for renewable energy is close to zero. In some cases, the subsidies are greater than all other costs, and energy is offered for a *negative price*. This has the counter-intuitive effect that a grid operator actually *earns money* by buying electricity from that company.

Energy from company B is generally more expensive, since it has a marginal cost (price of coal, labour wages, and so on), on top of paying back the investment.¹²

Besides offering their marginal price, generators will also state their *generation capacity*.¹³ For some generators, this will always be the same amount. For a solar park, however, this capacity varies drastically, and needs to be estimated.

Marginal emissions

The *environmental cost* of a generator is mostly dependent on its energy source. In the context of global warming, we are interested in the amount of *radiative forcing caused by greenhouse gases* that are emitted to generate energy, which is usually expressed as *equivalent kilograms of CO₂*. Just like the financial cost, we usually speak of the *marginal emission* of a certain generator: kgCO₂eq/kWh. See IPCC (2014) for a summary of marginal emissions of each energy source.

Phase two: grid operator

Now that all generators have offered a price, the grid operator needs to decide where to buy its energy from. Grid operators have a fairly good estimate for the load (energy demand) during the coming hour, based on the current load, historical load series, weather forecasts, sporting events, television programme schedules, and so on. Such a model is called a *load profile*.

By design, the total generation capacity is much greater than the expected load,¹⁴ so running every generator at full capacity would be problematic. As a grid operator, we need to tell each generator at what percentage of their capacity they should operate.

A complete set of generator instructions, called a *configuration*, might look something like Table 3.1. Note that generators could be told to operate at 0% of their capacity, which is equivalent to powering off the generator completely.

¹²In some cases, coal plants offer their electricity for a lower, or even negative, price, to avoid power off the plant. With the exception of open-cycle gas turbines, turning on non-renewable energy plants is expensive, and might take several hours. It might be cheaper for company B to offer their energy for free for one hour than to turn off the plant.

¹³This use of the word *capacity* is entirely different from the *capacity* of a capacitor, used in electrical engineering.

¹⁴to account for so-called *incident load*: the maximum amount of expected load. This amount is only likely to occur after a short blackout, when all consumer devices turn on simultaneously, and start cooling fridges and heating houses.

15 March 2019, 11:00-12:00		
generator	offered price	requested output
Sally's Solar Park	4 €/MWh	115 MW / 115 MW
Chris's Coal Plant	122 €/MWh	0 MW / 240 MW
Nellie's Nuclear Plant	45 €/MWh	1387 MW / 2500 MW
Steven's Solar Park	-2 €/MWh	23 MW / 23 MW
:	:	:

Table 3.1: A small section of a fictional configuration.

Some configurations are more expensive than others, and some will result in more greenhouse gas emissions than others. Perhaps surprisingly, most configurations are not even *admissible*: using them would cause some transmission lines to be overloaded, which could even result in a blackout.

More precisely, a configuration is called *ready to deploy* if it satisfies the following three conditions:

possible: For each generator, the power output dictated by a configuration must be a non-negative number, no greater than the maximum capacity of the generator.

balanced: When the dictated configuration is applied, total generation must equal total load, together with line losses.¹⁵

admissible: When the dictated configuration is applied, no line should be overloaded.

To determine whether a configuration is *admissible*, the grid operator can simply *calculate the line flows* that would be induced by that configuration, using a Power Flow (PF) algorithm, and check for any overloaded lines. Because power flow physics are quite well-understood, these results are accurate.

3.6.1 Optimum Power Flow

We can easily find a configuration that is both possible and balanced. First, set all generators to maximum capacity. We now have a *possible* configuration. By design, the total generation of this configuration is much greater than the total load. By scaling the output of all generators with the same factor $0 \leq \lambda \leq 1$, the configuration remains *possible*, and by the intermediate value theorem, a λ exists such that the configuration is *balanced*.

¹⁵Of course, the total load is not perfectly constant for one hour. To accommodate for this, the grid operator designates a single *load following* generator, which will vary its output continually to make sure that the total demand is met exactly. (This is equivalent to maintaining a constant AC frequency!) The bus that this generator is connected to is called the *slack bus* of the transmission network.

When trying out different *possible*, *balanced* configurations randomly, we will find that almost all of them are inadmissible; the subset of admissible configurations is actually quite small, and finding *any* ready-to-deploy configuration is a lot of work.

Once a ready-to-deploy configuration has been found, the grid operator now wants to minimise economic and environmental cost. Given this initial configuration, the associated cost can be calculated, since all generators have offered their price, and their environmental impacts are known. This ready-to-deploy configuration is not unique, and by varying the configuration only slightly, the configuration remains ready to deploy.¹⁶ By doing so, we might be able to reduce the (environmental) cost! By repeating this process, a local minimum can be found.

The problem of

*finding a ready-to-deploy configuration
that minimises the associated cost*

is called the *Optimum Power Flow (OPF)* problem.

Even with modern-day computers, solving this problem is a difficult task indeed, and is often simplified by making a slight modification to our process. Instead of using the Power Flow (PF) algorithm to check a configuration's admissibility, we use the so-called *Linearised Power Flow (LPF)* algorithm to check linear admissibility. This linearised version can be computed much more quickly, with only a small loss in accuracy. We will derive the equations describing these two algorithms in Chapter 4, and compare their results.

With our slight modification, we restate our problem as:

minimise *associated cost*
subject to *possibility*
and *balance*
and *linear admissibility*

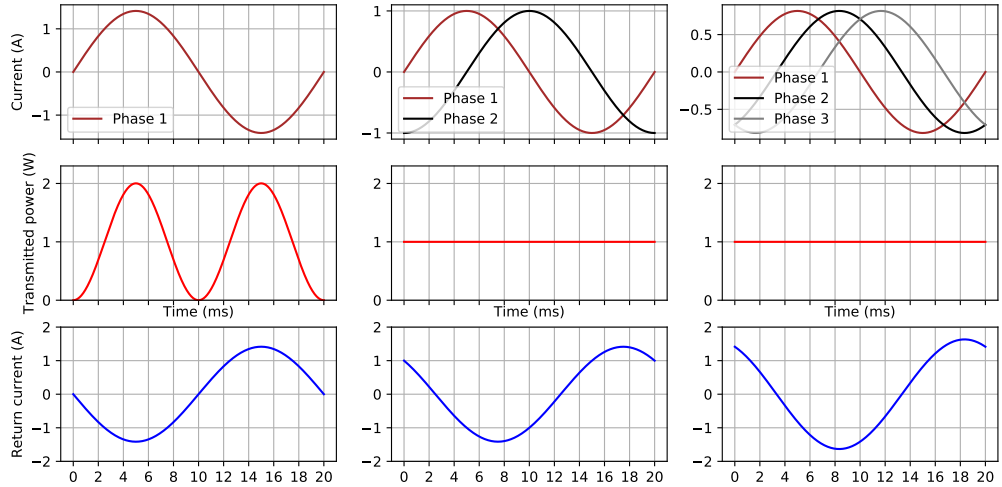
which is known as the *Linear Optimum Power Flow (LOPF)* problem. As suggested by the notation, this optimisation problem falls in the more general class of problems solvable using *linear programming*. First studied by Fourier in 1827, the field has seen many developments, most notably the *simplex* solution method developed by G. Dantzig in 1947.¹⁷ Nowadays, several high-performance linear programming solvers have been created, including the open source GNU Linear Programming Kit, which was used in this project.

Using the LPF algorithm introduces a small error. For this reason, the *admissibility* bounds are often scaled down by a contingency factor,¹⁸ creating a margin of error for line flows.

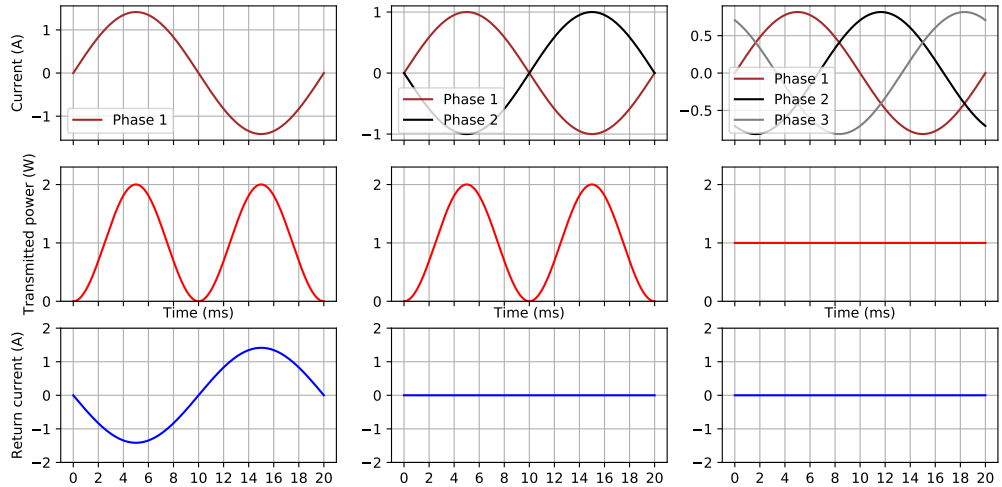
¹⁶As we will later learn, the function that maps a configuration to the vector of line flows that it induces is *continuous*. The set of vectors where each line flow is < 100% is an *open* box, and so its inverse image (the set of configurations that are ready to deploy) is also open.

¹⁷For the *simplex method*, see Matoušek and Gärtner (2007).

¹⁸A contingency factor of 0.7 is common.



(a) Phases distributed along half a cycle.



(b) Phases distributed along a full cycle.

Figure 3.1: Simulation of line current and transmitted power for one-phase, two-phase and three-phase transmission. The circuit consists of one, two or three identical resistors (1Ω), connected using the Wye configuration. Line voltage is chosen to produce a fixed amount of power (1 W).

Chapter four

Modelling Transmission Networks

In this chapter we will derive the *Linear Power Flow* (LPF) transformation: a linear map from the vector of power injections at the buses to the vector of currents flowing through the lines of the network.

It is a *right inverse* of K , which means that applying LPF to a power injection gives a flow that would induce that injection. There are many possible candidates for a right inverse. For example, one way to construct one is to fix a minimum spanning tree; when we set line currents outside of the tree to zero, all line currents inside the tree are uniquely determined.

Yet, only one right inverse is *physically correct*: the LPF. This function can be derived explicitly by constructing an electric circuit that represents the whole transmission network and everything connected to it, and applying Ohm's Law and Kirchoff's Laws to relate line currents to power injections. We linearise the resulting *node flow equations* to find the LPF matrix (page 43).

Using this linear map, we can transform the normal distribution of stochastic injections to a Gaussian distribution of line flows. Using the results of Chapter 2, we can estimate the overload probability of each line, resulting in a ranking of most vulnerable lines. Additionally, for each such line, we compute the most probable injection to cause the failure, and simulate the subsequent *cascading failures*.

4.1 The model

The LPF is essentially the *high-level model* used in the final chapters of this thesis (i.e. the transmission network is modelled as a linear transformation). In this chapter, we derive a closed-form expression for the LPF from a lower-level, *electrical* model. This derivation is based on the basic principles of *AC circuit theory*, which extends the more familiar concepts of DC circuits (consisting of constant voltage and current sources and resistors) to circuits with time-varying (often sinusoidal) voltage and current sources. (This is where *inductors* and *capacitors* come into play.)

Electric Power Systems by von Meier (2006) provides a very readable introduction into these subjects. Chapter 1 is an introduction to the physics of *electricity*; Chapter 2 introduces *DC circuit theory*; Chapter 3 concerns *AC circuit theory*, specifically in the context of AC power transmission.

For a fascinating, rigorous mathematical introduction into the subject, see *Mathematical*

ical Foundations of Network Analysis by Slepian (1968) or *Circuits, Matrices and Linear Vector Spaces* by Huelsman (2011).

4.1.1 Electrical model

We make a distinction between the *structure* and the *state* of the network. The structure is a directed graph, where each line is given an *admittance*. The state collects the (real and reactive) power injected at each bus, the (complex) voltage of each bus, and the (complex) current flowing through each line.

The use of complex-valued voltage and current (and therefore power) is essential when analysing AC circuits, even though we are only interested in *real* power. For example, we will find that the amount of real power transmitted over a line is approximately inversely proportional to the inductance of the line (the *imaginary* equivalent of resistance), and approximately proportional to the difference in phase angles at its ends (the *complex argument* of voltage).

4.1.2 Time invariance

The grid structure remains unchanged during normal operation, while the grid state is continually changing over time. For example, an important aspect of grid operation is *load profiling*: examining and predicting the total load connected to a node, as a function of time. As a result of changing loads, the flow of power in a grid is constantly changing.

One example of a change in grid structure is a *line failure*, which can be modelled as the removal of an edge from the graph. In some cases, the removal of an edge from the graph results in an unconnected graph (i.e. there exist two nodes with no sequence of lines connecting them). This scenario is called *power islanding*. Most transmission networks are designed in such a way that no single (or double) line failure can cause power islanding or a blackout, by increasing the *edge-connectivity* of the graph.

In the case of a *line overload*, however, a line failure is caused by an exceptionally high power flow, as a result of high supply or demand.¹ The failure of an overloaded line will cause a redistribution of power flow, since the power flowing through the failed line now needs to 'find another path' between the nodes. In a highly stressed network, this redistribution can cause a second failure, which can then cause a third failure, and so on, which can eventually cause a blackout. We will study these *cascading failures* in Section 4.10.

4.2 Grid structure

A transmission grid is modelled as a directed graph $(\mathcal{N}, \mathcal{L})$. As vertices we take the *nodes* of the network, which are those points where transmission lines connect to a generator, load, or to each other. Nodes are electrically distinct, in the sense that there is some

¹These high power injections are not necessarily located at the two endpoints of an overloaded line; it could also be a grid-wide pattern of power injections, all adding up to a high power flow on that line. We will study the *most likely power injection* in Section 4.9.3.

non-zero impedance between them, allowing them to sustain a potential difference. In a network of n nodes, they are represented by the natural numbers $1, \dots, n$, i.e. $\mathcal{N} = [n]$.

A pair of two distinct nodes (i, j) is contained in our set of lines \mathcal{L} if there is a transmission line connecting the nodes. The choice of line orientation can be arbitrary, as long as we have $(i, j) \in \mathcal{L} \Rightarrow (j, i) \notin \mathcal{L}$ for all lines $(i, j) \in \mathcal{L}$. This transmission line has non-zero impedance. (Otherwise i and j would be the same node.) In a network of m lines, lines are labelled $\mathcal{L}_1, \dots, \mathcal{L}_m$.

In literature on the subject, buses² are also called *vertices* or *nodes*, and lines can be called *edges*, *wires*, *cables* or *circuits*.

We model transmission lines as time-invariant impedances, which are assumed to be constant under any electric potential and current, allowing us to apply Ohm's Law. Instead of the impedance Z of a line, we use its *admittance* $Y = 1/Z \in \mathbb{C}$,³ and Ohm's Law becomes:

$$I = VY$$

This allows us to define the admittance between two unconnected nodes as 0. (i.e. no current is induced by a potential difference.) We define $\eta \in \mathbb{C}^m$ as the *admittance vector*, where η_l is the admittance of \mathcal{L}_l , for each $l \in [m]$.

Definition 4.2.1. To summarise, an (n, m) -grid structure is defined as a tuple $((\mathcal{N}, \mathcal{L}), \mathbf{K}, \boldsymbol{\eta})$, where:

- $n = \#\mathcal{N}$ is the number of nodes;
- $m = \#\mathcal{L}$ is the number of lines;
- $(\mathcal{N}, \mathcal{L})$ is a connected directed graph with $\mathcal{N} = [n]$;
- $\mathbf{K} \in \mathbb{R}^{n \times m}$ is the vertex-edge incidence matrix of $(\mathcal{N}, \mathcal{L})$;
- $\boldsymbol{\eta} \in \mathbb{C}^m$ is the line admittance vector.

4.3 Power grid state

The *state* of the network describes how the transmission network is being used (the (real and reactive) power injected at each node, and the voltage magnitudes) and how the electric circuit responds (voltage angles and (complex) line currents). More precisely, we use three physical quantities used in AC circuit analysis to describe the grid state:

Definition 4.3.1. A *grid state* of an (n, m) -grid structure is defined as a tuple $(\mathbf{S}, \mathbf{V}, \mathbf{I})$, where

- $\mathbf{S} \in \mathbb{C}^n$ is the *complex power injection vector*;
- $\mathbf{V} \in \mathbb{C}^n$ is the *bus voltage vector*;
- $\mathbf{I} \in \mathbb{C}^m$ is the *line current vector*. (Currents are directed along digraph edges.)

²'bus' is short for 'busbar': the latin 'omnibus' in conjunction with 'bar': some high-voltage cables are connected by welding them to a heavy metal bar.

³Written in Cartesian form, $Y = G + iB$, where G is the conductance, and B the susceptance of a line. Both have unit siemens (S), or mho (the reverse of 'ohm'), defined as $1 S = 1 \Omega^{-1}$.

4.4 State validity

Given an (n, m) -grid structure $((\mathcal{N}, \mathcal{L}), \mathbf{K}, \boldsymbol{\eta})$, only some states are physically possible. A state that satisfies Kirchoff's Laws and Ohm's Law will be called *valid*. Of course, since we are studying a real-world system, we are mainly interested in states that are valid, or at least close to being valid (in the sense of *DC-valid*, see Section 4.6).

4.4.1 Circuit representation

An (n, m) -grid structure $((\mathcal{N}, \mathcal{L}), \mathbf{K}, \boldsymbol{\eta})$ represents an electrical circuit, consisting of impedances and AC sources. A *valid* grid state $(\mathbf{S}, \mathbf{V}, \mathbf{I})$ corresponds to a physical state of the circuit. From the mathematical structure, we will construct the corresponding electric circuit in two layers, as follows:

In the first layer, each node i in \mathcal{N} becomes a node in the circuit. The value of V_i is the electric potential of that node, relative to ground.

A line $\mathcal{L}_k = (i, j)$ is modelled as an impedance element⁴ (—□—) with admittance η_k between the two nodes i and j . The value of I_k is the current flowing through the impedance from i to j .

See Figure 4.1 for the first constructed layer. This is not the final circuit: we have not yet added generators and loads to the circuit! Also, the transmission lines have no return wire. This means that there is no closed loop between two nodes, and therefore no energy can be transmitted.

To construct the second layer, we add a new component to each node $i \in \mathcal{N}$, which can be seen as the collection of AC sources (generators) and impedances (loads), connected in parallel between the node and ground. The exact way that loads and generators are connected to the node is not important,⁵ so we will simply state that this component:

- sustains a potential difference (which is V_i);⁶
- either supplies or draws a current, such that the amount of power generated or consumed by the component equals S_i (when S_i is positive or negative, respectively).

We will call this aggregation of generators and loads a *power injector* (—○—).

Each power injector is connected to a node on one end, and to a ground terminal on the other. In electric circuit theory, a ground terminal represents a direct connection to a universal ground: the 'zero' reference of electric potential. One could say that between

⁴complex-valued resistor

⁵This would be a circuit comprising the medium and low-voltage networks connected to the node, including every generator, fridge and phone charger that it serves. This is a common (and necessary) abstraction in power grid analysis.

⁶In physical systems, the *operating voltage* $|V_i|$ (remember that \mathbf{V} is complex) can be controlled by power plant operators by adjusting excitation current of a generator. The *phase angle* $\theta_j = \text{Arg}(V_j)$ can be controlled by adjusting the amount of energy (steam) supplied to a generator.

Both methods are an indirect form of control, which also affects all other nodes in the network. In fact, *maintaining* a constant operating voltage and phase angle is a complicated task, requiring continuous adjustments to generator operation. Section 4.3 of von Meier (2006) covers this topic in more detail.

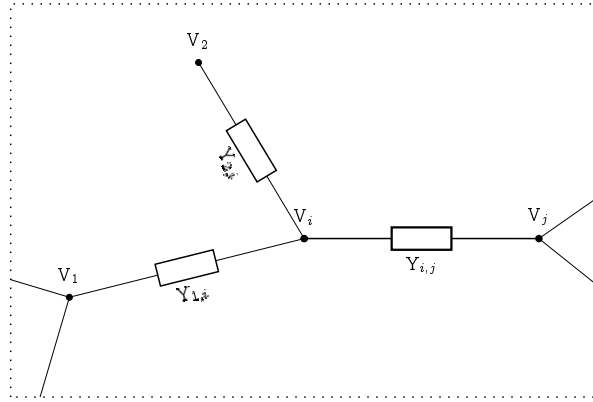


Figure 4.1: A section of a transmission network, showing the line (i, j) . Two more nodes, both connected to i , are also shown. Note that this is only one layer of the electric circuit used in the model. In the full model (Figure 4.2), each transmission line forms a closed circuit, allowing current to flow.

two different ground terminals, there exists a zero-impedance link connecting the two. We now have a simple closed circuit between any two nodes connected by a transmission line, consisting of a power injector for the first node, an impedance between the two nodes, a power injector for the second node and a ground link back to the first node.

This zero-impedance ‘ground link’ does not physically exist. Rather, it represents the ground wire of a three-phase transmission line. Because there is no return current and no electric potential across the return wire (see Section 3.4.1), we can set its impedance to zero. Another interpretation is that the single high-voltage line *represents the whole physical circuit* of three high-voltage wires and one return wire.

The complete, two-layer model is shown in Figure 4.2.

4.4.2 Kirchoff’s Voltage Law (KVL) & Ohm’s Law

For each line $\mathcal{L}_k = (i, j)$, we can apply Kirchoff’s Voltage Law to the loop “ground $\rightarrow i \rightarrow j \rightarrow$ ground”, as shown in Figure 4.2. This gives us:

$$V_i + \Delta V_k - V_j = 0,$$

where ΔV_k is the electric potential of the line impedance. This potential relates to the line current according to Ohm’s Law:

$$I_k = \Delta V_k \cdot \eta_k = (V_j - V_i) \cdot \eta_k.$$

Since the k th column of \mathbf{K} (which corresponds to the line $\mathcal{L}_k = (i, j)$) has exactly two non-zero entries: $K_{i,k} = 1$ and $K_{j,k} = -1$, we can write:

$$I_k = (V_j - V_i) \cdot \eta_k = -(K^* V)_k \eta_k.$$

This holds for every $k \in [m]$, and this system of equations can be written compactly as:

$$\mathbf{I} = i \operatorname{diag}(i\boldsymbol{\eta}) \mathbf{K}^* \mathbf{V}$$

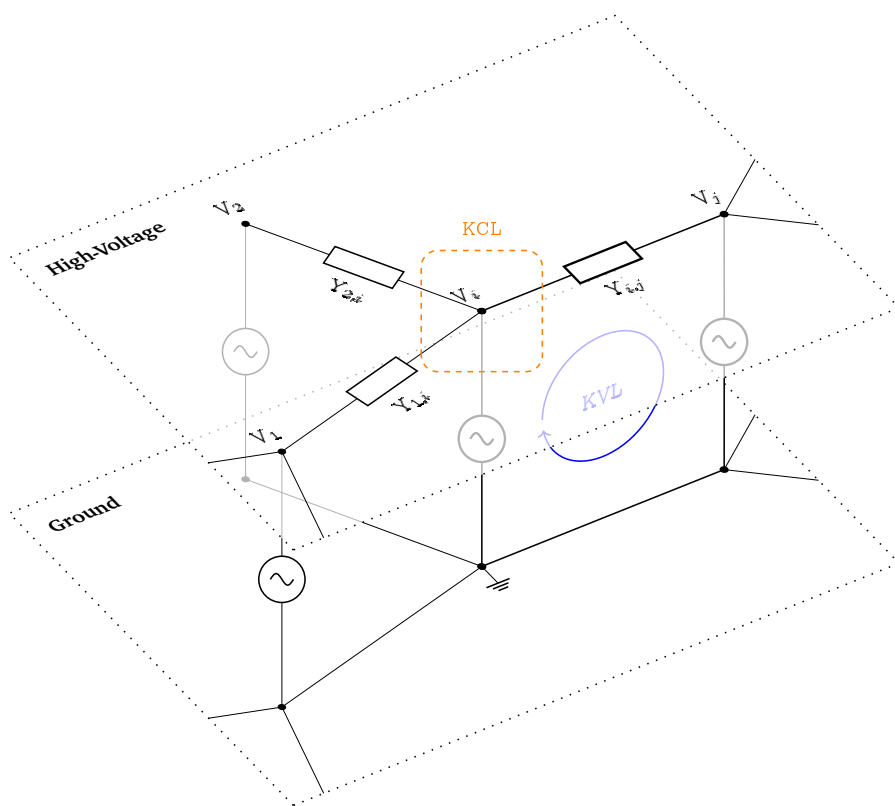


Figure 4.2: The electric model of the transmission network, showing the line (i, j) and two other nodes. A node is represented by a single component ($\textcircled{?}$), which is the aggregation of all generators and loads connected to that node. A transmission line is modelled as an impedance (\square), a complex-valued resistor. The ground 'wires' have zero resistance.

KVL is applied to each line, by traversing the loop drawn in blue.

KCL is applied to each node, by summing all currents entering and leaving the orange area.

Written in this form, we see that when $i\eta$, \mathbf{C} and \mathbf{V} are purely real, then \mathbf{I} is purely imaginary. Physically, this means that line current is always 90° out of phase with voltage differences. When phase angles are small, and voltage magnitude is constant, then the voltages ‘point roughly to the right’ in the complex plane. Therefore, their *differences* are almost purely imaginary.

4.4.3 Kirchoff’s Current Law (KCL)

Using KVL and Ohm’s Law, we found a relation between line current and node voltages. We can use KCL to relate the power injection to currents leaving and entering a bus.

We apply KCL to every high-voltage node in the electric circuit, as shown in Figure 4.2. For a bus $i \in [n]$, Kirchoff’s Current Law states:

$$[\text{sum of currents leaving the node}] - [\text{sum of currents entering the node}] = 0.$$

These currents are the currents of lines incident at the bus, together with the current ‘generated or consumed’ by the power injector. Complex power is given by:

$$\mathbf{S} = \overline{\mathbf{I}}\mathbf{V}.$$

In our case, \mathbf{I} is the current that we are looking for, flowing from the ground node to the high-voltage node at i , and \mathbf{V} is the potential difference between the high-voltage node and ground, which is \mathbf{V}_i . The amount of power generated or consumed is given by the grid state: $\mathbf{S} = \mathbf{S}_i$. The current through the power injector is now given by $\mathbf{S}_i \mathbf{V}_i^{-1}$.

The i^{th} row of \mathbf{K} corresponds to the bus i , and its entries are 1 for lines leaving i , and -1 for lines entering i . This allows us to write the sum of currents in a compact way:

$$\overline{\mathbf{S}_i \mathbf{V}_i^{-1}} + (\mathbf{K}\mathbf{I})_i = 0.$$

Taking the complex conjugate and multiplying both sides by \mathbf{V}_i gives $\mathbf{S}_i + \overline{(\mathbf{K}\mathbf{I})_i} \mathbf{V}_i = 0$ for each $i \in [n]$, or in matrix form:

$$\mathbf{S} + \overline{(\mathbf{K}\mathbf{I})} * \mathbf{V} = \mathbf{0}.$$

(The symbol $*$ denotes *point-wise* multiplication.)

4.4.4 Validity conditions

Instead of *requiring*⁷ the circuits laws to hold, we define them as an *optional property* of the grid state.

Definition 4.4.1. Given an (n, m) -grid structure $((\mathcal{N}, \mathcal{L}), \mathbf{K}, \eta)$, a grid state $(\mathbf{S}, \mathbf{V}, \mathbf{I})$ is *valid* if it satisfies the *KVL-Ohm equality*:

$$\mathbf{I} = i \text{ diag}(i\eta) \mathbf{K}^* \mathbf{V} \quad (\text{KVL-Ohm})$$

and the *S-KCL equality*:

$$\mathbf{S} + \overline{(\mathbf{K}\mathbf{I})} * \mathbf{V} = \mathbf{0}. \quad (\text{S-KCL})$$

⁷Slepian (1968) gives an *axiomatic* formulation of circuit theory.

Remark. In physical terms, the *KVL-Ohm equality* states:

Each line $\mathcal{L}_k = (i, j)$ satisfies Ohm's Law ($I = VY$), where:

$$I = I_k, \quad V = V_i - V_j, \quad Y = \eta_k$$

and the *S-KCL equality* states:

At each node i , the sum of power injected at the node, S_i , and power injected from the grid, must equal 0.

Proposition 4.4.2. *Given a grid structure and state as in Definition 4.4.1, the following are equivalent:*

- i. *The grid state is valid.*
- ii. *The grid state satisfies (KVL-Ohm) and (S-KCL).*
- iii. *The grid state satisfies (KVL-Ohm), and each node i satisfies the node flow equation, also called the power mismatch equation:*

$$S_i = i \sum_{j=1}^n \bar{L}_{i,j} |V_i| |V_j| e^{i(\theta_i - \theta_j)} \quad \text{for each } i \in [n], \quad (4.1)$$

$$\text{where } \mathbf{L} = \mathbf{K} \operatorname{diag}(i\boldsymbol{\eta}) \mathbf{K}^* \quad (4.2)$$

and $\boldsymbol{\theta} \in \mathbb{R}^n$ is the vector of voltage angles, i.e. $\theta_j = \operatorname{Arg}(V_j)$ (the principle argument of V_j). We call \mathbf{L} the nodal susceptance matrix (Ronellenfitsch et al., 2017).

Remark. Note that (4.1) does not depend on \mathbf{I} . This means that a valid state is uniquely determined by \mathbf{S} and \mathbf{V} , since \mathbf{I} can be computed from \mathbf{V} using (KVL-Ohm).

Remark. Writing in real and imaginary components, we get the node flow equations for real and reactive power for each node $i \in [n]$:

$$P = \Re(S_i) = \sum_{j=1}^n |V_i| |V_j| [\Im(L_{i,j}) \cos(\theta_i - \theta_j) - \Re(L_{i,j}) \sin(\theta_i - \theta_j)] \quad (4.3)$$

$$Q = \Im(S_i) = \sum_{j=1}^n |V_i| |V_j| [\Im(L_{i,j}) \sin(\theta_i - \theta_j) + \Re(L_{i,j}) \cos(\theta_i - \theta_j)] \quad (4.4)$$

In literature on the subject, the node flow equation is often given in this form. The summands in the expression above are essentially the two-dimensional rotation matrix of angle $\theta_i - \theta_j$, applied to the vector $(\Re(i\bar{L}_{i,j}), \Im(i\bar{L}_{i,j}))^*$.

We will later study so called *DC-valid* grid structures, where the values of \mathbf{L} are real. If so, (4.3) simplifies to:

$$P = \Re(S_i) = \sum_{j=1}^n \Re(L_{i,j}) |V_i| |V_j| \sin(\theta_j - \theta_i).$$

(Notice that we flipped θ_i and θ_j .) This tells us that in a network of just two nodes and one line with purely imaginary admittance, the amount of real power transmitted is proportional to $\sin(\theta_2 - \theta_1)$.⁸

Proof. (i) \iff (ii) is true by definition.

Suppose the grid state satisfies (KVL-Ohm). We have

$$\begin{aligned}\mathbf{S} + \overline{(\mathbf{KI})} * \mathbf{V} &= \\ \mathbf{S} + \overline{(i\mathbf{K}\text{diag}(i\boldsymbol{\eta})\mathbf{K}^*\mathbf{V})} * \mathbf{V} &= \\ \mathbf{S} + \overline{(i\mathbf{L}\mathbf{V})} * \mathbf{V} &= \mathbf{0}\end{aligned}$$

iff for each $i \in [n]$

$$\begin{aligned}\mathbf{S}_i &= - \left(\sum_{j=1}^n i\mathbf{L}_{i,j} \mathbf{V}_j \right) \mathbf{V}_i \\ &= - \left(\sum_{j=1}^n -i\bar{\mathbf{L}}_{i,j} \bar{\mathbf{V}}_j \right) \mathbf{V}_i \\ &= i \sum_{j=1}^n \bar{\mathbf{L}}_{i,j} \mathbf{V}_i \bar{\mathbf{V}}_j \\ &= i \sum_{j=1}^n \bar{\mathbf{L}}_{i,j} |\mathbf{V}_i| e^{i\theta_i} |\mathbf{V}_j| e^{-i\theta_j} \\ &= i \sum_{j=1}^n \bar{\mathbf{L}}_{i,j} |\mathbf{V}_i| |\mathbf{V}_j| e^{i(\theta_i - \theta_j)},\end{aligned}$$

proving (ii) \iff (iii).



4.5 Power Flow

In the previous section, we derived a fundamental result: the *node flow equation* (4.1). Recall from Section 3.5 that the *Power Flow problem* entails the following:

Given the production or consumption at each node,

find the current flowing through each line.

In the context of our electric model, this translates to:

Given an (n, m) -grid structure $((\mathcal{N}, \mathcal{L}), \mathbf{K}, \boldsymbol{\eta})$, and a power injection \mathbf{S} ,

find \mathbf{V} and \mathbf{I} such that $(\mathbf{S}, \mathbf{V}, \mathbf{I})$ is a valid state.

It turns out that the easiest way to solve this problem is to solve the node flow equation, obtaining \mathbf{V} . Once \mathbf{V} is known, one can easily compute \mathbf{I} using KVL-Ohm, giving a state $(\mathbf{S}, \mathbf{V}, \mathbf{I})$ that is valid by construction.

⁸The quantity $\theta_2 - \theta_1$ is called the *power angle* of the transmission line, a common measure of the amount of power being transmitted. A power angle greater than 45° will cause the nodes to lose synchronicity, making power transmission between the two nodes impossible. (von Meier, 2006) For long lines (over 100km), this *stability limit* places an upper limit on the amount of power that a line can transmit. For shorter lines, the *thermal limit* dominates.

The node flow equation is a system of non-linear equations, and no closed-form solution is known to exist in general. Fortunately, solving the node flow equation is essentially a root-finding problem. This means that well-established techniques, such as the Newton-Raphson algorithm, can be used to find a numerical solution.

The only difficulty lies in the *number of unknowns* ($2n$ real numbers⁹) and finding an *initial value* that converges to the solution. When studying the evolution of the grid state over time, we can use the solution of a previous iteration as initial value. In general, however, we need to come up with an initial guess.

The classical approach is to use the *flat start* as initial value: all voltage angles are set to 0, and magnitudes are all set to the same value (say, 380 kV). For small networks, the Newton-Raphson algorithm then converges to a valid state, with small power angles between lines, and voltage magnitudes close to the initial value. For larger networks, however, this initial value rarely converges, and a valid state can be ‘maddeningly difficult to obtain’ (Overbye et al., 2004).

Instead, a common approach is to approximate the grid structure and to linearise the laws of physics. The more approximations that we make, the easier it is to find a solution. A particular combination of approximations is known as the *DC approximation*, in which case a *closed-form* solution always exists, known as the *Linear Power Flow*. For accurate power flow analysis, this solution is then used as initial value for the original system of equations. In this thesis, however, we will only use the solution of the Linear Power Flow, as it is easier to compute and analyse. This is common practice when studying *cascading failures* (Nesti et al., 2018a; Ronellenfitsch et al., 2017; Purchala et al., 2005).

4.6 DC approximation

‘DC approximation’ is a name given to a collection of assumptions/approximations, described below. The name ‘DC’ refers to the approximation that the network is *decoupled*. Unlike the abbreviation might suggest (DC usually stands for ‘Direct Current’), the power grid is still modelled as an AC (Alternating Current) network. The first version of this technique was published by Stott and Alsac (1974), allowing the node flow equations to be solved efficiently using the computational power available at that time.¹⁰

Compare the following with Definitions 4.2.1 and 4.3.1.

Definition 4.6.1. Suppose $((\mathcal{N}, \mathcal{L}), \mathbf{K}, \boldsymbol{\eta})$ is an (n, m) -grid structure.

- If $i\boldsymbol{\eta} \in \mathbb{R}^m \subseteq \mathbb{C}^m$ (i.e. $\boldsymbol{\eta}$ has purely imaginary values) then the grid structure *satisfies the DC approximation*.¹¹

⁹ Actually, the voltage angle θ of one bus (the *slack bus*) is usually fixed to 0, since 4.1 only depends on differences in voltage angles. We then have $2n - 1$ unknowns.

¹⁰ Their method does solve the actual node flow equation, but they optimised the iterative root-finding process by *approximating the Jacobian*.

¹¹ Nesti et al. (2018a) write $\beta = i\boldsymbol{\eta}$. Transmission line impedance ($Z = R + iX$) is dominated by inductance, which is positive reactance (X). Resistance (R) is always positive for passive components. Therefore, Z lies in the top-right quadrant of \mathbb{C} . Then the admittance, $Y = 1/Z = G + iB$, lies in the bottom-right quadrant of \mathbb{C} . In the DC approximation, line conductance (G) is neglected, so ($Y = iB$ with $B < 0$). Therefore, $\beta_k = i\eta_k = iY = -B > 0$ is the *susceptance of line k, with reversed sign*.

For a grid state $(\mathbf{S}, \mathbf{V}, \mathbf{I})$ on the structure:

- If $\mathbf{S} \in \mathbb{R}^n \subseteq \mathbb{C}^n$ then the grid state *satisfies the DC approximation*. (Note that \mathbf{V} and \mathbf{I} need not be real-valued! We are still studying an AC circuit.)
- If $\mathbf{V} \in \mathbb{T}^n \cdot V_{op} \subseteq \mathbb{C}^n$ (i.e. $|V_i| = V_{op}$ for each node i) for some *operating voltage* $V_{op} \in \mathbb{R}_{\geq 0}$, then the grid state admits a *flat profile*.

In the special case $V_{op} = 1$, the grid state admits a *normalised profile*.

We note that $V_{op} = 1$ does not necessarily mean that the transmission network is operating at 1 V, it simply means that the network is operating at exactly *one unit of electric potential* (which could be set to 1 V, but also 380 kV, for example). This unit is known as a *power unit* (p.u.).

Compare the following with (KVL-Ohm) and (S-KCL).

Definition 4.6.2. Given an (n, m) -grid structure $((\mathcal{N}, \mathcal{L}), \mathbf{K}, \boldsymbol{\eta})$ and a grid state $(\mathbf{S}, \mathbf{V}, \mathbf{I})$ that both satisfy the DC approximation. The grid state is *approximately valid* if it satisfies the *approximate KVL-Ohm equality*:

$$\mathbf{I} = i \operatorname{diag}(i\boldsymbol{\eta}) i \mathbf{K}^* \boldsymbol{\theta} V_{op} \quad (\text{approx. KVL-Ohm})$$

and the *approximate S-KCL equality*:

$$\mathbf{S} + \overline{(\mathbf{K}\mathbf{I})} V_{op} = \mathbf{0}. \quad (\text{approx. S-KCL})$$

The approximate S-KCL equality can be obtained by replacing the \exp function in (4.1) by $z \mapsto 1 + z$ (the first two terms of the Maclaurin series of \exp):

Proposition 4.6.3. Given a grid structure state as in the previous definition, the state is approximately valid if and only if it satisfies the approximate KVL-Ohm equality and each node i satisfies the approximate node flow equation:

$$S_i = i \sum_{j=1}^n \bar{L}_{i,j} |V_i| |V_j| (1 + i(\theta_i - \theta_j)) \quad \text{for each } i \in [n]. \quad (4.5)$$

Proof. Suppose the approximate KVL-Ohm equality hold. The approximate node flow equality holds if and only if for each node i , we have:

$$\begin{aligned} S_i &= i \sum_{j=1}^n \bar{L}_{i,j} |V_i| |V_j| (1 + i(\theta_i - \theta_j)) \\ &= i \sum_{j=1}^n L_{i,j} |V_i| |V_j| - \sum_{j=1}^n L_{i,j} |V_i| |V_j| (\theta_i - \theta_j) \end{aligned}$$

We assumed a DC state ($S_i \in \mathbb{R}$):

$$\begin{aligned}
&= - \sum_{j=1}^n L_{i,j} |V_i| |V_j| (\theta_i - \theta_j) \\
&= - \sum_{j=1}^n L_{i,j} |V_i| |V_j| \theta_i + \sum_{j=1}^n L_{i,j} |V_i| |V_j| \theta_j \\
&= -\theta_i |V_i| \sum_{j=1}^n L_{i,j} |V_j| + |V_i| \sum_{j=1}^n L_{i,j} |V_j| \theta_j
\end{aligned}$$

We assumed a flat profile ($|V_i| = |V_j| = V_{op}$ for every $i, j \in [n]$):

$$\begin{aligned}
&= -\theta_i V_{op}^2 \sum_{j=1}^n L_{i,j} + V_{op}^2 \sum_{j=1}^n L_{i,j} \theta_j \\
&= -\theta_i V_{op}^2 \sum_{j=1}^n \bar{L}_{i,j} + V_{op}^2 \sum_{j=1}^n L_{i,j} \theta_j
\end{aligned}$$

The rows of \mathbf{L} add up to 0:

$$\begin{aligned}
&= 0 + V_{op}^2 \sum_{j=1}^n L_{i,j} \theta_j \\
&= V_{op}^2 \sum_{j=1}^n L_{i,j} \theta_j \\
&= (\bar{L}\theta)_i V_{op}^2 \\
&= \overline{(K \operatorname{diag}(i\eta) K^* \theta)_i} V_{op}^2 \\
&= -\overline{(K i \operatorname{diag}(i\eta) i K^* \theta V_{op})_i} V_{op} \\
&= -\overline{(KI)_i} V_{op}
\end{aligned}$$

which is equal to S_i if and only if the approximate S-KCL equality holds. \checkmark

Theorem 4.6.4. Suppose that a grid structure and state satisfy the DC approximation and that the state admits a flat, normalised profile. Then the approximated node flow equation is linear and real:

$$\boxed{\mathbf{S} = \mathbf{L}\boldsymbol{\theta}.} \quad (4.6)$$

Proof. In the proof of Theorem 4.6.3, we derived that the approximate node flow equation holds if and only if for each node i , we have:

$$S_i = (\bar{L}\theta)_i V_{op}^2.$$

Because \mathbf{L} is real-valued and $V_{op} = 1$, we find the result. \checkmark

4.6.1 Accuracy

The DC approximation is a useful tool for understanding the complex nature of transmission networks. Therefore, it is crucial to verify that the DC approximation is, in

fact, a good approximation, when real-world networks are studied. More precisely, one should ask:

1. How close is a DC-valid state to being valid? More precisely, when the approximate node flow equation (4.5) holds, what is the mismatch between the left hand and right hand side of the node flow equation (4.1)?
2. How close are real-world grid structures to satisfying the DC approximation?

The first question is answered in Proposition 4.6.6, where an upper bound is derived for the power mismatch. It shows that the mismatch is bounded by the *squares* of local differences in phase angles (i.e. $\theta_i - \theta_j$ for line (i, j)). Purchala et al. (2005) have shown that in the Belgian transmission network, all phase differences are below 7° , and 94% of lines have a phase difference below 2° .

The second question is answered by Nesti et al. (2018a), who confirm that the SciGRID network (which we will study in Part II) satisfies the criteria found by Purchala et al. (2005).

Lemma 4.6.5. *There exists $K \in \mathbb{R}_{\geq 0}$ such that*

$$|\exp ix - (1 + ix)| = K|x|^2 \quad \text{for every } -2\pi \leq x \leq 2\pi.$$

Proof. We provide a proof using *complex analysis*.¹² The complex (entire) function $z \mapsto \exp z$ is defined by the power series

$$z \mapsto \sum_{k=0}^{\infty} \frac{z^k}{k!} = 1 + z + z^2 \left(\frac{z^0}{2!} + \frac{z^1}{3!} + \dots \right)$$

which has infinite radius of convergence, and is continuous on \mathbb{C} .

The functions $z \mapsto \frac{1}{z^2}$, $z \mapsto \exp z$ and $z \mapsto 1 + z$ are all holomorphic on $\mathbb{C}^* = \mathbb{C} \setminus \{0\}$, and so the function

$$g : \mathbb{C}^* \rightarrow \mathbb{C} \quad g : z \mapsto \frac{1}{z^2}(\exp z - (1 + z)) \quad (4.7)$$

is holomorphic on \mathbb{C}^* , with a removable singularity at 0. The (unique) extension of g to \mathbb{C} is an entire function, and by construction:

$$\exp z = 1 + z + z^2 g(z) \quad \text{for each } z \in \mathbb{C}.$$

Since g is entire, it is continuous on \mathbb{C} . $I = [-i2\pi, i2\pi]$ is a compact subset of \mathbb{C} , so g is bounded on I , proving the result. \checkmark

Proposition 4.6.6. *Suppose $((\mathcal{N}, \mathcal{L}), \mathbf{K}, \boldsymbol{\eta})$ is an (n, m) -grid structure, with a state $(\mathbf{S}, \mathbf{V}, \mathbf{I})$ that admits a flat profile with operating voltage V_{op} .*

If the state is DC-valid, then there exists $K \in \mathbb{R}_{\geq 0}$ such that for each node i :

$$\begin{aligned} \left| \mathbf{S}_i - i \sum_{j=1}^n \bar{\mathbf{L}}_{i,j} |\mathbf{V}_i| |\mathbf{V}_j| e^{i(\theta_i - \theta_j)} \right| &\leq KV_{op}^2 \sum_{j=1}^n |\mathbf{L}_{i,j}| (\theta_i - \theta_j)^2 \\ &\leq KV_{op}^2 \|\boldsymbol{\eta}\|_{\infty} \|\mathbf{K}^* \boldsymbol{\theta}\|_2^2. \end{aligned}$$

¹²For an introduction, see Garling (2014).

Remark. This result states that if the grid state is *DC-valid*, and the power angles (i.e. $\theta_i - \theta_j$ for line (i, j)) are low, then the state is *close* to also being *valid*.

Quantitatively, it tells us that for a given node i , the 'error' resulting from using the approximate node flow equation (4.5) is proportional to the *squares* of phase angles of lines that connect to i .

Proof. Suppose $i \in [n]$.

Choose a $K \in \mathbb{R}_{\geq 0}$ for which Lemma 4.6.5 holds. The state is DC-valid, so we can substitute (4.5) for S_i :

$$\begin{aligned}
& \left| S_i - \sum_{j=1}^n \bar{M}_{i,j} |V_i| |V_j| e^{i(\theta_i - \theta_j)} \right| \\
&= \left| i \sum_{j=1}^n \bar{L}_{i,j} |V_i| |V_j| (1 + i(\theta_i - \theta_j)) - i \sum_{j=1}^n \bar{L}_{i,j} |V_i| |V_j| e^{i(\theta_i - \theta_j)} \right| \\
&= V_{op}^2 \left| \sum_{j=1}^n \bar{L}_{i,j} \left(e^{i(\theta_i - \theta_j)} - (1 + i(\theta_i - \theta_j)) \right) \right| \\
&\leq V_{op}^2 \sum_{j=1}^n |\bar{L}_{i,j}| \left| e^{i(\theta_i - \theta_j)} - (1 + i(\theta_i - \theta_j)) \right| \quad (\text{triangle inequality}) \\
&\leq KV_{op}^2 \sum_{j=1}^n |\bar{L}_{i,j}| (\theta_i - \theta_j)^2 \quad (\text{Lemma 4.6.5}) \\
&= KV_{op}^2 \left[\sum_{j=i}^n |\bar{L}_{i,j}| (\theta_i - \theta_j)^2 + \sum_{i,j \text{ connected}} |\bar{L}_{i,j}| (\theta_i - \theta_j)^2 + \sum_{i,j \text{ not connected}} |\bar{L}_{i,j}| (\theta_i - \theta_j)^2 \right] \\
&= KV_{op}^2 \left[|\bar{L}_{i,i}| (\theta_i - \theta_i)^2 + \sum_{i,j \text{ connected}} |\bar{L}_{i,j}| (\theta_i - \theta_j)^2 + \sum_{i,j \text{ not connected}} 0 \cdot (\theta_i - \theta_j)^2 \right] \\
&= KV_{op}^2 \sum_{\substack{j \neq i \\ i,j \text{ connected}}} |\bar{L}_{i,j}| (\theta_i - \theta_j)^2 \\
&\leq KV_{op}^2 \sum_{\substack{\mathcal{L}_k = (a,b) \in \mathcal{L}}} |\bar{L}_{a,b}| (\theta_a - \theta_b)^2 \\
&= KV_{op}^2 \sum_{\substack{\mathcal{L}_k = (a,b) \in \mathcal{L}}} |\eta_k| (K^* \theta)_k^2 \\
&= KV_{op}^2 \|\boldsymbol{\eta} * K^* \boldsymbol{\theta} * K^* \boldsymbol{\theta}\|_1 \quad (\text{in } \ell^1) \\
&\leq KV_{op}^2 \|\boldsymbol{\eta}\|_\infty \|K^* \boldsymbol{\theta} * K^* \boldsymbol{\theta}\|_1 \quad (\text{Hölder's inequality}) \\
&= KV_{op}^2 \|\boldsymbol{\eta}\|_\infty \|K^* \boldsymbol{\theta}\|_2^2
\end{aligned}$$



4.7 Nodal susceptance matrix

Theorem 4.6.4 shows that the *nodal susceptance matrix*, given by

$$\mathbf{L} = \mathbf{K} \operatorname{diag}(i\boldsymbol{\eta}) \mathbf{K}^*$$

is not just useful for compact notation: it relates phase angles to power injection, taking the grid structure into account ($\mathbf{S} = \mathbf{L}\boldsymbol{\theta}$).

However, for our purposes, we are more interested in the *inverse* of this function, which maps a power injection to the vector of phase angles that it induces at the buses. Unfortunately, the inverse does not exist: \mathbf{L} is an $n \times n$ matrix, but it does not have full rank. This can be seen by the fact that \mathbf{K} has rank $n - 1$, so the rank of \mathbf{L} is at most $n - 1$. We can be more precise:

Theorem 4.7.1. *Suppose that the entries of $i\boldsymbol{\eta}$ are non-zero.¹³ Then the nodal susceptance matrix, \mathbf{L} , has rank $n - 1$, and its kernel has a one-element basis:*

$$\ker \mathbf{L} = \operatorname{Span} \{(1, 1, \dots, 1)^*\}.$$

Proof. We have $\operatorname{rank} \mathbf{K} = n - 1$ (Theorem 1.3.2), so $\operatorname{rank} \mathbf{K}^* = \operatorname{rank} \mathbf{K} = n - 1$. We will prove $\operatorname{rank} \mathbf{L} = n - 1$ by showing that $\ker \mathbf{L} = \ker \mathbf{K}^*$. This tells us that they have the same nullity, and by the Rank-Nullity Theorem, the result follows.

Suppose $\boldsymbol{\theta} \in \ker \mathbf{K}^*$. Then

$$\mathbf{L}\boldsymbol{\theta} = \mathbf{K} \operatorname{diag}(i\boldsymbol{\eta}) \mathbf{K}^* \boldsymbol{\theta} = \mathbf{0},$$

i.e. $\boldsymbol{\theta} \in \ker \mathbf{L}$.

Conversely, suppose $\boldsymbol{\theta} \in \ker \mathbf{L}$. Then

$$\begin{aligned} \mathbf{L}\boldsymbol{\theta} &= \mathbf{0} \\ \Rightarrow \quad \mathbf{K} \operatorname{diag}(i\boldsymbol{\eta}) \mathbf{K}^* \boldsymbol{\theta} &= \mathbf{0} \\ \Rightarrow \quad \boldsymbol{\theta}^* \mathbf{K} \operatorname{diag}(i\boldsymbol{\eta}) \mathbf{K}^* \boldsymbol{\theta} &= 0 \\ \Rightarrow \quad (\boldsymbol{\theta}^* \mathbf{K} \operatorname{diag}(i\boldsymbol{\eta}) \mathbf{K}^* \boldsymbol{\theta})^* &= 0 \\ \Rightarrow \quad (\operatorname{diag}(i\boldsymbol{\eta})^{\frac{1}{2}} \mathbf{K}^* \boldsymbol{\theta})^* (\operatorname{diag}(i\boldsymbol{\eta})^{\frac{1}{2}} \mathbf{K}^* \boldsymbol{\theta}) &= 0 \quad (\operatorname{diag}(i\boldsymbol{\eta}) \text{ is self-adjoint}) \\ \Rightarrow \quad \left\| \operatorname{diag}(i\boldsymbol{\eta})^{\frac{1}{2}} \mathbf{K}^* \boldsymbol{\theta} \right\| &= 0. \end{aligned}$$

All entries of $i\boldsymbol{\eta}$ are non-zero, so $\mathbf{K}^* \boldsymbol{\theta}$ must be zero. It follows that $\boldsymbol{\theta} \in \ker \mathbf{K}^*$.

The given basis has the right number of elements, and we can see from (4.6) that $(1, 1, \dots, 1)^*$ is indeed an element of the kernel. 

Corollary 4.7.1.1. *If the entries of $i\boldsymbol{\eta}$ are non-zero, then the image of \mathbf{L} is the set of all power injections with zero sum.*

Proof. We have $\mathbf{L} = \mathbf{K} \operatorname{diag}(i\boldsymbol{\eta}) \mathbf{K}^*$, so $\operatorname{Im} \mathbf{L}$ is a linear subspace of $\operatorname{Im} \mathbf{K}$. Applying Theorem 1.3.2, we find that $\operatorname{Im} \mathbf{K}$ is the set of zero-sum injections, and that $\operatorname{Im} \mathbf{K}$ has dimension $n - 1$. The only linear subspace of $\operatorname{Im} \mathbf{K}$ with dimension $n - 1$ is $\operatorname{Im} \mathbf{K}$ itself, so $\operatorname{Im} \mathbf{L} = \operatorname{Im} \mathbf{K}$, proving the result. 

¹³An impedance element never has zero admittance: this would be equivalent to having no element at all.

In Theorem 4.6.4, we found the identity $\mathbf{S} = \mathbf{L}\boldsymbol{\theta}$, relating the power injection to the vector of voltage angles at the nodes. We now know that if \mathbf{S} has zero sum, there is a set of phase angles that are mapped to \mathbf{S} by \mathbf{L} . This set of solutions is a linear subspace of \mathbb{R}^n of dimension 1, and any two solutions differ by a constant angle.¹⁴

There are two paths to take after this point. One option is to fix the phase angle of the slack bus to 0, which uniquely defines all other phase angles. This corresponds to taking the $n - 1 \times n - 1$ submatrix of \mathbf{L} , by removing the row and column of the slack bus. This submatrix is then inverted, and a row and column of all zeroes is added (corresponding to the slack bus). This method is used by Brown et al. (2018).

A second method is to leave \mathbf{L} as-is, and to consider the *Moore-Penrose pseudoinverse* of \mathbf{L} . The resulting matrix, \mathbf{L}^+ , has the property that *if any solution to $\mathbf{S} = \mathbf{L}\boldsymbol{\theta}$ exists, one will be given by $\mathbf{L}^+ \mathbf{S}$.*¹⁵ Corollary 4.7.1.1 tells us that a solution exists if and only if \mathbf{S} has zero sum (which is a realistic assumption). This is the approach of Nesti et al. (2018a), which they interpret as 'distributive slack': not fixing a single slack bus (we will discuss this concept in Section 5.5.1).

4.8 Linear Power Flow

Physically, there is a *current* flowing along a line in the network, which has the function of transporting *energy*. Although the current is alternating, the average effect is a *flow of energy* from one bus to another. We define the *power flow* along a line as the rate of flow of energy, which is constant when the power injection is constant.

In the context of line overloads, we are only interested in line *current*, which can be seen as proportional to the amount of power being transmitted by the line. (Again, power is not a physical quantity that can be transmitted.) In a flat, normalised profile, power flow and line current are identical in magnitude. To follow general convention, we will talk about power flow instead of line current. For example, line ratings are often given in Watts, not Amperes.

Given an (n, m) -grid structure $((\mathcal{N}, \mathcal{L}), \mathbf{K}, \boldsymbol{\eta})$ and grid state $(\mathbf{S}, \mathbf{V}, \mathbf{I})$ that both satisfy the DC approximation, such that the state admits a flat profile, we define the *power flowing through line \mathcal{L}_k* as:

$$f_k = V_{op}(-iI_k). \quad (4.8)$$

This equation resembles¹⁶ the equation for electrical power ($P = VI$), but it is not a quantity of power being generated or consumed in a component! Rather, it should be seen as a quantity symbolising the amount of power that a line transmits.¹⁷ Equation (4.8) can be written in matrix form, giving the *vector of line flows*:

$$\mathbf{f} = V_{op}(-i\mathbf{I}). \quad (4.9)$$

¹⁴This makes sense physically: increasing the phase angle at each node by the same amount makes no difference to the grid state, since power transmission is related to *relative angles*: see Equation (4.5).

¹⁵In fact, the Moore-Penrose pseudoinverse solves the *linear least squares* problem.

¹⁶We multiply the current with $-i$ to account for the 90° phase shift between current and voltage in a pure inductor.

¹⁷Alternatively, this definition can be seen as a *change of unit* for electrical current.

We assume a normalised profile (i.e. $V_{op} = 1$), and we substitute (approx. KVL-Ohm) for \mathbf{I} :

$$\mathbf{f} = -iV_{op}\mathbf{I} = -iV_{op}^2 i \operatorname{diag}(i\boldsymbol{\eta})\mathbf{K}^*\boldsymbol{\theta} = \operatorname{diag}(i\boldsymbol{\eta})\mathbf{K}^*\mathbf{L}^+\mathbf{p}.$$

(We write \mathbf{p} instead of \mathbf{S} when \mathbf{S} is real-valued.)

We find the *Linear Power Flow equation*:

$$\mathbf{f} = \mathbf{F}\mathbf{p}$$

where $\mathbf{F} = \operatorname{diag}(i\boldsymbol{\eta})\mathbf{K}^*\mathbf{L}^+$

This is a linear transformation from a power injection vector \mathbf{p} to the line flow \mathbf{f} that induces it.

If the line thresholds are $\mathbf{W} = (W_1, \dots, W_m)^* \in \mathbb{R}^m$, then we can define the *normalised line flow* as:

$$\hat{\mathbf{f}} = \operatorname{diag}(\mathbf{W})^{-1}\mathbf{f} = \hat{\mathbf{F}}\mathbf{p},$$

where $\hat{\mathbf{F}} = \operatorname{diag}(\mathbf{W})^{-1}\mathbf{F}$ is the *normalised LPF*.

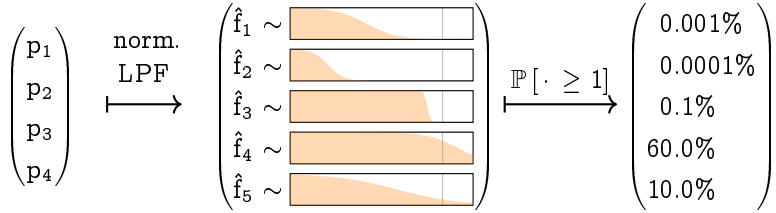
4.9 Stochastic power injections

Using the linear transformation \mathbf{F} that we just derived, we can compute the normalised line flow that a *zero-sum* power injection \mathbf{p} induces. This is a useful result: for example, one could check whether a generator configuration is *admissible* by writing down the injection \mathbf{p} associated to this configuration, and checking that no value of $\hat{\mathbf{F}}\mathbf{p}$ is greater in absolute value than 1. (Since we *normalised* the line flows, each line has unit threshold.) In a $(4, 5)$ -grid structure, this process might look something like:¹⁸



Things get even more interesting when \mathbf{p} is a *stochastic variable*. In this case, $\hat{\mathbf{f}}$ is also a stochastic variable! In fact, given a probability distribution function for \mathbf{p} , we can use $\operatorname{diag}(\mathbf{W})^{-1}\mathbf{F}$ to compute the *probability distribution function of $\hat{\mathbf{f}}$* . Using this probability distribution, we can now answer questions such as: “What is the probability that line i overloads?” ($\mathbb{P} [|\hat{f}_i| \geq 1]$) Or: “What is the probability that line i overloads, given that line j is operating at 95% capacity?” ($\mathbb{P} [|\hat{f}_i| \geq 1 \mid \hat{f}_j = 0.95]$).

¹⁸Here, we are actually showing the *absolute values* of $\hat{\mathbf{f}}$.



We will discuss the implications of having a stochastic power injection and the meaning of these absolute overload probabilities in Section 5.4.1. For now, assume that we are studying the injection and flow during a time window long enough for line failures to occur,¹⁹ but also short enough for fluctuations to be significant (and not ‘averaged out’). These assumptions should be seen as *embodied in the bus covariance matrix*, but for the remainder of this chapter, we make no formal assumptions about the covariance matrix.

4.9.1 Normally distributed power injection

Following Nesti et al. (2018a), we model \mathbf{p} to be *multivariate normally distributed*:

$$\mathbf{p} \sim \mathcal{N}(\boldsymbol{\mu}_p, \boldsymbol{\Sigma}_p)$$

where $\boldsymbol{\mu}_p$ is the mean power injection, which is the sum of deterministic generation and expected stochastic generation, minus the load. $\boldsymbol{\Sigma}_p$ is the *power injection correlation matrix*, which can be estimated from historical generation series. When power injection at different nodes is correlated (because of correlated weather), this matrix is non-diagonal.

Because $\hat{\mathbf{F}}$ is a linear transformation, the vector of normalised line flows $\hat{\mathbf{f}}$ is (multivariate) Gaussian distributed (Theorem 2.1.6), and its distribution is given by

$$\hat{\mathbf{f}} \sim \mathcal{N}(\boldsymbol{\mu}_f, \boldsymbol{\Sigma}_f), \quad \text{where} \quad \boldsymbol{\mu}_f = \hat{\mathbf{F}}\boldsymbol{\mu}_p \quad \text{and} \quad \boldsymbol{\Sigma}_f = \hat{\mathbf{F}}\boldsymbol{\Sigma}_p\hat{\mathbf{F}}^*. \quad (4.10)$$

For realistic networks we have $m > n$, which means that $\hat{\mathbf{F}}$ is not surjective. Then $\boldsymbol{\Sigma}_f$ is not injective, meaning that $\hat{\mathbf{f}}$ is Gaussian, but not normally distributed (Theorem 2.1.5).

4.9.2 Overload probabilities

For a line l , the probability distribution of the current through that line is simply the marginal distribution f_l . Therefore, the probability of an emergent failure of line l is given by:²⁰

$$\mathbb{P}[|f_l| \geq 1] = \mathbb{P}[f_l \leq -1] + \mathbb{P}[f_l \geq 1]$$

From Theorem 2.1.7 it follows that $f_l \sim \mathcal{N}(\mu_{fl}, \Sigma_{fl})$, and $\mathbb{P}[|f_l| \geq 1]$ can now be computed using standard techniques.

¹⁹i.e. long enough for line protection mechanisms to have an effect. The classical assumption is that lines switch off within one AC cycle (e.g. 20 ms for 50 Hz) when overloaded.

²⁰Remember that the *sign* of f_l corresponds to the *direction* of current through the line. The line orientations were chosen arbitrarily, and only have meaning in our bookkeeping.

The probability of *any* emergent failure is $\mathbb{P} [\exists_{l \in [m]} |f_l| \geq 1]$, which can be approximated by an upper and lower bound:

$$\max_{l \in [m]} \mathbb{P} [|f_l| \geq 1] \leq \mathbb{P} [\exists_{l \in [m]} |f_l| \geq 1] \leq \sum_{l \in [m]} \mathbb{P} [|f_l| \geq 1].$$

Trivially, the most likely line flow, given that any emergent failure occurred, coincides with most likely line flow, given that the most vulnerable line failed.

4.9.3 Most likely power injection

Now that we have identified the most vulnerable lines in the network, we naturally want to simulate the effect that the failure of one of these lines will have. When we remove the line from our model, we get a new LPF matrix, which can be used to check the currents through all other lines, after the initial failure. But what power injection should be used? Because we are studying the *hypothetical* failure of a line, we do not yet know the exact power injection that caused it.

The classical approach is to use the nominal power injection, μ_p . This is exactly what we would do when studying regular line failures (caused by a fallen tree, for example). In our case, however, we assumed that the line failed because of an *overload*, which tells us that the power injection must have deviated from its nominal value.

Because we have estimated a probability distribution for p , we can find the *most likely power injection, given that line l overloaded*. We can compute this injection explicitly, leveraging the fact that the LPF map is linear.

Theorem 4.9.1. *Suppose a grid with LPF \hat{F} has a $\mathcal{N}(\mu_p, \Sigma_p)$ -distributed power injection p . The most likely power injection $\tilde{p}^{(l)}$, given the emergent failure of a line l , is uniquely given by*

$$\tilde{p}^{(l)} = \mu_p + \frac{\text{sign}(\mu_{fl}) - \mu_{fl}}{\Sigma_{fl}} \Sigma_p \hat{F}^* e_l \quad (4.11)$$

when $\mu_{fl} \neq 0$. Otherwise, there are two injections that maximise the conditional probability of p , which are given by

$$\tilde{p}^{(l,+)} = \mu_p + \frac{1}{\Sigma_{fl}} \Sigma_p \hat{F}^* e_l \quad \text{and} \quad \tilde{p}^{(l,-)} = \mu_p + \frac{-1}{\Sigma_{fl}} \Sigma_p \hat{F}^* e_l.$$

Proof. The set of power injections associated with the failure event of line l is a union of two parallel planes in \mathbb{R}^n . Indeed, the condition $f_l = 1$ can be written as:

$$f_l = 1 \iff (Fp)_l = 1 \iff e_l^* \hat{F} p = 1 \iff \langle \hat{F}^* e_l, p \rangle = 1$$

which is the equation defining the plane with pillar $\hat{F}^* e_l$. Similarly, the condition $f_l = -1$ is satisfied if and only if p is contained in the plane with pillar $-\hat{F}^* e_l$.

We can now apply Theorem 2.2.3 to each pillar to find the mode of p , given $f_l = 1$, or

$f_l = 1$, respectively:

$$\begin{aligned}
\tilde{\mathbf{p}}^{(l,+)} &= \mu_p + \frac{1 - \langle \boldsymbol{\mu}_p, \hat{\mathbf{F}}^* \mathbf{e}_l \rangle}{\langle \Sigma_p \hat{\mathbf{F}}^* \mathbf{e}_l, \hat{\mathbf{F}}^* \mathbf{e}_l \rangle} \Sigma_p \hat{\mathbf{F}}^* \mathbf{e}_l \\
&= \mu_p + \frac{1 - \langle \hat{\mathbf{F}} \boldsymbol{\mu}_p, \mathbf{e}_l \rangle}{\langle \hat{\mathbf{F}} \Sigma_p \hat{\mathbf{F}}^* \mathbf{e}_l, \mathbf{e}_l \rangle} \Sigma_p \hat{\mathbf{F}}^* \mathbf{e}_l \quad (\hat{\mathbf{F}}^* \text{ is the } \textit{adjoint} \text{ of } \hat{\mathbf{F}}) \\
&= \mu_p + \frac{1 - \langle \boldsymbol{\mu}_f, \mathbf{e}_l \rangle}{\langle \Sigma_f \mathbf{e}_l, \mathbf{e}_l \rangle} \Sigma_p \hat{\mathbf{F}}^* \mathbf{e}_l \\
&= \mu_p + \frac{1 - \mu_{fl}}{\Sigma_{fl}} \Sigma_p \hat{\mathbf{F}}^* \mathbf{e}_l
\end{aligned} \tag{4.12}$$

$$\begin{aligned}
\tilde{\mathbf{p}}^{(l,-)} &= \mu_p - \frac{1 - \langle \boldsymbol{\mu}_p, -\hat{\mathbf{F}}^* \mathbf{e}_l \rangle}{\langle -\Sigma_p \hat{\mathbf{F}}^* \mathbf{e}_l, -\hat{\mathbf{F}}^* \mathbf{e}_l \rangle} \Sigma_p \hat{\mathbf{F}}^* \mathbf{e}_l \\
&= \mu_p + \frac{-1 - \langle \boldsymbol{\mu}_p, \hat{\mathbf{F}}^* \mathbf{e}_l \rangle}{\langle \Sigma_p \hat{\mathbf{F}}^* \mathbf{e}_l, \hat{\mathbf{F}}^* \mathbf{e}_l \rangle} \Sigma_p \hat{\mathbf{F}}^* \mathbf{e}_l \\
&\vdots \\
&= \mu_p + \frac{-1 - \mu_{fl}}{\Sigma_{fl}} \Sigma_p \hat{\mathbf{F}}^* \mathbf{e}_l.
\end{aligned} \tag{4.13}$$

By symmetry of the marginal distribution of f_l , it follows that in the unlikely case where μ_{fl} is zero, the line current is equally likely to deviate to the left as it is to deviate to the right, and both cases come with a different power injection. When μ_{fl} is non-zero, one of the two cases is more likely.

$$\begin{aligned}
\mu_{fl} > 0 &\iff \tilde{\mathbf{p}}^{(l,+)} \text{ is the most probable injection,} \\
\mu_{fl} = 0 &\iff \tilde{\mathbf{p}}^{(l,+)} \text{ and } \tilde{\mathbf{p}}^{(l,-)} \text{ are the two most probable injections,} \\
\mu_{fl} < 0 &\iff \tilde{\mathbf{p}}^{(l,-)} \text{ is the most probable injection.}
\end{aligned}$$

When $\mu_{fl} \neq 0$, we can use the sign function to combine Equations (4.12) and (4.13) into one, which gives the desired expression. 

4.10 Redistribution of flow

In the previous section, we studied normally distributed power injections, and we can now discover which lines are likely to fail, and what power injection was the most likely cause. The next step is to study the *redistribution of flow*: when overloaded lines are switched off (which happens almost instantly), the remaining lines in the network will have to take over their function, because *the power injection remains unchanged after a line outage*. In the simplest case of two parallel lines that connect two otherwise unconnected grids (say, a geographical island connected to the mainland via two cables), the failure of one line will force the other line to carry its original current, plus the current that would normally flow through the failed line.

Except for special cases like these, this *redistributed flow* is, in general, hard to compute without the tools developed in this section. The general case not only consists of all possible line failures, we also want to study all *possible combinations* of line failures.

We will discuss two methods to solve this problem: the Direct and the Optimised methods. The first method simply considers the graph obtained by removing the failed lines from the network, and then recalculates (LPF) for the network. Calculating the Moore-Penrose inverse of \mathbf{L} is computationally expensive²¹, and every combination of line failures requires this calculation.²² A second method, first introduced by Guler et al. (2007), utilises the LPF of the original network to derive the redistribution of flow. This Optimised method is computationally less expensive, and provides additional insight into the effect of line outages, that would not be obtained when discarding the original network.

4.10.1 Direct method

For the Direct method, we simply recompute the LPF for the perturbed network. To avoid reducing the dimension m , and recalculating \mathbf{K} , we set the admittance of each failed line to zero.

More formally, suppose $((\mathcal{N}, \mathcal{L}), \mathbf{K}, \boldsymbol{\eta})$ is an (n, m) -grid structure with $\mathcal{Z} \subseteq [m]$ a collection of $v \in [m]$ lines that fail. For an injection $\mathbf{p} \in \mathbb{R}^n$, the line flows *before* the failures of \mathcal{Z} are given by:

$$\mathbf{f}^{\mathcal{Z}} = \text{diag}(i\boldsymbol{\eta})\mathbf{K}^* (\mathbf{K}\text{diag}(i\boldsymbol{\eta})\mathbf{K}^*)^+ \mathbf{p} \quad (4.14)$$

(by definition of \mathbf{F}) and the line flows *after* the failures are given by:

$$\mathbf{f}^{\mathcal{Z}} = \text{diag}(i\boldsymbol{\eta})\mathbf{K}^* (\mathbf{K}\text{diag}(i\boldsymbol{\eta})\mathbf{I}_{[m] \setminus \mathcal{Z}}\mathbf{K}^*)^+ \mathbf{p}, \quad (4.15)$$

where $\mathbf{I}_{[m] \setminus \mathcal{Z}}$ is the identity matrix, with diagonal entries set to zero for line numbers contained in \mathcal{Z} . By taking the product $\text{diag}(i\boldsymbol{\eta})\mathbf{I}_{[m] \setminus \mathcal{Z}}$, we are essentially setting the admittance of failed lines to zero, which corresponds physically to a circuit break.

4.10.2 Optimised method

Theorem 4.10.1. *Suppose $((\mathcal{N}, \mathcal{L}), \mathbf{K}, \boldsymbol{\eta})$ is an (n, m) -grid structure, with LPF \mathbf{F} . Suppose that $\mathcal{Z} \subseteq [m]$ is a collection of $v \in [m]$ lines that fail. For a given injection $\mathbf{p} \in \mathbb{R}^n$, the line flows before the failures of \mathcal{Z} are given by:*

$$\mathbf{f} = \mathbf{F}\mathbf{p} \quad (4.16)$$

$$(4.17)$$

and the line flows after the failures are given by:

$$\mathbf{f}^{\mathcal{Z}} = \mathbf{f} - \mathbf{M}\mathbf{N}(\mathbf{N}^*\mathbf{M}\mathbf{N})^+ \mathbf{N}^*\mathbf{f} \quad (4.18)$$

where $\mathbf{M} = \mathbf{F}\mathbf{K} - \mathbf{I} \in \mathbb{R}^{m \times m}$ and $\mathbf{N} = (\mathbf{e}_{\mathcal{Z}_1} \cdots \mathbf{e}_{\mathcal{Z}_v}) \in \mathbb{R}^{m \times v}$, the matrix that is zero everywhere, except for the entries (\mathcal{Z}_i, i) (for $i \in [v]$), where it has value 1.

²¹Scientific computing libraries generally calculate \mathbf{L}^+ using the Singular Value Decomposition of \mathbf{L} .

²²Calculating the LPF of the SciGrid network ($n = 489$, $m = 895$) takes approximately 700 ms, excluding the additional overhead of copying the unperturbed network.

Remark. This expression for $\mathbf{f}^{\mathcal{Z}}$ also contains a pseudo-inverse, which might not look computationally advantageous, compared to the Direct method. Note, however, that right multiplying by \mathbf{N} corresponds to taking the *submatrix of column numbers* \mathcal{Z}_1 through \mathcal{Z}_v , and left multiplying by \mathbf{N}^* gives the submatrix of *row numbers* in \mathcal{Z} . This means that \mathbf{M} only needs to be computed once, after which most matrix multiplications in (4.18) can done by *indexing appropriately*, for any combination of line failures. Additionally, if the number of failed lines is small, the product $\mathbf{N}^*\mathbf{M}\mathbf{N}$ will be a small matrix, drastically improving performance. Lastly, this expression only requires (pseudo-)solving the system of equations $(\mathbf{N}^*\mathbf{M}\mathbf{N})\boldsymbol{\alpha} = \mathbf{N}^*\mathbf{f}$, which can be done more efficiently than computing the full pseudo-inverse. (The same optimisation can be also applied to the Direct method.)

Several proofs to this theorem exist. The first proof, by Guler et al. (2007), iterates over the failed lines, proving the result by natural induction. (Guo et al., 2009) provide two additional proofs, which follow from a careful analysis of the Direct method, where they *remove the columns of K* that correspond to failed lines. An entirely different, fourth proof, due to Ronellenfitsch et al. (2017), uses the formalism of *graph cycles*, which form a basis for $\ker \mathbf{K}$. Their article is truly fascinating, as it explores how flow redistributions are composed of loop flows. Additionally, they derive a more general result, where the grid perturbation is expressed as a *change in line admittances* η .²³ Taking the limit $\eta_l \rightarrow 0$ then corresponds to the removal of the line.

Before providing this fourth proof, we will try to deduce the result from intuitive reasoning, to better understand the found expression.

Intuitive argument. Both \mathbf{f} and $\mathbf{f}^{\mathcal{Z}}$ are induced by the same power injection, i.e. $\mathbf{K}\mathbf{f} = \mathbf{K}\mathbf{f}^{\mathcal{Z}} = \mathbf{p}$. This means that the difference between the two, which is the change in flow right after the line failures, is an *element of the kernel of K*. We denote this difference by $\Delta\mathbf{f} := \mathbf{f}^{\mathcal{Z}} - \mathbf{f}$.

For each $l \in \mathcal{Z}$, the current through line l must become zero. This imposes the condition

$$\Delta\mathbf{f}_l = \mathbf{f}_l^{\mathcal{Z}} - \mathbf{f}_l = -\mathbf{f}_l, \quad (4.19)$$

or more compactly,

$$\mathbf{N}^* \Delta\mathbf{f} = -\mathbf{N}^* \mathbf{f}. \quad (4.20)$$

Let us first consider the case of a single failure: $\mathcal{Z} = \{l\}$, that does not cause the network to become disconnected. We are looking for a $\Delta\mathbf{f} \in \ker \mathbf{K}$, under the condition that $\mathbf{f}_l^{\mathcal{Z}} = -\mathbf{f}_l$. The first choice that might come to mind is to fix a basis of $\ker \mathbf{K}$ consisting of *unit loop flows* in the graph. We can pick a unit loop flow that is non-zero at l , and scale by $\pm\mathbf{f}_l$ to find the desired flow difference.

Although this does satisfy the condition at l , it is in general not the flow that will be *induced* in the perturbed network, which is uniquely determined by power flow physics. There are many linear combinations of unit loop flows that satisfy the condition at l , one of which is the correct one.

Suppose that the network is unused ($\mathbf{p} = \mathbf{0}$). We now *force* a current of 1 through line l and we fix all other line currents to 0. This line flow vector is given by \mathbf{e}_l . The result

²³Some transmission networks deploy adjustable inductors that clamp onto transmission lines, to steer the flow of current, making this generalisation especially relevant.

of this flow will be a power injection which remains zero everywhere, except at the two nodes that $\mathcal{L}_l = (i, j)$ connects. This power injection is given by \mathbf{Ke}_l .

On the other hand, if we were to apply the injection \mathbf{Ke}_l to the network, allowing current to flow naturally, we would find the vector of line currents \mathbf{FKe}_l , which in general does not equal \mathbf{e}_l ! Of course, the natural line flow in l will still be relatively large, but some power will be transmitted along different routes. For example, in a circular network of four buses and four lines of equal admittance, with $l = 1$, we find²⁴

$$\mathbf{FKe}_1 = \begin{pmatrix} 0.75 \\ -0.25 \\ -0.25 \\ -0.25 \end{pmatrix}, \text{ with difference } \mathbf{FKe}_1 - \mathbf{e}_1 = \begin{pmatrix} -0.25 \\ -0.25 \\ -0.25 \\ -0.25 \end{pmatrix}.$$

Because \mathbf{F} is the right-inverse of \mathbf{K} , we find that $\mathbf{K}(\mathbf{FKe}_l) = \mathbf{Ke}_l$, which means that the *difference between a natural flow and a forced flow*, $\mathbf{FKe}_1 - \mathbf{e}_1$, is an element of the kernel of \mathbf{K} .

We have not yet satisfied the condition (4.20). Given a power injection \mathbf{p} and unperturbed flow $\mathbf{f} = \mathbf{Fp}$, we can *scale* the above difference with some $\alpha \in \mathbb{R}$:

$$\Delta\mathbf{f} = (\mathbf{FKe}_l - \mathbf{e}_l) \alpha$$

with α such that

$$\Delta\mathbf{f}_l = -\mathbf{f}_l$$

is satisfied. If the network remains connected, α is given by $-\mathbf{f}_l / (\mathbf{FKe}_l - \mathbf{e}_1)_l = \mathbf{f}_l / (1 - (\mathbf{FK})_{ll})$. We state, *without proof*, that this is indeed the flow difference dictated by power flow physics.²⁵

In our above example, we find $\alpha = 3$, which gives

$$\Delta\mathbf{f} = \begin{pmatrix} -0.75 \\ -0.75 \\ -0.75 \\ -0.75 \end{pmatrix}, \text{ and the redistributed flow: } \mathbf{f}^Z = \mathbf{f} + \Delta\mathbf{f} = \begin{pmatrix} 0.00 \\ -1.00 \\ -1.00 \\ -1.00 \end{pmatrix}.$$

Of course, we could have found this result quite easily: after the first line fails, the unit of power simply traverses the loop in the other direction (hence the flipped sign in \mathbf{f}^Z).

In the general case of multiple line failures, we essentially apply the above procedure to each failed line, and add the resulting differences. If we were to use this method *iteratively*, by considering the failed lines in some chosen order, we run into the following issue, when more than one line is removed: when removing the second line from the network, we will find a difference flow that sets the second line current to zero. Unfortunately, this difference flow will also change the current of the first line, which is then no longer zero. If we then consider the first line again, we will also affect the second line, et cetera.

²⁴The series combination of lines 2, 3 and 4 has a third of the admittance of line 1, so their current must equal a third of the current through line 1.

²⁵If we assume the Theorem to be true, one could work backwards from (4.18) to find this result.

To avoid this cat-and-mouse game, we need to find all scaling factors $\alpha_1, \dots, \alpha_v$ *simultaneously*. By virtue of linearity, the v conditions imposed by (4.20) form a set of *linear conditions* on $\boldsymbol{\alpha} = (\alpha_1, \dots, \alpha_v)^*$.

For each line $l \in \mathcal{Z}$, the natural-forced difference is $\Delta\mathbf{f}^l := \mathbf{F}\mathbf{K}\mathbf{e}_l - \mathbf{e}_l$. When combining all differences for $l \in [m]$ as columns of a matrix, we find:

$$\begin{pmatrix} | & & | \\ \Delta\mathbf{f}^1 & \dots & \Delta\mathbf{f}^m \\ | & & | \end{pmatrix} = \mathbf{F}\mathbf{K} - \mathbf{I} = \mathbf{M}$$

The sub-matrix of differences for $l \in \mathcal{Z} \subseteq [m]$ is given by:

$$\begin{pmatrix} | & & | \\ \Delta\mathbf{f}^{\mathcal{Z}_1} & \dots & \Delta\mathbf{f}^{\mathcal{Z}_v} \\ | & & | \end{pmatrix} = \mathbf{M}\mathbf{N}$$

Note that $\mathcal{Z}_1, \dots, \mathcal{Z}_v$ do not need to be ordered.

A linear combination of $\Delta\mathbf{f}^{\mathcal{Z}_1}, \dots, \Delta\mathbf{f}^{\mathcal{Z}_v}$ with scale factors $\alpha_1, \dots, \alpha_v$ is given by

$$\Delta\mathbf{f}(\boldsymbol{\alpha}) = \mathbf{M}\mathbf{N}\boldsymbol{\alpha}. \quad (4.21)$$

Condition (4.20) then becomes:

$$\mathbf{N}^*\mathbf{M}\mathbf{N}\boldsymbol{\alpha} = -\mathbf{N}^*\mathbf{f} \quad (4.22)$$

with pseudo-solution

$$\boldsymbol{\alpha} = -(\mathbf{N}^*\mathbf{M}\mathbf{N})^+ \mathbf{N}^*\mathbf{f}. \quad (4.23)$$

Finally, combining (4.21) and (4.23) gives:

$$\Delta\mathbf{f} = -\mathbf{M}\mathbf{N}(\mathbf{N}^*\mathbf{M}\mathbf{N})^+ \mathbf{N}^*\mathbf{f},$$

in agreement with the result. 

A rigorous proof of Theorem 4.10.1 is given in Ronellenfitsch et al. (2017). This only needs to be adapted to our notation.

In (4.23) we take the *pseudo-inverse*, instead of the general inverse, to account for a set of failures that disconnects the network. We discuss the implications of this modification in Section 6.6.2.

Part II

Predicting failures in Germany's grid

Chapter five

Methods

In the remaining chapters of this thesis, we apply the theory developed in Part I to a real-world problem, to demonstrate its usefulness and its limitations. The goal of the model described in this thesis can be summarised as follows:

Given:

- A real-world *grid structure*;
- hourly *load series*;
- hourly *generation series*.

Predict:

- ‘*Top 10*’ of lines most vulnerable to an emergent failure;
- for each vulnerable line: the most likely *cascading line failures*.

The model, in particular the use of a bus covariance matrix to study cascading line failures, was proposed by Nesti et al. (2018a). Following their approach, the model is applied numerically to the SciGRID dataset (Matke et al., 2016). This dataset is an approximation of the transmission network in Germany, including grid structure, generation capacity, hourly load series and hourly renewable generation series.

As discussed in Section 3.4.2, transmission lines can fail for a number of reasons, and this model only studies one specific type of failure: *short-term changes in renewable generation*.

Line overloads are not the most common, but the most imminent type of failure in a network, in the sense that grid operators need to continually monitor the *configuration* (distribution among the nodes of power generation) to ensure that no line will overload. This strongly constrains the capability of the transmission network. At any point in time, there could be many configurations that are environmentally (or *economically*) better than the current configuration, but they might lead to a line overload.¹ Turning

¹It is for this reason that the Optimal Power Flow problem is computationally difficult solve: it often takes many iterations until a generation distribution is found that does not cause any transmission line to be overloaded.

off functioning wind turbines is known as *wind curtailment*, and switching off solar panels is called *solar curtailment*.²

In China, where roughly a quarter of the world's wind generation capacity is installed, wind curtailment amounted to 16% between 2010 and 2016. (Ye et al., 2018)

5.1 Constructing a complete dataset

European grid operators have detailed datasets that describe the grid structure and state of the transmission network, but these are not (yet) publicly available. We use the work of Brown et al. (2018), which combines open datasets from different sources, to obtain an approximate representation of the German transmission network.

5.1.1 Grid structure

The *European Network for Transmission System Operators for Electricity* (ENTSO-E) was established in 2008 to promote the integration between the electricity markets of European Union member states, and to increase public transparency of these markets. ENTSO-E provides a number of public datasets, including historical hourly load series, international energy flows and yearly generation series. An up-to-date map can be viewed, containing almost all high-voltage transmission lines in Europe, and lines outside of Europe that are part of the synchronous grid of Continental Europe. Unfortunately, this dataset is not available in a computer-readable format,³ and only gives the operating voltage and number of parallel circuits of a line.

Luckily, the SciGRID project has assembled an open source dataset of grid structure, using an entirely different source. The OpenStreetMap project is a detailed, open source world map, maintained by a community of mappers. The map is so detailed, in fact, that it not only contains most transmission lines and substations of Europe, it even contains observations of the number of parallel circuits, the number of wires per cable⁴, the frequency⁵, the name of the grid operator, the operating voltage⁶ and the names of the two buses that it connects. From these characteristics, line resistance and inductance can be estimated. The SciGRID dataset has aggregated OpenStreetMap data, and highly simplified the network, resulting in a complete grid structure.

²Wind turbines can indeed be turned off, by twisting the rotor blades towards 0° pitch and applying the *brakes*. In large turbines, common types are drum brakes (similar to a back-pedalling brake for bikes) and disk brakes. Brakes are especially important during maintenance. Solar panels are switched off using a simple mechanical or electronic switch (a relay). (Denholm et al., 2015)

³they provide a more on this later

⁴You can sometimes see that instead of a single high-voltage cable, there are *three* wires right next to each other. These three lines carry the same current: they are connected every few metres. This increases the total surface area of the cable with relatively low increase in volume (i.e. cost).

⁵which is always 50 Hz in Europe

⁶This can be deduced from the physical size of the insulators between the cable and the transmission tower (or you could ask the operator).

5.1.2 Grid state

For our analysis, we need the *hourly* generation series (for each generator at each node), and the hourly load series (aggregated at each node). This data is not publicly available. Yet, previous work (Brown et al., 2018) has shown that these values can be estimated for the German network by combining public sources, in particular:

- SciGRID, which is based on OpenStreetMap data, for the grid structure (as discussed above);
- Data published as part of the German Renewable Energy Sources Act (*Erneuerbare-Energien-Gesetz*), for the location and capacities of solar and wind sources;
- Andresen et al. (2015) provide a world map of hourly solar and wind *potential*, based on weather data and forecasts, for hourly wind and solar series;
- Federal Network Agency of Germany (*Bundesnetzagentur*), for the location and capacities of all other energy sources;
- Global Domestic Product (GDP) and population density of districts (*Landkreise*) of Germany, for load sizes and locations;
- ENTSO-E hourly load series, for hourly load series.

We now have all the data that we need, except for the hourly generation series of *non-stochastic* energy sources. To fill this gap, Brown et al. (2018) use the clever solution of running an Optimal Power Flow (OPF) simulation for each hour, to determine the cheapest generator configuration. The rationale behind this method is that grid operators *use this exact method* to determine the hourly generator configuration. As long as the marginal costs of each generator are realistic, we hope to find a realistic generator configuration this way.

Clearly, the resulting dataset is an *estimation*, and any results that follow from it should be taken with a grain of salt.

Brown et al. (2018) have developed the *Python for Power System Analysis* (PyPSA) toolbox for solving the OPF problem, which they have made publicly available as free software.⁷ We have used PyPSA for our analysis.

5.1.3 A note on larger datasets

Although the full ENTSO-E network can only be viewed on their official website, Hörsch et al. (2018) were able to extract this information into a usable format. They provide the tools to construct a full dataset for European load and generation, but this process is too computationally demanding to take on in this thesis.

In fact, the limitation of our dataset does have a number of benefits. There are obvious computational benefits, which allow us to study the network without simplification,⁸ and the network is small enough for individual lines to be studied. One additional

⁷under the *GPLv3 licence*

⁸In larger datasets, the set of buses often needs to be clustered to solve the OPF problem.

advantage is that the distribution of installed renewable generation is consistent within Germany (see Figure 6.5), while a European dataset would see large differences among countries (which all have different policies). Finally, Germany has the highest share of stochastic⁹ generation among European countries: in 2011, 41% of solar energy and 31% of wind energy in the European Union was generated in Germany¹⁰

5.2 LPF

As part of the OPF results calculated using PyPSA, we also get the *line currents* for each hour. When calculating the currents using the LPF (applied to the power injections given in the OPF results), we find results that are very similar, but not exactly the same. The largest *relative* discrepancies take place on lines with the smallest thresholds. Figure 5.1 shows the current of each line at 11:00, as given by the OPF results, and calculated using the LPF. It looks like these errors are not the result of a *systematic* error in the calculation of the LPF (the LPF is using the same line impedances, for example), and we assume that the result given by PyPSA is *more accurate*. More importantly: the line flows given by PyPSA are on the edge of the feasibility region, giving us the kind of critically loaded state that we are interested in. The result of applying the LPF overestimates the current through some lines, beyond the feasibility limit of the OPF.

This discrepancy needs to be investigated further,¹¹ but for now, we will continue our analysis by adding this discrepancy as *error-correction term* to the LPF:

$$\text{LPF}_{new} : \quad \mathbf{p} \quad \mapsto \quad \text{LPF}_{old}(\mathbf{p}) \quad + \quad (\mathbf{f}_{\text{PyPSA}} - \text{LPF}_{old}(\mathbf{p}_{nom})).$$

where $\mathbf{f}_{\text{PyPSA}}$ is the nominal flow given in the OPF results, and \mathbf{p}_{nom} is the injection found by the OPF.

5.3 Exploratory data analysis

We are interested in the fluctuations of renewable generation, and how these fluctuations are correlated among different buses. Let us first take a look at the generation series provided by our dataset. For each bus, we know the amount of installed capacity for solar and for wind (expressed in MW), and we have hourly values for the *saturation* of these generator types (i.e. what percentage of installed capacity is actually being generated at that time).

For bus ‘*Emden-Borßum*’,¹² which is one of the five buses with an offshore wind park, the hourly generation capacity of wind offshore, wind onshore and solar during the first two weeks of January is given in Figure 5.2. Generation series for other buses look very similar (although most buses do not house offshore wind generation).

We can see a clear correlation between offshore and onshore wind generation. This should come as no surprise, since the offshore wind park and the onshore wind turbines

⁹This does not include renewable deterministic generation, notably hydroelectricity.

¹⁰Sources: *European Wind Energy Association* and *EuroObserv'ER*

¹¹By studying the source code of PyPSA in more detail, for example.

¹²This is the 228th bus, and has name ‘270’ in the SciGRID dataset.

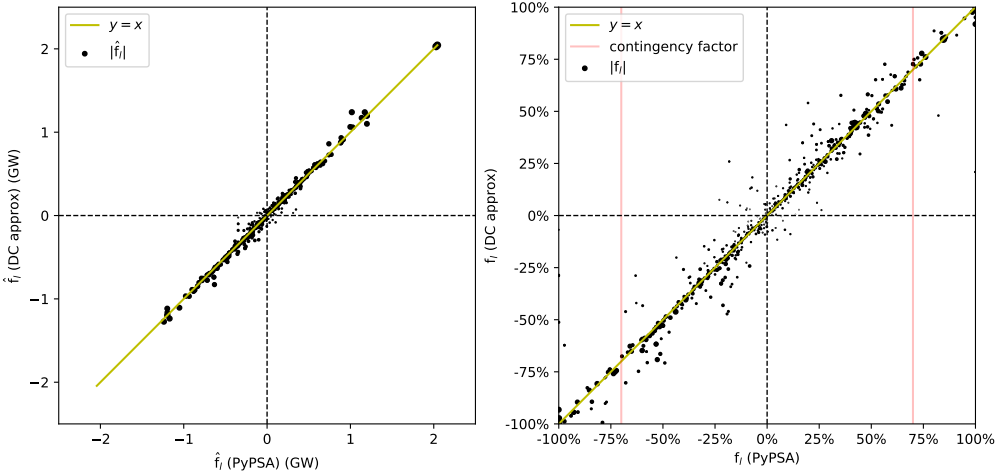


Figure 5.1: Line flow (left) and saturation (right) computed using the LPF and as computed by PyPSA.

are in close proximity (both are close to ‘*Emden-Borßum*’), and are therefore exposed to similar weather. We also notice that the offshore generation is often *saturated*: the saturation is capped at 100%. When examining this phenomenon for all five offshore generators, we find that, on average, offshore generation was saturated ($\geq 95\%$) during 34% (SD 8%) of measured hours. Saturation is rare for onshore wind generation (2.4%, SD 1.6%) and solar generation (< 0.5% for all buses). This saturation might be an artefact of the used dataset.

In the solar generation series, one can clearly identify the daylight hours, which span about 8 hours in January.¹³ We see some sunny days (day 3, for example), overcast days (day 5), and cloudy days (the last two days). The low efficiency on cloudy days might be a little extreme, but the generation series look to be realistic in general. The solar and wind series also agree with historical weather data.

5.3.1 Geographical correlation

By superimposing the generation series of multiple buses, we can see how strongly they are correlated. Figure 5.3 shows the *midday* solar generation values of different buses. When choosing buses randomly (Figure 5.3a), we see some overall correlation in generation. For example, on January 13, all buses experience low solar generation.

In Figure 5.3b, we first choose an arbitrary initial bus (79 was chosen in the figure), and then look at all buses that are in close proximity of the first bus. The generation series of buses chosen this way are clearly *more correlated* than those of randomly selected buses.

¹³In Germany. For comparison: a day is 16 hours long in July.

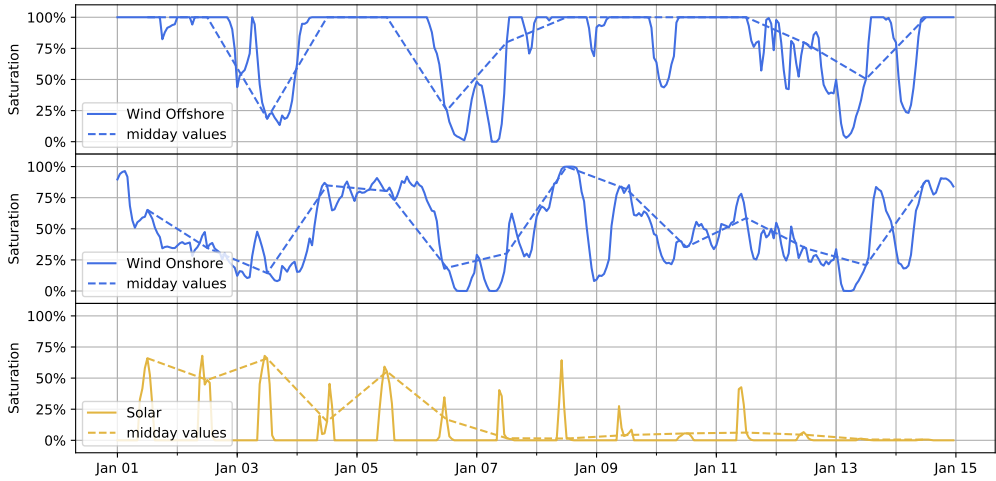


Figure 5.2: Renewable generation capacity at bus ‘Emden-Borßum’ during the first two weeks of January. A dashed line is drawn through all midday (12:00) values for later reference.

5.4 Stochastic power injection

We model the power injection as a *stochastic variable*. In particular, we will assume that the power injection is (multivariate) normally distributed, and we can use historical generation series to estimate this distribution.

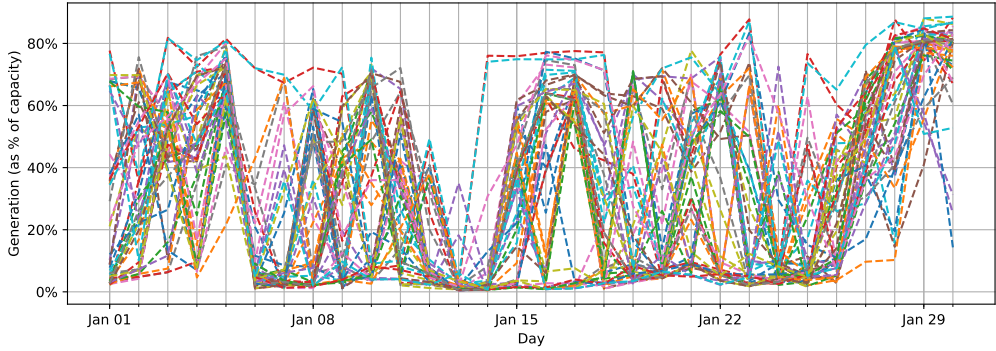
Besides its useful mathematical properties, the normal distribution is a natural choice for modelling the ‘noise’ of injected power, as each bus is the *accumulation of all generators and loads* connected to the bus. When their individual contributions are *random* (but not necessarily normally distributed), their combined effect will resemble a normal distribution by the Central Limit Theorem.

Of course, the Central Limit Theorem can only be applied to individual contributions that are *independently* distributed, which is not the case when studying renewable generation. For example, the amount of solar power generated at a bus is the sum of power generated by all individual solar panels in the region, but their fluctuations are *highly correlated*; not independent.

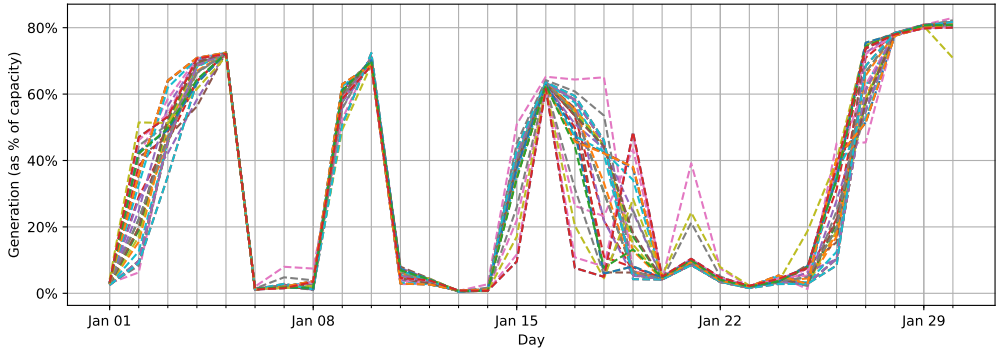
5.4.1 Generation forecast

Grid operators use *forecasting models* to predict the amount of stochastic power generated in the near future to guide their decisions. Advanced models use precise weather forecasts, and extrapolate the expected amount of stochastic generation. A cruder method is to simply look at past generation values of a single bus to predict future generation. We will discuss two models that use this latter method: the *ARMA model* and the *persistent forecast model*.

No forecast can be completely accurate: the real power injection will differ from the predicted injection by some error. This is where the *stochastic* part of our model becomes



(a) 50 randomly selected buses.



(b) All 34 buses that are within 100 km of bus 79.

Figure 5.3: Superposition of midday solar generation values at different buses.

useful: **we model this error to be normally distributed.** As covariance matrix, Nesti et al. (2018a) propose *computing the error values for historical generation series*, and using their covariances as covariance matrix for the normally distributed (future) errors.

This way, the normal distribution captures only correlations in forecast errors, and not correlations in the generation series themselves. This is desirable, because line overloads do not necessarily occur because of large or small amounts of stochastic generation: as long as this amount is known *ahead of time*, the grid operator will adjust the generator configuration to maintain a feasible state. Rather, line overloads may occur when there is a large, sudden fluctuation in stochastic generation that was not predicted by the grid operator (i.e. a large forecast error.)

While we do not know what forecast models are used by the grid operators in Germany, they are certainly beyond the scope of this thesis. So instead of using realistic forecast models, we use a *placeholder model*. Nesti et al. (2018a) use two ARMA models for this purpose (one for wind, one for solar). Their results turn out to be hard to reproduce because the generation series are poorly described by an ARMA model. This is especially true for solar generation series: an ARMA model cannot accurately capture the characteristic shape that we see in Figure 5.2, requiring additional tricks to produce a result.

Because of the possibly unnecessary complexity of these ARMA models, we introduce a

simpler model: the *persistent forecast model*, which predicts the future generation to be equal to the present generation. Although this model does not necessarily provide an accurate forecast, it is sufficient for the purpose of having a placeholder model.

5.4.2 Persistent forecast model

Suppose that (X_1^i, \dots, X_T^i) is the measured (solar or wind) generation series at a node i (T is the number of hours in the series). Given our *persistent forecast* model, we predict the next value to be:

$$X_{T+1}^i \approx X_T^i.$$

If X_{T+1}^i is known, the *prediction error* is defined as $\epsilon_T^i = X_{T+1}^i - X_T^i$.

For all buses, we compute the $T - 1$ prediction errors for the generation series of January. We compute the *sample covariance of these error series*.

5.4.3 Bus covariance matrix

We find covariance matrices for solar generation and wind generation. Following Nesti et al. (2018a), we use these matrices to construct the two *bus covariance matrices*:

$$\Sigma_{\text{day}} = \Sigma_{\text{wind}} + \Sigma_{\text{solar}} \quad \Sigma_{\text{night}} = \Sigma_{\text{wind}}.$$

5.5 Most likely power injection

The most likely power injection, given the failure of a line, can be computed directly using Theorem 4.9.1. This method is numerically stable, even when the failure probability is, to numerical approximation, equal to 0. Also, while the proof of Theorem 4.9.1 uses (the existence of) the inverse of Σ_p , it is not required in the final expression.

When examining the result of this calculation for a number of lines, we found two problems with the final result, which are most prominent on stable lines (those with negligible overload probability).

5.5.1 Non-zero net injection

First, the most likely injection might not have zero sum. We can safely apply the matrix F to an injection p that does not have zero sum. Nevertheless, under our assumptions, p must have zero sum. As part of the DC approximation, we found that the power injection is the image of $L = K \text{diag}(i\eta) K^*$, applied to the vector of phase angles, θ (Equation 4.6). From Theorem 1.3.2 it then follows that the power injection should have zero sum.

Instead of concluding that our model, and the results that follow, are therefore entirely invalid, we will simply *ignore this problem*. We do so with the same reasoning as Nesti et al. (2018a): in reality, the total power injection is never exactly of zero sum. As discussed in Section 3.3, turning any grid-connected device on or off will change

the total injection. This does *not* cause the power grid to ‘promptly vanish in a puff of logic’, but rather, it physically causes a *change of AC frequency*. This change in frequency is then measured by grid operators and generators, who react by changing their energy output to compensate for the change in frequency. This feedback loop is *stable* (von Meier, 2006), as long as frequency changes are small, and the demand can be met.¹⁴

The generators (or rather, the buses that they are connected to) that respond to a change in AC frequency are called the *slack buses* of the network, and they are chosen by the grid operator. In our discussion of the energy market (3.6), we assumed, for didactic simplicity, that a single generator is assigned to be the slack bus.

Nesti et al. (2018a) assume, for mathematical simplicity, that all generators play this role, which is called *distributive slack*. The individual amounts of change in generation is chosen such that the line flows after all generators have settled into a zero-sum are exactly equal to $\mathbf{F}\mathbf{p}^{init}$, where \mathbf{p}^{init} is the initial, non-zero power injection. This redistributed injection is given by:

$$\mathbf{p}^{slack} = \mathbf{K}\mathbf{F}\mathbf{p}^{init}.$$

When \mathbf{p}^{init} does have zero sum, we find $\mathbf{p}^{slack} = \mathbf{p}^{init}$, since \mathbf{F} is the right-inverse of \mathbf{K} , when restricted to the set of zero-sum injections.

5.5.2 Unrealistic renewable fluctuations

The second problem with the most likely injection is that it might not be realistic, simply because there are not enough solar panels and wind turbines to produce the predicted injection. A simple way to check this condition is to calculate the predicted increase in renewable generation at each node, and compare it to the installed capacity.

5.6 Cascading line failures

Given the most likely injection for an assumed initial failure, we can compute the corresponding line flows using the (error-corrected) LPF. This gives us the set of lines that become overloaded, which includes the assumed initial line. Any other lines that fail in this first stage are said to *fail jointly* with the initial failure. The overloaded lines form our set of failed lines: we model the failure after a line overload to be *instant*.

Next, we compute the redistributed flow using the Optimised method (Theorem 4.10.1), and overloaded lines are added to our list of failed lines. Lines that were overloaded in the previous stage remain failed.¹⁵ This process is repeated until no new lines fail.

To evaluate whether a set of failed lines causes a power island to emerge, we study the rank of $\mathbf{N}^*\mathbf{M}\mathbf{N}$ in Equation (eq:lineflowsafterfailures). When this submatrix does not have full rank, the network must be disconnected.

¹⁴Note that this is a one-sentence simplification of the study of *grid stability*.

¹⁵In reality, modern circuit protection devices will automatically attempt to reconnect the line a couple of times, in case the fault was only temporary (von Meier, 2006). For simplicity, we will ignore such mechanisms in our model.

Chapter six

Results

In this final chapter, we discuss the results of applying our theory to the SciGRID dataset. We would like to reiterate that this data is aggregated from different sources, most of which are *not* physical measurements, but ‘educated guesses’.

With this in mind, we proceed with our analysis, not necessarily with the goal of providing accurate operational advice for German grid operators, but to demonstrate that the model can be applied to real-world transmission networks. By studying a representative dataset, we can study the strengths and weaknesses of the model. Finally, we hope that this model will provide *qualitative insight* into the complex behaviour of grid failures, not specific to this dataset.

6.1 SciGRID data

The SciGRID dataset needs to be translated into the language of our model. It contains more information than we need, and it is not yet in the desired format.

6.1.1 Structure

(*A more detailed analysis of dataset properties is available on the GitHub repository.*)

Before any processing, we find that the SciGRID network (obtained from PyPSA example code, the exact dataset used by Nesti et al. (2018a)) contains 585 buses, 1423 generators (of all sources) and 489 loads. It also contains 38 storage units (all are pumped hydroelectric), but these were excluded from our analysis.¹ There are 852 transmission lines in the dataset, at possible voltage levels 220 kV and 380 kV, and there are 96 transformers (between these two voltages). Transmission lines have per-kilometre estimates for admittance, from which the total admittance can be deduced.

Voltages

In our model, we *normalise* the grid voltage. To do so, we multiply all line admittances by the *square* of their operating voltages, after which all voltages can be assumed to be

¹More specifically, they were used in solving the OPF problem, but their initial charge was set to zero.

1, and a unit of current is proportional to a unit of transmitted power. Of the 585 buses, 192 are part of one of the 96 *voltage pairs*: these are two buses at the same location, with the same name (except for the voltage suffix), connected via a transformer. By merging these pairs, we find 489 geographically unique buses, at normalised voltage. From now on, we will refer to these (possibly merged) buses as the buses of the network: $n = 489$, $\mathcal{N} = [489]$.

Loads

There is exactly 1 load connected to each bus. In reality, there are of course thousands of loads connected to a bus: the load in the dataset is the *aggregated* load at that bus. We have hourly time series (i.e. amount of MW being consumed) for each node in the year 2011, which only includes active power consumption.

Generators

Generators are connected to the geographically closest bus, and there is at most one generator per bus of each type.² This means that generation is *aggregated*: multiple generators of the same type are combined into one. There are 489 solar generators, 488 onshore wind generators and 5 offshore wind generators. Offshore wind generators are connected to buses at the north coast of Germany. This means that every bus houses stochastic generation. Their geographic distribution is shown in Figure 6.5.

Lines

Line voltages and admittances are normalised as described above. For each line, we have the names of the two original buses that it connects, which can easily be converted to the new bus collection.

During the study of cascading failures, we found that the network contains *parallel lines*: lines that connect the same pairs of buses. In some cases, there are up to four different lines that are all parallel. When examining these cases on OpenStreetMap, we find that there are indeed parallel lines in the physical network. This is reflected by the *lengths* of parallel lines, as given by SciGRID: these are not the great-circle distances between buses, but rather the distance measured along the line (which makes some turns and bends).

Because our model only holds for *digraphs*, which cannot have parallel lines, we *combine* parallel lines by summing their (voltage normalised) admittances, and summing their thresholds.³ Nesti et al. (2018a) do not mention this anomaly, and use the original set of lines. For comparison, we computed some results for both versions of the network, and found the results to be somewhat similar, in general. Because we did not consider

²In order of installed capacity: *Wind Onshore* (37 GW), *Solar* (37 GW), *Hard Coal* (25 GW), *Gas* (24 GW), *Brown Coal* (21 GW), *Nuclear* (12 GW), *Run of River* (4 GW), *Other* (3 GW), *Wind Offshore* (3 GW), *Oil* (2.7 GW), *Waste* (1.6 GW), *Storage Hydro* (1.4 GW), *Multiple* (0.15 GW) and *Geothermal* (32 MW).

³The results regarding the kernel of K, and the Optimised method for analysis cascading failures, break down without this property.

the case of parallel lines in our model, combining parallel lines in the dataset seems like the *correct* choice.

Of the 852 original lines, there are 705 unique links between original buses before normalising voltages, and there are 695 unique links between buses. There are never two parallel lines with opposite orientation. These 695 lines were used in our model, and will be referred to as simply the *lines* of the network: $m = 695$.

6.1.2 State

Our dataset contains hourly values for load and stochastic (wind and solar) generation for the year 2011. Deterministic generation is estimated using the OPF algorithm, as implemented by PyPSA (Brown et al., 2018), a Python package designed for this purpose. Following common practice, we first multiply all line thresholds by a *contingency factor*: 0.70. This forces the optimisation process to leave a safety margin at every line, and also accounts for the error of using the DC approximation. Figure 6.1 shows the resulting injection at 1 January 2011 at 11:00. Line currents can then be computed using the LPF.

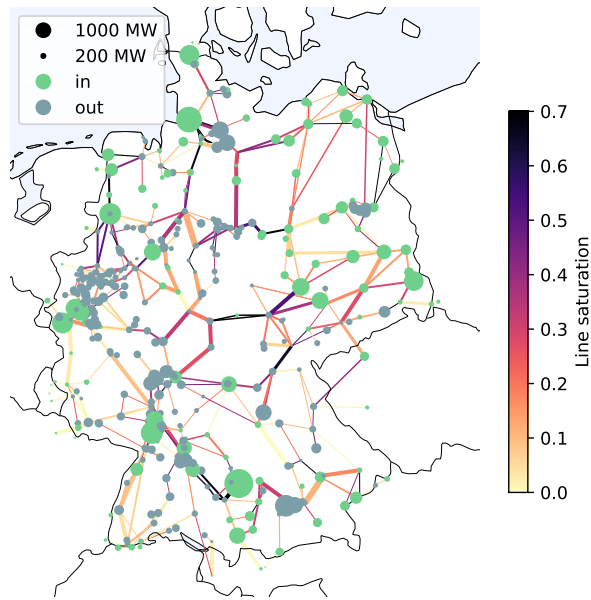


Figure 6.1: Nominal line flow during 11:00-12:00, as fraction of line capacity. Node size represents net power injection. When generation exceeds load, the injection is positive (green), otherwise negative (greyish blue). *Compare with Figure 1a of Nesti et al. (2018a).*

6.2 Bus covariance

As discussed in Section 5.4.2, we estimate the bus covariance matrix from historical errors in our forecast. We find *high* covariances among nodes, which we expected from

our preliminary analysis. Because renewable generation data is extrapolated directly from (coarse) weather data, the generation series of nearby buses are almost identical. The covariance of buses, calculated using the difference series, is visualised in Figure 6.2.

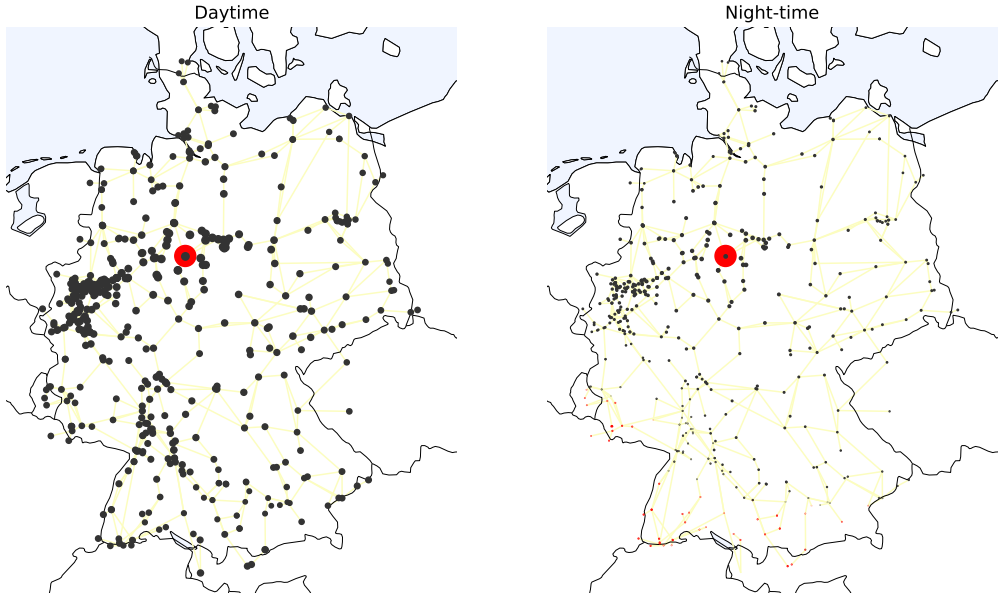


Figure 6.2: Covariance of all buses, relative to the circled bus. Dot size represents normalised covariance. (Normalised using installed renewable capacity at the node.)

6.3 Line covariance

By incorporating bus covariances in our model (which result from correlated weather), we hope to find new structure in the line covariances. To assess the effect of estimating bus covariances, we compare three possible bus covariance matrices:

1. *The identity matrix*: all bus injections are independently Gaussian distributed with the same variance. (They are almost IID, but their means differ.)
2. *The diagonal of estimated variances*: all bus injections are independently Gaussian distributed, but their variances and means differ.
3. *The estimated covariances*: the vector of bus injections is (multivariate) Gaussian distributed. All bus injections are, in general, dependent on each other, and their variances and means differ.

It is well known that local changes to the grid structure have long-range effects. For example, Withaut and Timme (2013) showed that *adding* a new line to a heavily congested, but stable network can cause the failure of another line, possibly far away from

the added line.⁴ This is reflected in our model by the fact that line currents have non-zero covariance, even when bus injections are independently distributed. (In this case, $\Sigma_f = \mathbf{F}\mathbf{I}\mathbf{F}^* = \mathbf{F}\mathbf{F}^*$, which is generally not a diagonal matrix.) Figure 6.3a and Figure 6.3b show the covariances of all lines, relative to a chosen line. We see that covariance is generally high for lines that are close, but there are some clear exceptions. There seems to be a general trend that lines are highly (positively or negatively) correlated when they are close, and *oriented in the same direction* (e.g. East-West) as the chosen line.

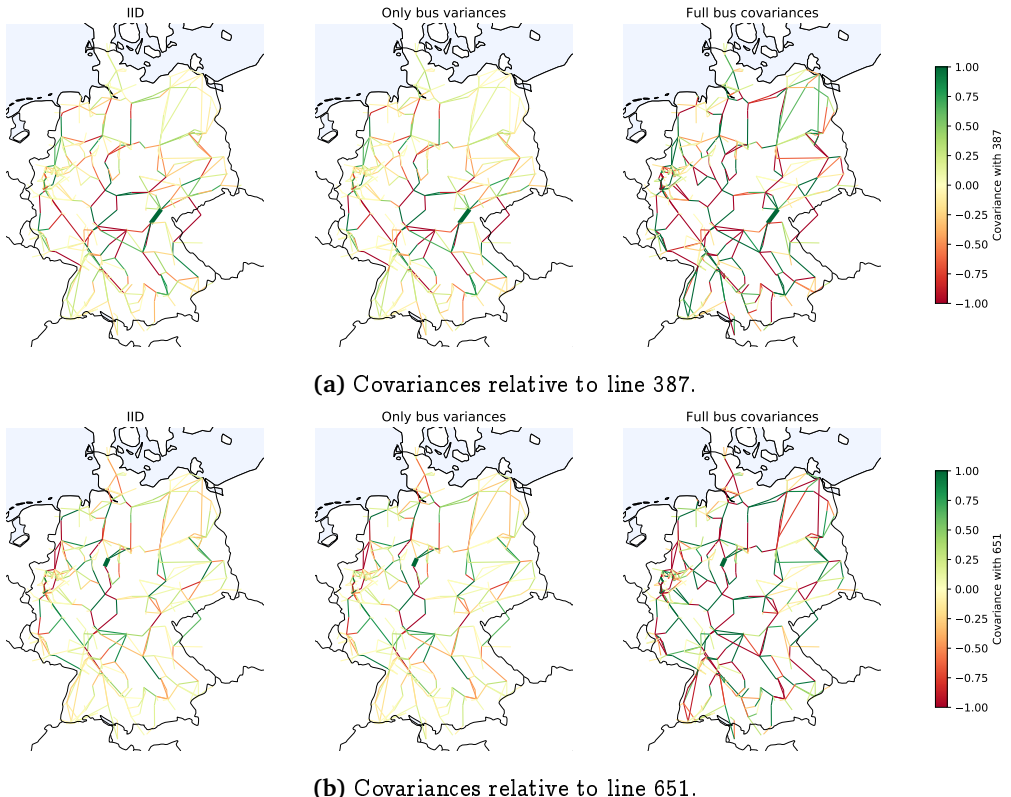


Figure 6.3: Covariance of all lines, relative to the enlarged line. Normalised using installed renewable capacity. Signs (red or green) can be chosen arbitrarily. Absolute covariance is therefore proportional to color *saturation*.

The covariance of a random pair of lines is relatively high when their physical separation (measured either in kilometres or in graph distance) is low. Because weather is correlated, even at high distance, using the bus full covariance might result in higher covariances between lines with high separation. (This was concluded by Nesti et al. (2018a).)

Using a different bus covariance matrix will likely result in a overall increase or decrease of line covariances. Note, however, that scaling the covariance matrix *uniformly* does change absolute overload probabilities, but it does not change the *ranking* of most vulnerable lines, and it does not change most likely injection: a uniform factor in Σ_p

⁴The counter-intuitive fact that adding a line, or increasing the impedance of existing lines, can make a network *more* congested, is known as *Braess' Paradox*. Similarly, some line failures can be prevented by switching off other lines in the network.

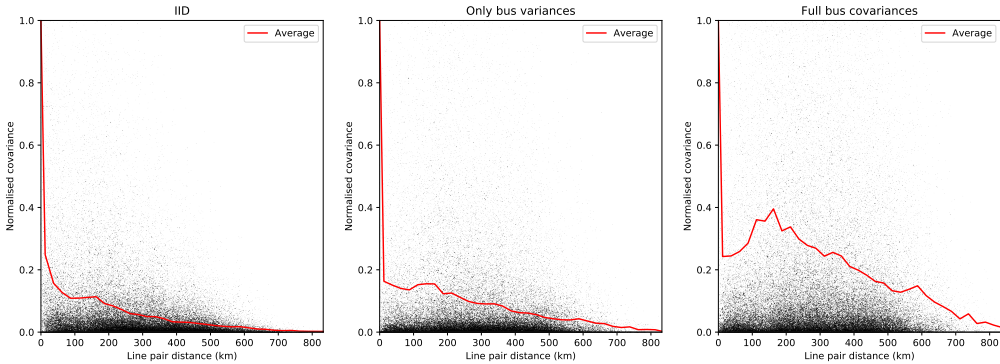


Figure 6.4: For 10^5 random pairs of lines, the covariance and distance (between line centres) is shown, for three possible bus covariance matrices. The averages (over 25 km) show that correlated buses increase long-range correlations in line flows. Covariances are normalised using average line variance.

disappears in Equation (4.11).

This makes it difficult to compare the three bus covariance matrices, as any absolute difference in line covariance should be ignored. Instead, we will examine the covariance of two lines, *relative to their own variances*. This way, the effect of any absolute, proportional increase in covariance is avoided. First, let us choose a number of lines, and examine the covariances of all other lines with the chosen line, relative to its variance.

In particular, we are interested in the decay of covariance over distance. Jung and Kettemann (2016) studied the decay of the Line Addition Distribution Factor (difference in flow after adding a line) over distance, also using the SciGRID network. This is not the same as covariance, of course, but both are measures of the *global effect* of local changes in flow. They first determined the largest 2-connected component of the network, and removed all other lines from the model. In the remaining network, they studied the 880 possible additions of short new lines, and found a general *exponential* decay of change in currents as a function of graph distance.

To study the decay of covariance, we collect the geographical separation and covariance (resulting from the three possible bus covariance matrices) of 10^5 random pairs of lines in the network. Because of power flow physics, these covariances are highly spread out. However, when averaging the covariances in groups of 25 km (Figure 6.4), we find are able to see the differences in decay.

By doing so, we find an important result. When we model bus injections to be uncorrelated (first two graphs in Figure 6.4), we find *some* correlation in line flows, which are due to power flow physics.⁵ On average, these correlations decrease as the distance between two lines increases, as shown by the red line.⁶ On the other hand, when we include *covariances among bus injections* in our model (last graph in Figure 6.4), we find a *relative increase in long-distance correlations of line flows*, compared to the

⁵ As an example, consider the n -loop network. Here, two neighbouring lines are highly correlated, since they always transmit roughly the same amount of power. (The difference is the amount of power injected at their common node.)

⁶ We might expect this decay to be *exponential* (based on the work of Jung and Kettemann (2016), for example), but this is not the case.

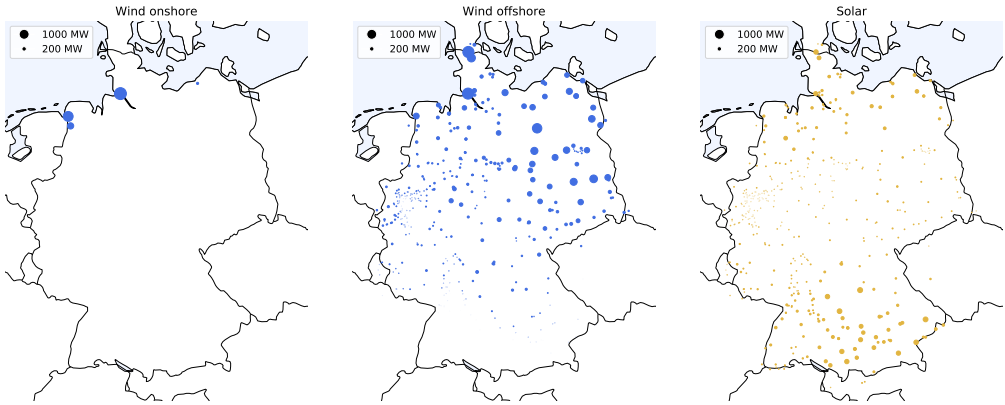


Figure 6.5: Installed stochastic capacity per source: wind onshore, wind offshore, solar.

uncorrelated case. This is one of the main results of Nesti et al. (2018a), which they demonstrate only on the n -loop network. Figure 6.4 validates that the result also holds for the SciGRID network.

Curiously, in the range 25 km - 150 km, the average correlation of line flows *increases* with higher line distances. The reason for this phenomenon is unclear, but one could investigate this further by examining line pairs of these short distances individually.

6.4 Most vulnerable lines

Using the nominal injection at 1 January, 11:00, we compute the failure probability of each line. The 30 most vulnerable lines are given in Table 6.1 (first two columns) and their positions are given in Figure 6.6. In the SciGRID dataset, lines are not numbered randomly. Rather, we find that two consecutive line numbers often correspond to two lines that are in close proximity. In the case of lines 651 and 652, for example, the two lines are connected in *series*. As a consequence of power flow physics, their line flows highly correlated.

We identify the same vulnerable lines as Nesti et al. (2018b), but the ranking is different. This can be attributed to two differences in approach. First, we have combined parallel lines,⁷ which changes the vulnerability order significantly. It is unclear why this changes the result. For comparison, the ranking that we get *without* combining parallels was also computed, which is more similar than of Nesti et al. (2018b). The second major difference is the use of a different covariance matrix, although it is reassuring to see that the same lines are identified.

6.4.1 Properties of vulnerable lines

As can clearly be seen in Table 6.1, most lines that are vulnerable to emergent failures are nominally being used at 70% percent of their capacity. (This is exactly the *contingency factor* used in the LOPF calculation.) This is explained by the low standard deviations

⁷ all 30 most vulnerable lines were not part of a parallel combination

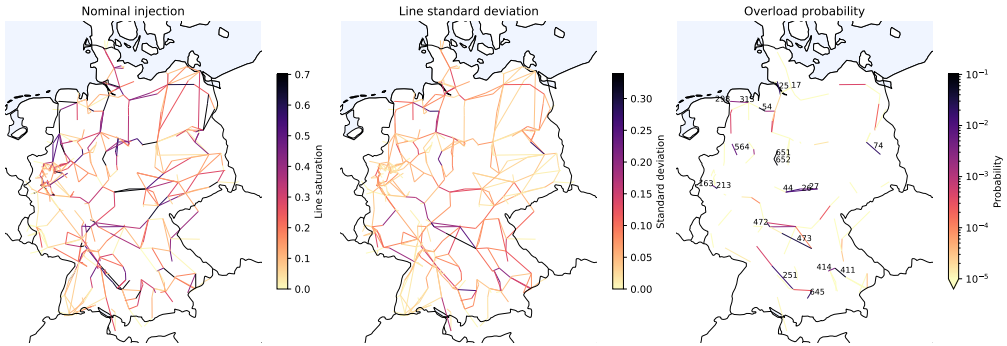


Figure 6.6: Visualisation of μ_f , Σ_f and $(\mathbb{P}[|f_l| \geq 1])_{l \in [m]}$ at 1 January, 11:00. The 20 most vulnerable lines are labelled.

of line flows. In fact, when we scale the covariance matrix uniformly by a factor close to zero, this effect is exaggerated.⁸

The 10 most vulnerable lines are not significantly long or short. They average 43 km (SD 30 km), compared to 36 km (SD 35 km) for *all* lines in the network. From Figure 6.6 we can make the interesting observation that vulnerable lines are generally oriented radially towards the *Ruhr*, a density populated area in western Germany.

Vulnerable lines have significantly lower thresholds. On average, the 10 most vulnerable lines can transmit 554 MW (SD 219 MW), while the grid-wide average is 1385 MW (SD 1052 MW). Indeed, a change in injection has an *absolute* effect on line flows; lines with low thresholds that are operating at the contingency limit (70%) need only a small amount of additional power to overload.

There is a difference in line *impedance*: $3.9 + 18.9i\Omega$ (SD $3.3 + 12.5i\Omega$) compared to the average of all lines, $2.0 + 12.0i\Omega$ (SD $2.6 + 13.6i\Omega$). This higher reactance means that vulnerable lines have higher *susceptance*, making them more sensitive to changes in node voltages. Grid operators have some control over these values, and lowering the line reactance might make these lines less vulnerable. To study these questions further, we need to also take *reactive power* into account, which we omitted in the DC approximation.

6.5 Most likely injection

In addition to the failure probability, we compute the most likely injection to cause that failure using Theorem 4.9.1. The reader is invited to examine these injections themselves using Interactive Figure 6.8. The most likely fluctuation of three lines is given in Figure 6.7a. As expected, we find that vulnerable lines (most likely) fail due to small fluctuations in the injection, while robust lines only fail because of extreme, highly unrealistic fluctuations.

⁸This is a *large deviations* result of the normal distribution: if we have $X \sim \mathcal{N}(0, \sigma^2)$, then the marginal distribution of $X \mid X \geq 1$ becomes increasingly concentrated around 1 as σ tends towards zero. See e.g. Touchette (2011).

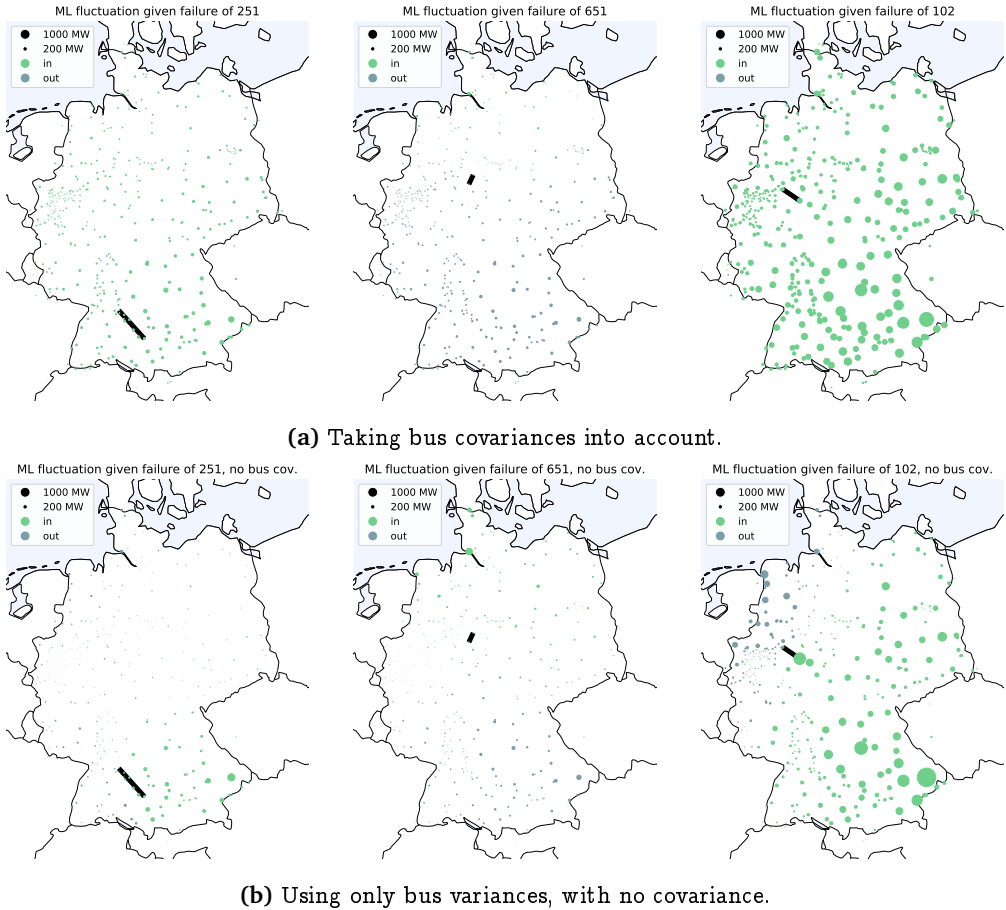


Figure 6.7: The most likely fluctuation given the failure of lines 251 (1.60% overload probability), 651 (9.56%) and 102 ($< 10^{-15}$). By including bus covariances (top), we find the most likely fluctuation to be more spread out. Zero-sum correction (distributive slack) is not applied.

6.5.1 Geographic distribution of fluctuations

In general, the most likely fluctuation is not concentrated at the two endpoints of the line, but rather, it consists of small, grid-wide fluctuations. This is due to high bus covariances, but also due to power flow physics. To examine the contribution of bus covariances, we also compute the most likely injection using only the diagonal of bus variances, see Figure 6.7b. For these three lines, we find that the fluctuations are indeed more evenly distributed when bus covariances are taken in account.

To study this hypothesis more objectively, we need a measure of how ‘spread out’ the fluctuation is. One possibility is to use the *standard deviation* of the 489 entries of a fluctuation: when a fluctuation is more evenly distributed (geographically), we expect the standard deviation of individual fluctuations to be lower. When computing these values for the 50 most vulnerable lines, we find no significant result: the average of the 50 standard deviations in fluctuations is 22.0 MW (SD 6.5 MW) for correlated buses and 22.6 MW (SD 9.5 MW) for uncorrelated buses. Taking a lower number of lines does not

improve the result. Curiously, when *all* lines are considered (including the 584 lines with negligible overload probability⁹), the average standard deviation is actually *higher* with correlated buses: 1245 MW (SD 9244 MW) versus 418 MW (SD 1036 MW) for uncorrelated buses. However, because we are mainly interested in the most vulnerable lines, we will leave this anomaly for what it is. Regarding the first 50 lines, it seems like a different approach is needed, and we are unable to confirm our hypothesis.

6.5.2 Bus extensions

Since we did not incorporate the *installed stochastic capacity* in our model, it is possible that the predicted most likely injection dictates that some buses are generating more stochastic power than what is installed. To evaluate this problem, we retrieve the total amount of installed stochastic capacity for each bus from our dataset (taking the sum of solar and wind). For a given point in time, the generation values then tell us how much a bus can fluctuate upwards (more generation) and downwards.

Given a most likely injection, we can compute whether the fluctuation at each bus is within the possible bounds, and if not, by how much the bounds must be extended for the most likely injection to be possible. In Table 6.1, the number of buses that needs to be extended is given, along with the total amount of extended capacity. For simplicity, we make no distinction between an extension upwards or downwards. An extension upwards means that more solar panels or wind turbines would be needed for the injection to be possible.¹⁰ An extension downwards is harder to justify, but one could say that it means that the amount of stochastic generation *before* the fluctuation must have been higher, replacing non-stochastic generation at that node.

For the most vulnerable lines, we find that the *number* of extended buses can be quite high, but the total amount of addition capacity is low, in general. For reference, buses in the network have an average installed capacity of 76 MW (solar); 82 MW (wind).

6.5.3 Cascades

Using the most likely injection, we simulate the resulting cascade. The results for all lines are given in Interactive Figure 6.8. The number of lines that either failed jointly with the initial failure, or failed during the subsequent cascade, is also given in Table 6.1. This extends the result of Nesti et al. (2018b), which only provides the failure probability. We find that among the 10 most vulnerable lines (at 11:00), only the failures of lines 298, 25 and 645 result in a power island. We will discuss these lines in more detail in Section 6.5.4, but for now, we note that these failures quickly result a power island. (For 298 and 645, this happens the first stage.) At this point, our model becomes unreliable (see Section 6.6.1).

6.5.4 Evolution of line vulnerabilities

Of course, the method above can be applied to any nominal injection, not just the injection at 1 January, 11:00. By applying the method to every hour of the first day, we

⁹i.e. less than 10^{-15} , the numerical margin of error in our case

¹⁰This implies an inaccuracy in our dataset.

find 24 different rankings, one of which is given in Table 6.1. This allows us to not only identify lines that are vulnerable at a given point in time, but to find lines that are a *consistent vulnerability*, based on the general use of the transmission network.

Instead of providing 23 additional tables, we have summarised the results of a full day in Figure 6.9. Here, we see that some lines (like 337) are only vulnerable at one point during the day, while others (298 and 54) have a consistently high overload probability. There is a clear distinction between daytime and night-time, since the time of day determines which covariance matrix is used in the calculation. In fact, this highlights how a change in covariance influences results: some lines are only vulnerable because of the covariances brought upon by solar generation, while others are relatively unaffected.

A most striking result is that the overload probabilities of 25 and 298 are perfectly *constant* for sustained periods, and both are likely to cause a cascade, resulting in an average of 108 and 76 failures, respectively. When examining these two lines in more detail, we find that both are *branches out of the network towards coastal cities of the North Sea*, with high-capacity offshore wind generation. These generators were operating at full capacity during the studied day,¹¹ which would cause a constant¹² power injection. Because the lines are *branches* out of the larger graph, the flow through the line is exactly equal to the power injection at its end, and therefore constant.

Regarding the subsequent cascades of these two lines, it seems like our model falls short of giving an accurate redistribution of flow, due to the singularity caused by their removal. (No flow redistribution exists that would not change the injection.)

6.6 Discussion

6.6.1 Cascading failures

Following Nesti et al. (2018a), we identify the lines most vulnerable to emergent failures, and we give the absolute overload probabilities (first two columns of Table 6.1). We extend the original result by also stating the (most likely) total fluctuation and the sequence of cascades. Additionally, we assess the final stage of the cascade (i.e. the *severity* of the emergent failure) using the final number of failed lines, and we determine whether a power island emerged in the process. These results are given in the table.

This allows us to make the important observation that most vulnerable lines do *not* result in a severe cascade of failures. This means that the network will remain operational after the emergent failure, and once the nefarious fluctuation has passed, the failed line can be operational again. For some vulnerable lines, our model does predict a significant amount of cascaded failures. However, when looking at these cases individually, we find that they are all lines that branch out of the network, quickly resulting in a power island. After the power island occurred, the simulated cascades are likely erroneous. We suspect that the emergent failure of these lines will indeed cause a power island to form, but that the remainder of the network will remain operational.

¹¹according to our dataset

¹²except for the local energy usage, which is relatively small

OVERLOAD PROBABILITY			MOST LIKELY INJECTION			CASCADE	
l	$\mathbb{P}[f_l \geq 1]$	mean $\pm SD$	total fluctuation	extended buses (add. capacity)		failed lines per phase (disconnected)	power island?
651	9.55 %	0.70±0.23	3.8 GW	43 (62 MW)		1	no
652	8.95 %	0.68±0.24	3.9 GW	46 (82 MW)	(2)		yes
411	7.06 %	0.70±0.20	5.0 GW	6 (12 MW)		1	no
54	6.21 %	0.61±0.25	2.5 GW	3 (1 MW)		1	no
298	3.45 %	0.70±0.17	1.1 GW	3 (0 MW)	(1 » 3 » ... » 65)		yes
473	3.13 %	0.37±0.34	7.1 GW	10 (52 MW)		1	no
213	2.37 %	0.70±0.15	6.9 GW	103 (569 MW)	2 » 3 » 4 » 5		no
25	2.11 %	0.70±0.15	2.1 GW	0 (0 MW)	2 » 4 » (5 » 50 » ... » 102)		yes
645	2.02 %	0.70±0.15	4.4 GW	15 (70 MW)	(1 » 5 » ... » 53)		yes
74	1.96 %	0.43±0.28	6.5 GW	12 (52 MW)		1	no
472	1.76 %	0.43±0.27	8.3 GW	11 (84 MW)		2	no
251	1.60 %	0.70±0.14	7.6 GW	11 (111 MW)	2 » 5 » (10 » 19 » ... » 177)		yes
44	1.31 %	0.70±0.14	9.1 GW	9 (33 MW)	1 » 2		no
26	0.980%	0.70±0.13	9.4 GW	9 (46 MW)	1 » 3 » (8 » 23 » ... » 117)		yes
17	0.871%	0.70±0.13	6.5 GW	70 (324 MW)		3	no
163	0.645%	0.70±0.12	9.1 GW	143 (1137 MW)	2 » 3 » 4		no
564	0.585%	0.70±0.12	5.9 GW	1 (2 MW)		2	no
27	0.542%	0.69±0.12	10.1 GW	10 (69 MW)	2 » 3 » (5 » 8)		yes
414	0.406%	0.47±0.20	9.8 GW	12 (140 MW)	2 » 3 » 4 » (6 » 10)		yes
315	0.246%	0.70±0.11	2.0 GW	0 (0 MW)	(2 » 7 » 13)		yes
461	0.237%	0.46±0.19	10.7 GW	15 (234 MW)	2 » 4 » 5		no
627	0.160%	0.57±0.15	8.3 GW	23 (169 MW)		2	no
531	0.151%	0.18±0.28	5.2 GW	14 (56 MW)	(3 » 11 » ... » 159)		yes
534	0.113%	0.63±0.12	4.3 GW	2 (8 MW)	3 » 5 » (8 » 12 » ... » 184)		yes
460	0.052%	0.38±0.19	12.5 GW	20 (396 MW)	3 » 6 » 7 » 8 » (11 » 12)		yes
257	0.048%	0.51±0.15	10.3 GW	21 (417 MW)	3 » 6 » (8 » 11)		yes
624	0.047%	0.42±0.17	5.5 GW	13 (53 MW)	3 » 6 » 9 » 15 » (21»...»137)		yes
561	0.045%	0.68±0.10	4.7 GW	1 (2 MW)	3 » 9 » 16 » (21 » ... » 200)		yes
569	0.042%	0.61±0.12	8.4 GW	19 (87 MW)	1 » (4 » 179 » ... » 219)		yes
563	0.034%	0.69±0.09	4.5 GW	2 (8 MW)	3 » 8 » (16 » 52 » ... » 151)		yes

Table 6.1: The 30 most vulnerable lines at 1 January, 11:00. For each line, we have the absolute overload probability and the mean and standard deviation of line saturation. For the most likely injection, the total change (fluctuation) in injection is given, and the number of buses for which renewable generation would need to be extended for the most likely injection to be possible.

The number of failed lines in each cascade stage is shown. Stages in parentheses correspond to a disconnected network. (The first number is greater than 1 when there are *joint failures*.) The final column states whether the last cascade stage is disconnected (i.e. whether a power island emerged).

6.6.2 Power islands

The Optimised method computes redistributed flows efficiently, and its derivation (Section 4.10.2) provides us with a more intuitive understanding of flow redistribution. Examining results for individual lines (e.g. see Interactive Figure 6.8) shows realistic results. Yet, as the analyses of lines 25 and 298 demonstrate, the method is likely erroneous when the network becomes *disconnected* after the line removal(s), i.e. when a power island occurs.

In fact, in its original form (Ronellenfitsch et al., 2017), the optimised method is only defined when the network remains connected. While this is a limitation of the Optimised method, it is, more generally, a limitation of using DC approximated power flow. In this approximation, we assume the network to be in a *state of equilibrium*: generation matches load exactly.

In our case, the use of a stochastic injection means that we generally do not have a zero-sum injection, contradicting the assumption. This contradiction is usually justified using the concept of (distributive) slack: an overall increase or decrease in generation will occur (to compensate for the non-zero net injection), without changing the line flows.

Yet, when studying cascading failures, we are looking at a time frame much shorter than the time it takes to reach equilibrium. This shorter time scale generally requires an analysis of an entirely different nature: this is the study of *transient stability*, which is far beyond the scope of this thesis.

Overall, a better understanding of the physics that underlie line failures is required to study cascading failures, especially in cases where power islanding occurs.

6.6.3 Previous work (Nesti et al., 2018a)

This thesis was inspired by the model and case study of Nesti et al. (2018a). While many of the future research topics proposed by this article remain open, we have been able to independently verify their results. While our model is based on the original, there are some fundamental differences between the two. Therefore, the differences in our results provide valuable insight into the accuracy of either model.

There are two important modifications that we chose to make to the original model. First of all, our model does not use ARMA forecasting, but a much simpler *persistent forecast* as placeholder. For wind generation series, the resulting covariance matrices turn out to be very similar. We cannot comment on the similarity in solar covariances, as we were unable to reproduce these results.

A second difference is the use of a different method for computing the redistributed flow, which is based on Ronellenfitsch et al. (2017). There is no clear practical benefit to using the Optimised method, except for computational cost. Still, our use of this method has led to the insight that a DC approximated model is not well-suited for disconnected networks, when a large power imbalance exists among connected islands.

This Optimised method requires the network to be a *digraph*, which does not allow for parallel lines to exist. For this reason, we have combined parallel lines in our network, taking their physical properties into account. Strangely, this increases the discrepancy

between the line flows computed by the LPF, and those given by the OPF algorithm. This effect could be investigated further by studying smaller test networks.

Evaluation of results

We performed a careful analysis of the results that follow from the SciGRID application, identifying new problems in the model of Nesti et al. (2018a). For example, we find that for almost all lines, the most likely power injection requires an extension of stochastic capacity at multiple buses. For some lines, this extension is relatively small, and it does not invalidate the result. For other lines, a significant extension is needed. We suspect that the required extensions will be much greater when analysing a point in time when renewable generation is already high. A better understanding of the origin of our dataset is needed to evaluate the significance of this problem.

This problem could be addressed *within the framework of our model* by imposing additional conditions on the most likely injection. In its current form, the problem of finding the most likely injection is an optimisation problem with *linear boundary conditions* (as given in the proof of Theorem 4.9.1). Because the boundary conditions can be written as a *half-plane in \mathbb{R}^n* , we were able to derive a closed form solution. We could include the upper and lower limits of stochastic generation as addition linear conditions, which will likely make a closed-form solution unobtainable. Instead, non-linear optimisation methods could be used to find the most likely injection, given these additional conditions.¹³ See Chertkov et al. (2011) for a study using this approach.

6.6.4 Future

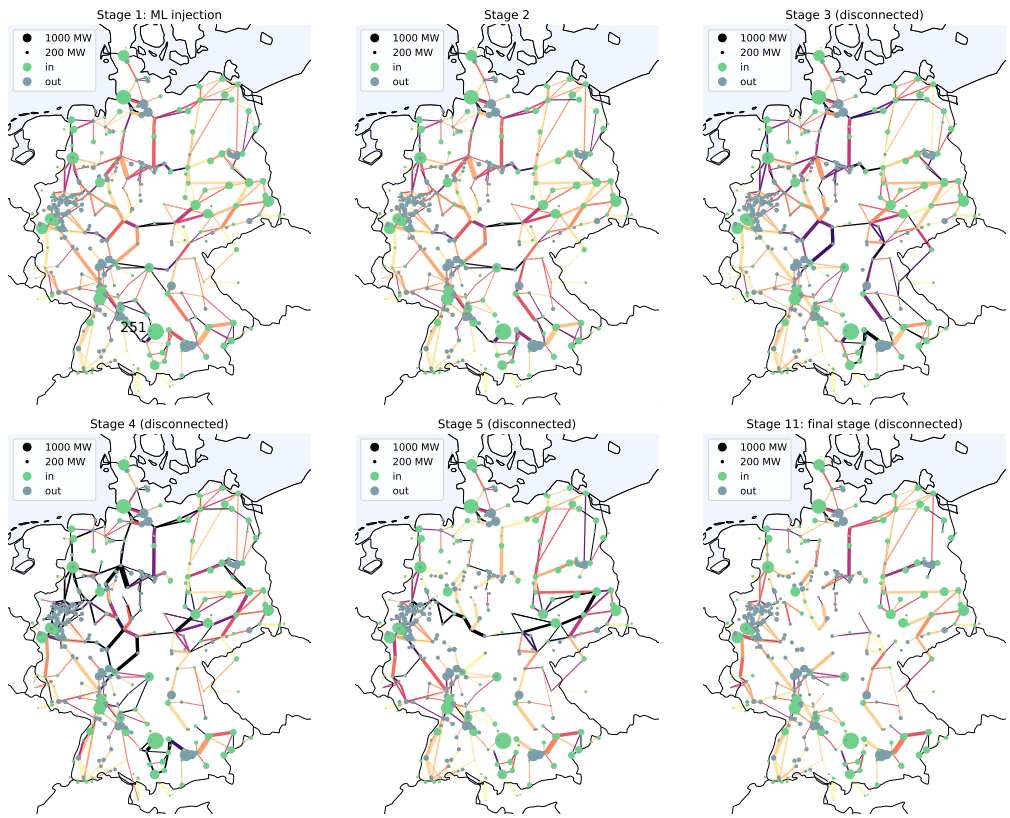
There are many aspects of this analysis that could be studied in more detail; some are mentioned throughout this chapter. Regarding our case study, the first shortcoming that could be addressed is the fact that we have only thoroughly looked at data of January 1st. Like Nesti et al. (2018a), most of our results are computed for the nominal injection at 11:00. Additionally, we have computed our main result for the remaining 23 hours of the day, which includes hours where the *night* covariance matrix is used (see Figure 6.9). While we can directly compute results for the remaining days of January and the remaining months of 2011, we have not yet analysed these results.

While our dataset provides an interesting case study, it does have some limitations. First of all, the dataset does not consist of physical measurements: it is constructed by combining various data sources, most of which are in turn obtained from modelling. Because of the numerous steps needed to construct our final dataset, it is hard to quantify the inaccuracy of our results.

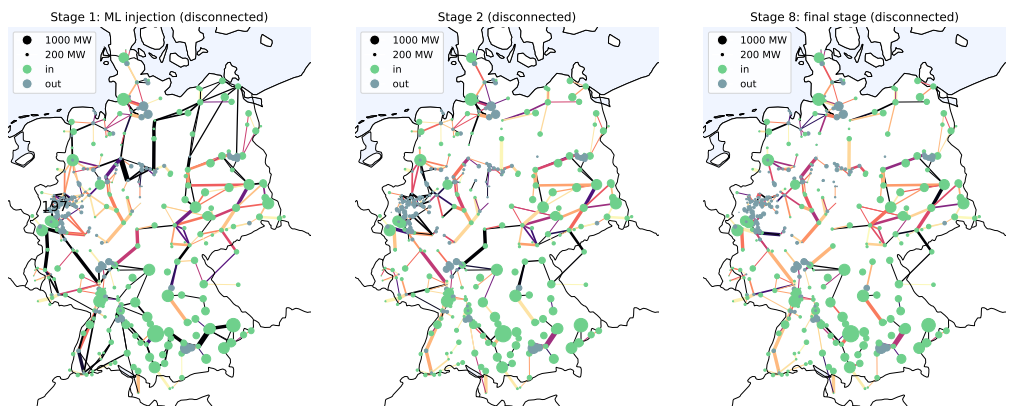
Crucially, our dataset does not allow us to *verify our results*, since it is *too coarse* to contain fluctuations, and it provides no historical data on line failures. High-resolution stochastic generation datasets do exist, possibly for all nodes of a realistic transmission network. However, to the best of our knowledge, no dataset exist that contains continuous measurements of line currents and overloads.

¹³In fact, if we use this more general method to find the most likely injection, we could enforce the power injection to have zero sum by imposing one additional linear condition: $\sigma(\mathbf{p}) = 0$. Although this would solve the problem of having a most likely injection with non-zero sum, there is no physical argument for this imposing this condition.

Many smaller datasets exists that can be analysed using our methods. Most notably, the *IEEE test networks* can be extended with fictional stochastic generation, as demonstrated by Nesti et al. (2018a) and Chertkov et al. (2011). These smaller networks would allow us to more easily inspect the behaviour of individual lines in the network. Another way to construct a smaller network could be to take a *subsection* of the SciGRID network.



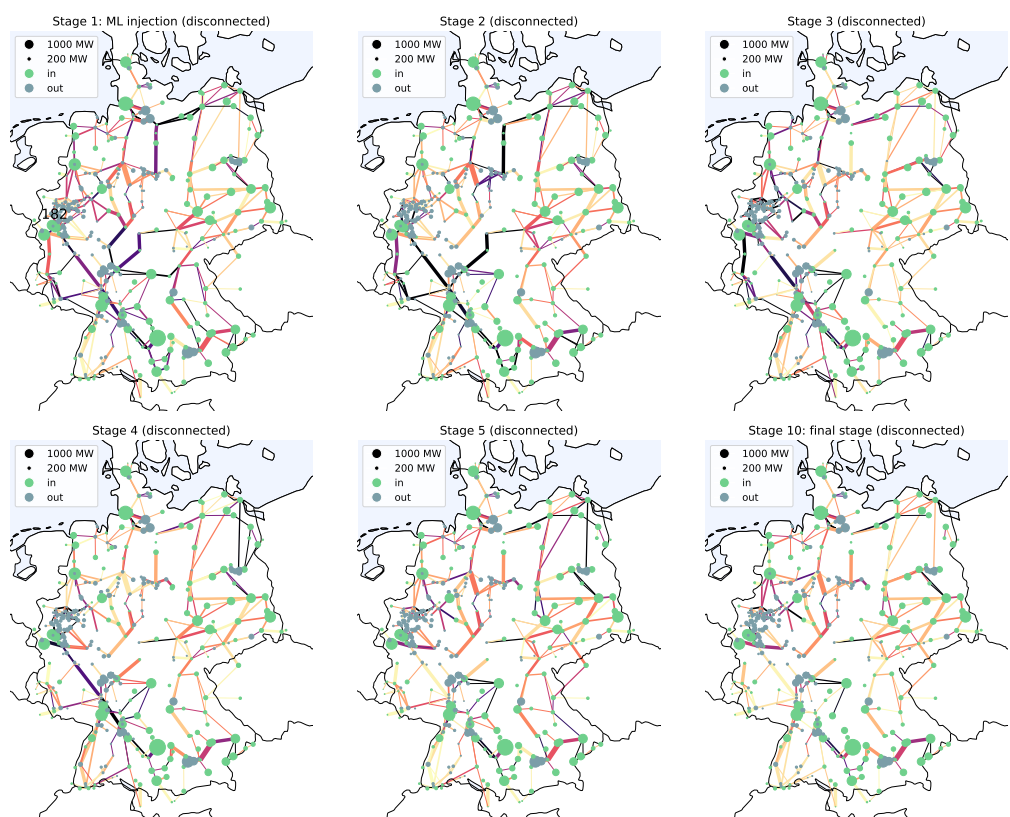
(a) Assumed failure of line 251.



(b) Assumed failure of line 197.

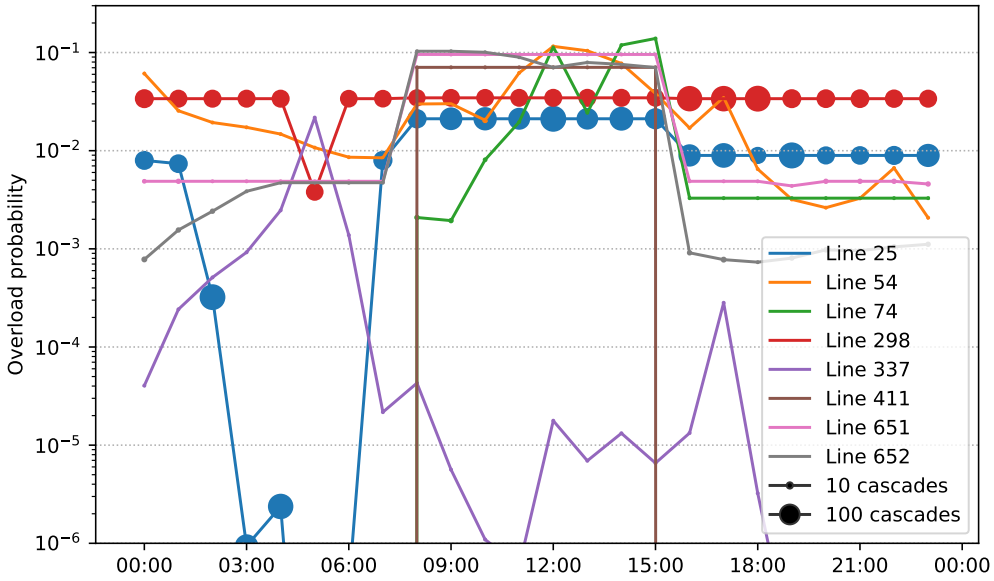
Interactive Figure 6.8: Simulated cascade stages after one assumed emergent failure. Node sizes represent the most likely injection. Long cascade sequences are truncated.

This figure is interactive: to view animated cascade simulations for all lines of the network, visit fonsp.com/grid.

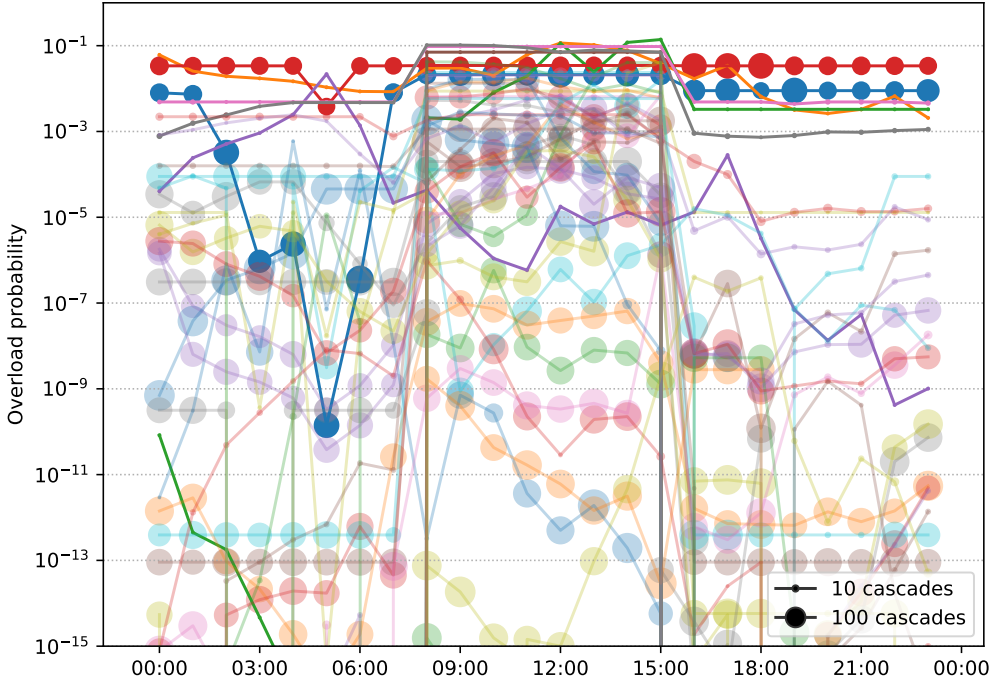


(c) Assumed failure of line 182.

Interactive Figure 6.8: (continued)



(a) All lines that are, at any time during the day, among the 3 most vulnerable lines.



(b) All lines that are, at any time during the day, among the 20 most vulnerable lines.

Figure 6.9: Evolution of absolute failure probabilities during 1 January 2011. Dot sizes represent final number of lost lines after the most probable cascade.

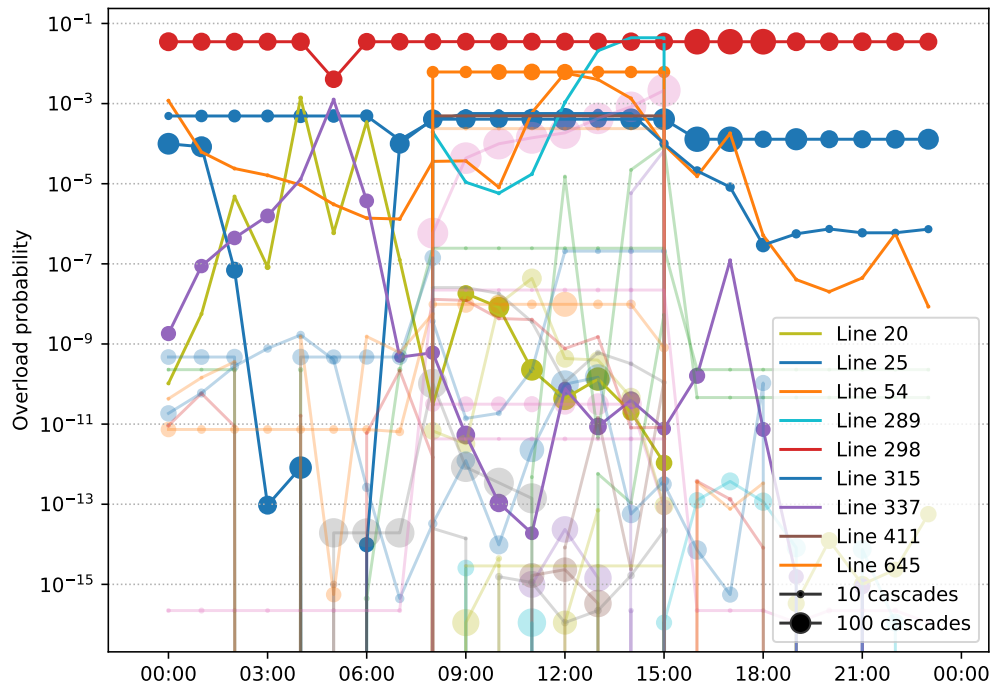


Figure 6.10: For reference, the same as Figure 6.9b, but computed using *uncorrelated* injections.

From the author

Thank you for reading my bachelor thesis! I hope that I have been able to express my enthusiasm and fascination for the subject. It has been a wonderful experience to work on this thesis, and I am especially proud to have worked on a problem that is the subject of current research.

I would like to thank my supervisors, Henk and Eric, for taking the time to guide me through this process, for communicating their knowledge and for supporting my unusual choice of subject.

I have been fortunate enough to speak with Tommasso Nesti and Bert Zwart, who, together with Alessandro Zocca, authored the article that this thesis was inspired by. Their comments helped me to better understand the context and interpretation of their model. I also wish to thank Uli Zeitler for discussing the physical properties of AC transmission lines and Klaas Landsman for helping me find the right thesis subject.

I am very grateful to my family and friends for the wonderful four years in Nijmegen. I would like to thank my friend Merlijn Kersten for his enthusiasm and advice during the past few months, and I thank my brother Thijs van der Plas for giving me a pair of shoulders to stand on.

-fons

Bibliography

- Andresen, G. B., A. A. Søndergaard, and M. Greiner
2015. Validation of Danish wind time series from a new global renewable energy atlas for energy system analysis. *Energy*.
- Brown, T., J. Hörsch, and D. Schlachtberger
2018. PyPSA: Python for Power System Analysis. *Journal of Open Research Software*, 6(1):4.
- Chertkov, M., M. Stepanov, F. Pan, and R. Baldick
2011. Exact and efficient algorithm to discover extreme stochastic events in wind generation over transmission Power Grids. In *IEEE Conference on Decision and Control and European Control Conference*, Pp. 2174–2180. IEEE.
- Denholm, P., M. O'connell, G. Brinkman, and J. Jorgenson
2015. Overage from Solar Energy in California: A Field Guide to the Duck Chart. Technical report, National Renewable Energy Laboratory.
- Garling, D. J. H.
2014. *A course in mathematical analysis. Volume III, Complex analysis, measure and integration*. Cambridge: Cambridge University Press.
- Guler, T., G. Gross, and M. Liu
2007. Generalized Line Outage Distribution Factors. *IEEE Transactions on Power Systems*, 22(2):879–881.
- Guo, J., Y. Fu, Z. Li, and M. Shahidehpour
2009. Direct calculation of line outage distribution factors. *IEEE Transactions on Power Systems*, 24(3):1633–1634.
- Hörsch, J., F. Hofmann, D. Schlachtberger, and T. Brown
2018. PyPSA-Eur: An open optimisation model of the European transmission system. *Energy Strategy Reviews*, 22:207–215.
- Huelsman, L. P.
2011. *Circuits, matrices and linear vector spaces*, dover ed. edition. Mineola N.Y.: Dover Publications.
- IPCC
2014. Annex III: Glossary. In *Climate Change 2013: The Physical Science Basis. Contribution of Working Group III to the Fifth Assessment Report of the Intergovernmental Panel on Climate Change*, S. Schrömer, T. Bruckner, L. Fulton, E. Hertwich, A. McKinnon, D. Perczyk, J. Roy, R. Schaeffer, R. Sims, P. Smith, and R. Wiser, eds.

- Jung, D. and S. Kettemann
 2016. Long-range response in ac electricity grids. *Physical Review E*, 94(1):012307.
- Kirtley, J. L.
 2010. *Electric power principles: sources, conversion, distribution, and use*. John Wiley & Sons, Ltd.
- Matke, C., W. Medjroubi, and D. Kleinhans
 2016. SciGRID - An Open Source Reference Model for the European Transmission Network (v0.2).
- Matoušek, J. and B. Gärtner
 2007. *Understanding and using linear programming*. Springer.
- Nesti, T., A. Zocca, and B. Zwart
 2018a. Emergent Failures and Cascades in Power Grids: A Statistical Physics Perspective. *Physical Review Letters*, 120(25):258301.
- Nesti, T., A. Zocca, and B. Zwart
 2018b. Supplemental Material for: Emergent failures and cascades in power grids: a statistical physics perspective. Technical report.
- Overbye, T., Xu Cheng, and Yan Sun
 2004. A comparison of the AC and DC power flow models for LMP calculations. *37th Annual Hawaii International Conference on System Sciences, 2004. Proceedings of the*, 00(C):9 pp.
- Pestman, W. R.
 1998. *Mathematical statistics - an introduction*. Nijmegen: Walter de Gruyter.
- Purchala, K., L. Meeus, D. Van Dommelen, and R. Belmans
 2005. Usefulness of DC power flow for active power flow analysis. *IEEE Power Engineering Society General Meeting, 2005*, Pp. 2457–2462.
- Ronellenfitsch, H., D. Manik, J. Hörsch, T. Brown, and D. Witthaut
 2017. Dual Theory of Transmission Line Outages. *IEEE Transactions on Power Systems*, 32(5):4060–4068.
- Slepian, P.
 1968. *Mathematical Foundations of Network Analysis*, volume 16 of *Springer Tracts in Natural Philosophy*. Berlin, Heidelberg: Springer Berlin Heidelberg.
- Stott, B. and O. Alsac
 1974. Fast Decoupled Load Flow. *IEEE Transactions on Power Apparatus and Systems*, PAS-93(3):859–869.
- Touchette, H.
 2009. The large deviation approach to statistical mechanics. *Physics Reports*, 478(1-3):1–69.
- Touchette, H.
 2011. A basic introduction to large deviations: Theory, applications, simulations.

von Meier, A.

2006. *Electric Power Systems*. Hoboken, NJ, USA: John Wiley & Sons, Inc.

Witthaut, D. and M. Timme

2013. Nonlocal failures in complex supply networks by single link additions. *Eur. Phys. J. B*, 86:377.

Ye, Q., L. Jiaqi, and Z. Mengye

2018. Wind Curtailment in China and Lessons from the United States. Technical report, Brookings.

The code used to generate this document (\LaTeX) and the embedded figures (Python 3.7 with numpy and matplotlib) is available¹⁴ at the *GitHub repository*:

github.com/fonsp/grid-analysis

The Interactive Figure contains its own source code (JS with D3.js):

fonsp.com/grid

If you have any comments, I would love to hear from you!

fonsvdplas@gmail.com

¹⁴open source, under the MIT Licence